UNIVERSITY OF CAPE TOWN

DOCTORAL THESIS

Quantum Chaos and Phase Transitions

Author:
Nitin Gupta

Supervisors:
Prof. Jeff Murugan
Dr. Dario Rosa
Dr. Shajidul Haque

Presented to the Department of Mathematics and Applied Mathematics at the University of Cape Town as a partial fulfillment of the requirements for the Doctor of Philosophy degree in Applied Mathematics.

March 11, 2025

University of Cape Town

The copyright of this thesis vests in the author. No quotation from it or information derived from it is to be published without full acknowledgement of the source. The thesis is to be used for private study or non-commercial research purposes only.

Published by the University of Cape Town (UCT) in terms of the non-exclusive license granted to UCT by the author.

University of Cape Town

Abstract

Quantum materials permeate the modern world - these are systems that exhibit quantum mechanical properties, like topological phases and superconductivity, at macroscopic scales. The principles governing quantum materials include entanglement and coherence phenomena which are fundamentally quantum mechanical in nature, without classical counterparts. The semiconductors in mobile phones, computers, and solar cells; light emitting diodes (LEDs); sensors in medical equipment and other precision devices; Maglev trains and particle accelerators - all utilize quantum materials in one form or another. The trajectory of modernization over the past century has been significantly shaped by developments in quantum materials, underscoring the importance of studying their phases in detail.

This thesis focuses on one aspect of the research program to improve the understanding of quantum materials: mathematical probing for the presence of quantum phases (QPs) of matter and the transitions (QPTs) among them. Specifically, it proposes that Krylov Complexity can be utilized to detect QPs and QPTs. Krylov Complexity is a quantity that has been recently proposed in the physics literature as a measure of chaotic nature of a quantum system *i.e.* it encodes the information transport properties of a system - exponential signatures in the Krylov Complexity typically characterize a chaotic quantum system. A priori, one may not expect Krylov Complexity to be sensitive to the presence of QPs and QPTs. This thesis gives evidence contrary to this expectation. The results demonstrate that Krylov Complexity exhibits distinctive signatures at the boundaries of QPs, such as sharp peaks or discontinuities, which correspond to the quantum critical points.

Numerous techniques have been developed to study quantum materials both theoretically and experimentally: Tensor Network Methods, Renormalization Group Theory, Scanning Tunnel Microscopy, Hall Effect Measurement etc. This thesis highlights the simplicity and effectiveness of Krylov Complexity, which utilizes known information from studying Hamiltonians of many-body quantum systems with minimal additional computation.

In summary, through a comprehensive review of the theoretical framework underpinning Krylov Complexity, this thesis provides compelling evidence that it is a simple yet effective tool for probing QPs and QPTs, thereby opening new avenues for understanding quantum materials, their phases, and the transitions among these phases.

Declaration

A part of the content of this thesis is stems from publications with a set of collaborators spanned by: {{University of Warsaw, Poland: Pawel Caputa, and Sinong Liu}, {University of Cape Town, South Africa: Cameron Beetar, Shajidul Haque, Jeff Murugan, and Hendrik JR van Zyl }}.

The following list links the chapters of this thesis to the corresponding publications, resulting from collaborations with the above-mentioned individuals, that they are based on:

Chapter 4: Pawel Caputa, Nitin Gupta, S. Shajidul Haque, Sinong Liu, Jeff Murugan, and Hendrik J. R. Van Zyl. Spread complexity and topological transitions in the Kitaev chain. *JHEP*, 01:120, 8 2023;

Chapter 5: Cameron Beetar, Nitin Gupta, S. Shajidul Haque, Jeff Murugan, and Hendrik J. R. Van Zyl. Complexity and operator growth for quantum systems in dynamic equilibrium. *Journal of High Energy Physics*, 2024(8):156, Aug 2024.

I, the undersigned, as the author of this work, hereby declare that this thesis has not been submitted, either in the same or different form, to this or any other university for a degree and that it represents my own work - along with citations, where appropriate - with the exception of quotes, which are attributed to their authors. Furthermore, I have explicit written permission of the co-authors, listed above, of the above-mentioned publications to exclusively include the publications in this work and that the publications shall not form the basis of another thesis by themselves or their students.

Nitin Gupta

Signature: _____ March 11, 2025

Acknowledgment

Throughout my academic journey I've received invaluable support of many people and organizations, and here's a small attempt to try to express my gratitude to a subset of them.

First and foremost, I am deeply grateful to my advisor Jeff Murugan, without whose support this thesis would not have come to fruition. He has been instrumental in my development as a physicist, and his contributions are too many to be listed individually. In particular, his patient support, belief in me, and the healthy environment he has fostered in Quantum Gravity & Strings Laboratory (QGaSLab) will remain an ideal. I shall continue to be inspired by him for a long time indeed.

Thanks are also due to my other supervisors, Dario Rosa and Shajid Haque, for innumerable long discussions, guidance, and collaborations. A special vote of thanks go to my office-mate Jaco van Zyl for entertaining my never-ending questions. Thanks also extend to all my collaborators: Pawel Caputa, Sinong Liu, Cameron Beetar, and Jaco van Zyl; along with the members of the QGaSLab (and by extension, HEPCAT) for camaraderie including Ru, Zayd, and Thato.

I'm very grateful to the Science Faculty at the University of Cape Town (UCT) for the Science Faculty PhD Fellowship that funded the bulk of my studies during the PhD, which were supplemented through tutorship support by, primarily, the National Institute for Theoretical and Computational Sciences (NITheCS, previously NITheP), and the Department of Mathematics at UCT. I would also like to extend my thanks to the following individuals and organizations (in no particular order) for supporting my doctoral journey through support in one form or another: Amanda Weltman, Arpan Bhattacharyya, Tomaž Prosen, Xue-Yang Song, Adrian (Hoi-Chun) Po, NITheCS, IIT Gandhinagar, QISS Consortium, University of Ljubljana, ICTP, and HKUST. A special vote of thanks go to the Galileo Galilei Institute in Florence for inviting me to the winter school on the Theory of Fundamental Interactions in 2020 - which inspired me to continue with a path in academia.

My journey in Cape Town would not have been so enjoyable without my friends Bikash, Atiq, and Toma - thanks for all the hikes, the celebrations, the food-coma, and for being there. I'd also like to thank the members of the Badminton and Table Tennis sports clubs at UCT for the numerous enjoyable practice sessions. I was only able to explore Cape Town to my heart's content due to the encouragement I received from the Motorcycle Owners' Club (MOCT) - thanks for helping me overcome my fears of riding in strong winds and all the great advice.

To my girlfriend Arifa for sticking with me through thick and thin, and for her suffering & love through long years of separation, thank you! Finally, I'd like to thank my parents for their constant support, encouragement, and understanding for the path I've chosen.

Contents

"To explain all nature is too difficult a task for any one man or even for any one age. 'Tis much better to do a little with certainty, and leave the rest for others that come after you."

- Isaac Newton

1 Introduction

"All things appear and disappear because of the concurrence of causes and conditions. Nothing ever exists entirely alone; everything is in relation to everything else"

- Buddha

Goldilocks zone, honeycomb's hexagonal shape, Fibonacci spiral patterns, fish school movements, coral reef growths, water striders, bird migration, bacterial quorum sensing (including bio-luminescence), and symbiotic relationships[1]: What do all these phenomena have in common? Well, on one hand they're all phenomena that have fascinated human beings for millennia; and on the other, these phenomena share a striking natural tendency to optimize processes. Upon observation, it is easy to note that most natural phenomena, whether organic or inorganic, have evolved in a manner that minimizes the difficulty or cost of performing actions. This optimization assumes various shapes *e.g.* optimal arrangement patterns (honeycomb's hexagonal shape or Fibonacci pattern), energy conservation (water striders, bird migratory patterns), behavioral efficiency (bacterial quorum sensing, swarm behavior) etc. As curious beings, rather safe from predatory worries, we tend to have spare thought to study these patterns in more detail.

An *Ariadne's Thread* tying the study of these optimization phenomena is the notion of studying how difficult or complex it is to perform a particular task. Shifting gears to academia, this notion has been extensively studied in the field of computer science [12–14]. Computational complexity, colloquially, measures the difficulty or cost of performing an action or implementing a task. The earliest usage of an explicit notion of complexity in physics literature was in the terms of measuring complexity, or difficulty of preparation, of a quantum circuit - as a precursor to the anticipation of constructing quantum computers which were expected to have vastly different computational complexity than their classical counterparts. Those anticipations have since been realized [15], though, to an extent [16]. In contemporary physics, complexity enjoys a broader appreciation and applicability[2].

After the initial, somewhat lackluster, forays in quantum circuits during early 2000s, the study of complexity has garnered signification attention initiated by its successes in elucidating black hole physics [18–20]. In modern times, quantum complexity is a widely studied object, primarily in connection with its ability to diagnose quantum chaos [21–25]. This thesis is devoted to a recently introduced avatar of complexity, Krylov complexity [26], which adapts the ubiquitous Krylov subspace methods [27] to the study of quantum complexity. Krylov subspace methods enjoy wide applicability since they serve as a map from a high-dimensional

[1] See [3–11], respectively.

[2] In fact, a notion of complexity was recently used by Jared Lichtman to assist in his proof of the Erdős Primitive Set Conjecture [17]. Lichtman's method included computing the size of a primitive set, which is akin to the difficulty or cost of assembling the set elements - and hence, a valid definition of complexity, considering that there are no mathematical restrictions placed upon which quantity can serve as complexity.

linear problem, *e.g.* a system of linear equations, to an (often) easier to solve lower-dimensional problem [28]. This is precisely what they do for quantum complexity as well. In the context of studying transport properties in quantum many-body systems, this takes the form of *e.g.* understanding dynamical evolution of an operator and the corresponding linear problem is the Heisenberg's equation for the operator under study. Krylov subspace methods map the Hamiltonian time-evolution into a tridiagonal form [26], leading to significant reduction in computation difficulty and making many analytical calculations tractable. A numerical implementation of it via Lanczos algorithm [29] does suffer from numerical instabilities [30] - however, this can be combated to an appreciable extent via methods like Full Orthogonalization [31–34].

The central premise of this thesis is our proposal that Krylov complexity serves as an efficient and rigorous diagnostic of transitions between quantum phases of matter *e.g.* topological phases and PT-symmetric phases. The motivation behind this is two-fold. First, Krylov complexity is computed using a super-operator Liouvillian whose spectrum consists of differences of energies of eigenstates of the Hamiltonian, and consequently captures the dynamical phase transitions. Secondly, Krylov complexity has been shown to have a geometric interpretation [35], and since phase transitions like topological phase transitions involve a change in geometry, Krylov complexity manages to capture these transitions. We test our hypothesis for two cases: the Kitaev chain [36], and the linearly-coupled Bateman oscillator [37]. In both cases, our results [1, 2] indicate a sharp and precise correlation between Krylov (spread) complexity and quantum phase transitions. We demonstrate that not only can Krylov complexity detect quantum phase transitions, it is quite robust in its sensitivity the phase transitions as well as the dynamics of the system. We have not been alone in conjecturing that Krylov complexity be utilized to detect quantum phase transitions. There have been other works, concurrent with the execution of this thesis, that concur with our results - for different models. Of particular note are, applications to detecting dynamical phase transitions in the LMG model [38], to detecting de-confinement phase transitions in $SU(N)$ Yang Mills theory [39], and to MBL phase transitions [40]. One might wonder on the necessity of introducing another probe of phenomena which can be diagnosed via existing means. A rather impractical answer is, intellectual curiosity. More practically though, throughout the development of physics it has been observed that a new perspective to look at the same phenomena has often resulted in unexpected advances[1]. Krylov complexity is exactly this new perspective to look at quantum materials and their phases. Lastly, as well shall see, Krylov complexity is generically simple in its formulation as well as execution *vis a vis* other popular non-experimental probes like Tensor Network Methods, Renormalization Group Theory, Density Matrix Renormalization Group etc.

This thesis is structured simply, in Ch.2 we first give a broad-strokes overview of quantum chaos from its historical development to contemporary usage as well as probes that diagnose it; then in Ch.3 we take a deep dive into the theoretical framework that formalizes the construction of Krylov complexity, apply the same construction to develop Krylov complexity for operators as well as states, review a unifying mechanism for them both, provide one approach to extending these definitions to continuous theories, identify some com-

[1] An example of this is the SYK Model: it is widely believed to be - not just chaotic, but maximally so. As we shall see later, the defining characteristic of quantum chaos is the BGS conjecture which cannot be applied to the SYK model as it lacks a classical counterpart. How, then, does one classify the model as chaotic? This is through the study of complexity (among other probes of chaos), whose profile allows one to make statements about scrambling dynamics of a system - independent of the BGS. In a sense, this is how machine learning works: learn from a control data-set and make predictions for the other data.

putational approaches that simplify the calculation of Krylov complexity, and finally discuss a more detailed motivation that indicates the reasons one may expect Krylov complexity to be able to probe quantum phase transitions *a priori*; then in Chs. 4 and 5, we test our hypothesis and demonstrate that there indeed exists correlations in the form of characteristic signatures in Krylov complexity coinciding with the critical points of quantum phase transitions; and, a final Ch.6 compiles all the discussion into one short narrative, and provides some promising avenues to extend this thesis into innovative research directions.

2 Complexity through the Ages: The Chaos Origins

"Chaos is found in greatest abundance wherever order is being sought. It always defeats order, because it is better organized."

- Terry Pratchett

This chapter is devoted to introducing the background of quantum complexity via its historical development and to describe its status in contemporary theoretical physics. Complexity has been an usual suspect in the field of computer science but the interest of physicists in complexity is rather recent. The study of quantum complexity in theoretical physics has seen a strong revival in the past decade. It was reintroduced to the community by Susskind [19, 20] in the context of black hole physics and quantum information transport/scrambling. Susskind's works proposed that the difficulty of sending information through an Einstein-Rosen bridge, aka wormhole, is related to the computational complexity of the operators used to generate the relevant signal. In particular, the operators with low complexity cannot sustain information transport through the wormhole, while those with high complexity can. It served to elucidate that even though firewalls (a la AMPS [41]) may technically exist for black holes, they are quite unlikely to do so due to the extraordinarily high complexity associated to their existence. Inspired from gaining such deep insights into a strongly interacting system in a complicated setup, physicists began formalizing the notion of quantum complexity. Since then, there has been a flurry of activity surrounding the study of quantum complexity in various quantum systems and, primarily, it has assimilated as part of the standard toolkit to study information transport or scrambling in quantum mechanical systems and is widely employed as a probe of quantum chaos.

2.1 Quantum Chaos: The Founding Years

We shall now turn our attention to the field of quantum chaos as the development of complexity, in general, and Krylov complexity, in particular, has followed the advances in exploring the chaotic properties of quantum mechanical systems. Classically, chaotic phenomena are well known, and, by-and-large, are characterized as an exponential sensitivity to changes in initial conditions *i.e.* classically chaotic systems demonstrate very different phase-space trajectories upon a slight deviation in the initial conditions. The (highest) factor in the exponential is often understood to demonstrate the presence or absence of chaos and is termed as *Lyapunov exponent*, λ_L. Some well-known examples of classically chaotic systems include the three-body problem [42], the double pendulum [43], the Lorenz attractor [44], and billiards under various boundary conditions [45, 46]. The most accessible and intuitive understanding of classical chaos in these models, and others, is through the trajectory definition provided above. However, to extend this definition to quantum mechanical models is not very straightforward due to the Heisenberg uncertainty principle leading to an absence of phase-space trajectories in quantum mechanics.

The first hurdle to studying quantum chaos is to come up with a correct rigorous definition. This hasn't been without some debate. In particular, [47] argued that the term "quantum chaos" is a misnomer as there is no exponential sensitivity to initial conditions - but rather, there exist novel quantum phenomena which indicate the existence of chaos in the corresponding classical theory, which [47] dubbed as *quantum chaology*. For the duration of this work, as is prevalent in literature, the usage of the phrase "quantum chaos" refers precisely to this notion - though the author of [47] may not concur with the terminology. More explicitly, after precisely defining probes of quantum chaos, one aspect is the study of transport properties of quantum systems whose classical counterparts are chaotic and understand the generic behavior of those probes; while the other aspect, is to employ those probes in purely quantum mechanical systems like the Sachdev-Ye-Kitaev model and learn about these quantum-only systems by the generic behavior of the probes. In a sense, this is a theorist's version of a controlled experiment with the former serving as the control.

Even though phase-space trajectories may be the simplest understanding of chaos in classical systems, they cannot be extended to quantum systems. In view of this, we turn to other probes of classical chaos - the most robust among which is the energy level statistics, which can indeed be extended to quantum systems. This diagnostic of chaos was initially introduced in physics literature as a result of the discovery of Random Matrix Theory behavior in spectra correlations of heavy nuclei in a series of seminal works by Wigner [48–50] and Dyson [51–54]. The next seminal works [55,56] by Bohigas-Gianonni-Schmidt firmly established the study of quantum chaos as an important field in its own right. Their conjecture, colloquially known as the *BGS conjecture*, posits that the quantum mechanical systems whose classical counterpart exhibit chaotic signatures have certain properties that are described by Random Matrix Theory (RMT). More specifically, the energy level statistics or spectral correlations of a quantum chaotic system are governed by random matrix theory and the spectral level repel each other *i.e.* the spectral correlations follow the same distribution as ensembles of large random matrices, whose elements are randomly draw from *e.g.* various ensembles of random Hermitian matrices like the Gaussian Unitary Ensemble (GUE), Gaussian Orthogonal Ensemble (GOE), and Gaussian Symplectic Ensemble (GSA) - corresponding to the system's symmetry. The symmetry in the case of the latter two (GOE and GSE) is time reversal symmetry with a difference in spins demarcating them: GOE describes integral spins and GSE describes half-integral spins; while, GUE is more generic in the sense that it describes, according to the BGS conjecture, (chaotic) systems that break time-reversal symmetry. More formally, this classification is also referred as the Dyson's *Threefold Way* [54][1].

Furthermore, the work by BGS brought evidence that universality in RMT-like spectral correlations for chaotic systems is not exclusively a feature of systems with a large number of degrees of freedom, as was widely believed (primarily owing to Wigner and Dyson) prior to their work. To this date, the BGS proposal remains a conjecture with no formal proof - however, there is a convenient convergence of ever increasing instances of coincides where the proposal stands faithful, and currently is widely believed to hold true. We note that the quantum chaotic computations are actually performed in the $\hbar \to 0$ limit and are termed semi-classical to distinguish them from the non-determinism of purely classical phenomena like fluid turbulence

[1] In 1995, Altland and Zirnbauer extended this classification to ten symmetry classes, sometimes also called as the *Tenfold Way*, by incorporating particle-hole symmetry into the Threefold Way which only considers time-reversal symmetry [57].

or the irregular orbits of certain planetary satellites, and at the same time harkening back to the classical understanding of chaos captured via spectral statistics.

A critique of the historical development of quantum chaos would be remiss to not mention instances where its working definition, the BGS conjecture, does not work so well or outright fails. A classical example is the kicked rotor. The classical kicked rotor describes a freely rotating stick with some moment of inertia which is subjected to periodic kicks. For sufficiently strong kicks, the classical kicked rotor exhibits chaotic signatures [58, 59] - however, the quantum version of the same exhibits suppression of classical diffusion due to *Anderson localization*[1]. This is in sharp contrast to the behavior one may expect following the BGS conjecture and is a purely quantum effect arising from interference. Just as Anderson localization imparts subtlety to the applicability and interpretation of BGS conjecture in non-interacting systems, its generalization to interacting systems via Many-Body Localization [61] also follows the same behavior behavior; and while in the former phenomenon the localization is a consequence of disorder, it is both disorder and interaction for the latter. Another aspect of quantum chaos that needs a careful look through the lens of BGS conjecture is the phenomenon of quantum scars. Certain quantum mechanical systems [62, 63][2], with chaotic classical counterparts, host specific states called *scar states*, or simply scars. Scars represent condensation of quantum probabilities along certain classical periodic trajectories and as they are the imprints of classical behavior in a quantum system they are called as scars or "memory" of the classical theory on the quantum one[3]. It has been shown that certain measures of quantum chaos (including, Krylov complexity) may fail to capture chaotic signatures if these measures are applied to scar states [64]. This is less of a failure of the measure than a direct consequence of the definition *i.e.* the spectral statistics themselves do not follow Wigner-Dyson (or RMT-like) statistics and are rather Poissonian, signaling integrable dynamics [65, 66] in the presence of scars. Hence, this represents a direct challenge to the BGS conjecture. Finally, the transition from quantum to classical in the $\hbar \to 0$ limit may not be very smooth - leading to very different signatures in quantum systems compared to their classical counterparts and hence, the BGS conjecture may not be directly applicable.

2.2 Quantum Chaos: Paradigm Shift to Contemporary Developments

While initial few decades of the work on quantum chaos focused on rigorously establishing a working definition of quantum chaos, the late 1990s saw a natural paradigm shift to exploring the nature of quantum chaos in various quantum mechanical setups. Among the most prominent work that characterized this paradigm shift was the seminal work by Srednicki [67] on Eigenstate Thermalization Hypothesis.

The Eigenstate Thermalization Hypothesis (ETH) is a fundamental statement on how isolated quantum systems, *i.e.* quantum systems without the presence of a bath, approach thermal equilibrium. ETH postulates that for a generic (large) class of quantum systems the expectation values of observables in individual

[1] Initially, this suppression was observed in numerical simulations and dubbed "dynamical localization" but it was later realized that this is nothing but the Anderson localization [60].

[2] There is a blog-post by Terrence Tao on the presence of scars in quantum billiards!

[3] An alert reader might find this terminology quite ironic considering that, fundamentally, every classical observation is a coarse-graining of some quantum phenomena.

energy eigenstates are consistent with the predictions of statistical mechanics. Importantly, ETH posits that individual energy eigenstates behave as if the system has reached thermalization[1] - without requiring any averaging over states, which is usually the case in statistical mechanics. The hypothesis has proved useful to elucidate connections between quantum mechanics and thermodynamics - specially in the framework of out-of-equilibrium dynamics such as quantum chaos or quenching. The ETH serves as a correspondence principle between thermalization for the classical systems and that for the quantum systems. For classical systems, thermalization traditionally assumes the guise of phase space ergodicity while such a notion cannot be extended to quantum systems due to the Heisenberg uncertainty principle rendering traditional phase space obsolete. The key input to propose ETH is the insight that for quantum chaotic systems each energy eigenstate may infact exhibit properties of thermal equilibrium. This insight, while initially a conjecture, was more-or-less proved a couple of decades later in [70] where the titular question, "Does a single eigenstate encode the full Hamiltonian?", was answered in affirmative. Furthermore, ETH provided a bridge between the observation that isolated quantum systems appeared to thermalize while they would be expected to preserve information due to isolation. ETH can be formulated as an ansatz on the matrix elements of the energy eigenstates of a Hamiltonian,

$$\boxed{\langle E_m \mid \mathcal{O} \mid E_n \rangle \equiv \mathcal{O}_{mn} = \mathcal{O}(\overline{E})\, \delta_{mn} + e^{-\frac{S(\overline{E})}{2}} f_{\mathcal{O}}(\overline{E}, \omega)\, R_{mn},} \tag{2.1}$$

where, $\mathcal{O}_{mn}$ is the matrix element of operator $\mathcal{O}$ in eigenstate of Hamiltonian, $\overline{E} = \left(E_m + E_n\right)/2, \omega = E_m - E_n$, and $S(E)$ is the thermodynamic entropy at energy E. Importantly, $\mathcal{O}(\overline{E})$ and $f_{\mathcal{O}(\overline{E},\omega)}$ are smooth functions of their respective arguments such that $\mathcal{O}(\overline{E})$ is the expectation value of the microcanonical ensemble at energy $\overline{E}$ and R_{mn} is a random variable with vanishing mean and unit variance. Clearly, there is an exponential suppression of off-diagonal terms with increasing entropy such that these terms vanish in the thermodynamic limit - this implies that in the thermodynamic limit the dynamics are governed by diagonal terms *i.e.* expectation values of $\mathcal{O}$ in the individual eigenstates. As a result observables obeying (2.1) are expected to relax to thermal values (the diagonal elements) within a time-scale much shorter than the ones required for decoherence of the energy eigenstates (proportional to inverse energy level spacings). However, there is no agreed classification of which generic operators satisfy (2.1) but it is understood to hold true for physical observables to which statistical mechanics applies as discussed in [71]. [70] argues that ETH can apply to observables with support on at-most half of the system's size. ETH conjecture has been a particular landmark in describing quantum chaotic systems as it describes why isolated quantum systems exhibit thermalization even though they are described by unitary dynamics through the linear Schrödinger equation. However, there are a few known shortcomings of ETH hypothesis. As our final remarks on ETH, we note its shortcomings:

- ETH is expected to fail to describes states at the edge of the spectrum as these states are generally non-chaotic. This is because the behavior of edge states often deviates away from the bulk states, and RMT is not applicable to them - thereby, rendering ETH non-applicable to edge states in these cases. Even for bulk states, the ETH may break down due to glassy or sub-diffusive dynamics;

[1] Thermalization here is defined *a la* von Neumann *i.e.* an operator is said to thermalize if the long-time average of its expectation value should be close to the microcanonical prediction. In other words, during the dynamical evolution of the system, if the operator's expectation value remains close to the microcanonical expectation value at most last times then the observable has thermalized. This is known as the *quantum ergodic theorem* or "normal typicality", and was proved by von Neumann [68, 69].

- ETH doesn't completely capture the behavior of systems quenched from a non-integrable point to an integrable point. In such cases, even if the initial state is thermal, the system doesn't necessarily thermalize according to the usual thermodynamic ensembles. This brings forth the importance of the role of the sparsity of the energy density after the quench in preventing thermalization in integrable systems;
- ETH is quite generic in its applicable, and as such it does not explain the dynamics to thermalization in specific systems and, in particular, it doesn't provide an explanation for the relaxation timescales involved *i.e.* while it provides an explanation for observations thermalizing - it doesn't account for specifics of the problems under consideration: the observable being studied, the Hamiltonian capturing the system, initial state of the system etc.

In short, ETH extends the RMT postulate to describe quantum systems which one may naively expect to follow unitary dynamics but for experimental and numerical observations which are indicative of thermalization for most generic systems. For an excellent authoritative account of ETH, including more details on its relations and compatibility with RMT, see [72].

The final note-worthy contribution that we briefly touch upon is in the context of Hamiltonian-evolution of generic operators in chaotic quantum many-body systems. This contribution takes the shape of, at-this-point quite unsurprisingly, another hypothesis known as Operator Growth Hypothesis (OGH) [26][1]. The operator growth hypothesis posits a generic growth pattern for most operators of a chaotic quantum system via the Lanczos coefficients (see Ch.3), which capture the entirety of the dynamical information of a system. Colloquially, the hypothesis is formulated as the condition that the (off-diagonal) Lanczos coefficients, b_n, should grow as quickly as possible. This maximum growth is linear for higher than one dimensions with logarithmic corrective contributions in one dimension. More formally, the statement of the hypothesis reads, if a Hamiltonian H governs the unitary time-evolution of an infinite non-integrable quantum many-body system in greater than one dimension then for a local operator O, with no involution with any of the sub-extensive conserved quantities, in the thermodynamic limit the Lanczos coefficients are,

$$\boxed{b_n = \alpha\, n + \gamma + \mathcal{O}(1),} \tag{2.2}$$

with $\alpha > 0, \gamma$ being real constants. The constant α characterizes universality classes of quantum many-body systems *i.e.* it captures the growth of generic operators under Hamiltonian dynamics [27] and displays characteristic behavior for different classes of systems. This behavior for different classes of dynamics shall be complied as a table in the next section.

2.3 Hailing Quantum Chaos

Having gone through the development of quantum chaos as a field in its formative years, having understood the principles that govern the modern studies, as well as classification of quantum many-body systems as

[1] The same work [26] that formulated this hypothesis also introduced another notion capturing the quantum chaotic dynamics in many-body systems, Krylov complexity - the central tool and object of interest for this thesis.

chaotic or non-chaotic, we shall now compile a brief overview of the standard probes with demonstrated capabilities to capture chaotic behavior - the final entry in which shall be our object of interest, Krylov complexity. For a more detailed discussion on each of the probe see the recent review [73] and a somewhat dated reference [74], covers the earlier probes of quantum chaos very well.

1. *Random Matrix Theory*: First and foremost, the earliest diagnostic of quantum chaos was through the RMT-like behavior in spectral correlations. As mentioned before, for a quantum mechanical system with energy levels following a Wigner-Dyson distribution pattern the dynamics is classified, by definition via BGS conjecture, as chaotic; while, Poissonian distribution pattern signals integrable dynamics. The former, is characterized by phenomenon like "level repulsion" or "avoided level-crossing" wherein nearby energy levels repel each other under perturbation. For quantum systems with chaotic classical counterparts, his is understood as a manifestation of diverging phase-space trajectories of the coarse-grained classical system in the spectral correlations, again via the BGS conjecture. The joint probability distribution for the eigenvalues ($\{\lambda_i;\ i = 1, \cdots, N\}$) in the Threefold Way *i.e.* elements of the corresponding matrix drawn randomly from GUE/GOE/GSE, is given as,

$$p\left(\lambda_1, \lambda_2, \cdots, \lambda_N\right) = \frac{1}{Z_\beta} \prod_{k=1}^{N} e^{-\frac{\beta}{4}\lambda_k^2} \prod_{i<j} \left|\lambda_i - \lambda_j\right|^\beta, \tag{2.3}$$

with Z_β being a normalization constant and β, referred to as the Dyson index in physics literature, fixing the source probability distribution from which the matrix elements are drawn: $\beta = 1$ for GOE, $\beta = 2$ for GUE, and $\beta = 4$ for GSE. Clearly, there's a zero probability for eigenvalues coinciding indicating the level-repulsion or avoided-crossing characteristics for quantum chaotic dynamics.

2. *Spectral Form Factor*: Spectral Form Factor (SFF) is motivated through a desire to construct an observable that captures the RMT-like spectral correlations in physics [75]. SFF is defined as square of the Fourier transformation of the spectral density. For a Hermitian Hamiltonian represented through a N-dimensional square matrix, the SFF is given as,

$$\mathrm{SFF}(t) \equiv \frac{1}{N^2} \sum_{i,j=1}^{N} e^{it\left(\lambda_i - \lambda_j\right)} = \left|\frac{1}{N} \mathrm{Tr}\, e^{iHt}\right|^2, \tag{2.4}$$

where $t > 0$ is the Fourier transform variable identified as the physical time. The SFF is generally computed for ensembles of Hamiltonians and the trace in its definition is over some ensemble. It encodes both short as well as long range correlations in the spectrum and hence serves as a robust probe of quantum chaos. For chaotic systems, it shows a characteristic behavior termed as dip-ramp-plateau as demonstrated in Fig.(1). Importantly, SFF is not self-averaging and needs an average to be taken over some ensemble (or disorder) which implies that its numerical implementation requires a good amount of resources in most interesting cases, and may not be particularly reliable. For a review of the computation of SFF for different classes of random matrices, see [76]. Another similar probe, however somewhat non-mainstream, is *Loschmidt echo* [77] which quantifies the degree of irreversibility

via Hamiltonian evolution, and can be interpreted as the *fidelity* of a quantum state to remain unaffected under perturbation if the corresponding system is described through a Hermitian Hamiltonian. Sometimes even entanglement entropy is employed as a probe of quantum chaos [78].

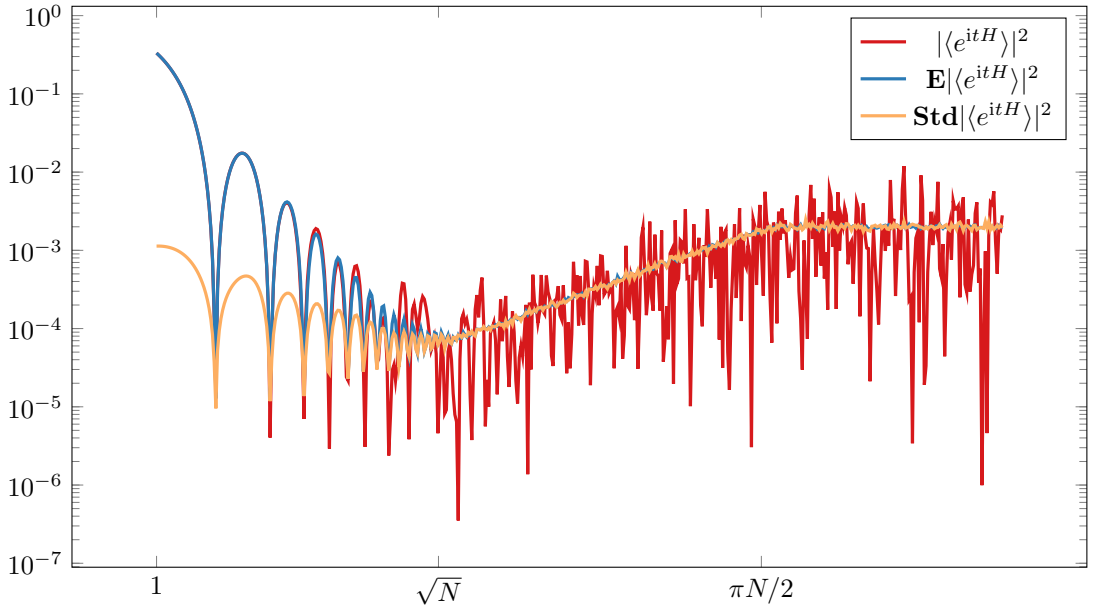

Figure 1: Characteristic *dip-ramp-plateau* behavior of SFF for quantum chaotic systems. This log-log plot displays the behavior of SFF of a random Hamiltonian that's assembled randomly from a GUE. The red line corresponds to the SFF of a single realization, the blue to its expectation value on the ensemble, and the red to its standard deviation on the ensemble. The latter two are obtained for a sample of width 500. The dip is a system specific indicator of loss of constructive interference, present at $t = 0$, in the various phases in the trace of the Fourier transform. The universal features include the ramp indicating quantum chaos, while the plateau regime indicates discreteness in the energy levels (and is generic for thermal or integrable systems both). Clearly, SFF is not self-averaging and the universal features become apparent after some kind of averaging - typically, this takes the form of a disorder average (*e.g.* in SYK model) or an ensemble average (*e.g.* random unitaries drawn from GUE ensemble, as in this case). This figure is taken from [76].

3. *Out-of-Time-Order Correlators:* Out-of-Time-Order Correlators (OTOCs) while first introduced in 1969 [79], have seen a sharp resurgence in interest in the past decade owing to a series of works by Shenker and Stanford [80–82] in the context of AdS/CFT correspondence or gauge-gravity duality and studying scrambling operator dynamics. Their work was supplemented by others [83–85] which helped establish OTOCs as a sharp tool to capture quantum chaotic dynamics and has since garnered significant attention [24, 86–92]. It is defined as the out of time order part of the following 4-pt correlator [88],

$$C(t) = -\left\langle [W(t), V(0)]^2 \right\rangle_\beta , \tag{2.5}$$

where $W(t)$ and $V(0)$ are operators at time t and 0 respectively, and $\langle\cdot\rangle_\beta$ represents a thermal inner product or average. This definition can be seen as an application of the correspondence principle to the diverging phase-space trajectories definition of classical chaos. Considering an OTOC defined out of the position and momentum operators in a quantum mechanical system, $C(t) = -\left\langle \left[x(t), p(0)\right]^2 \right\rangle$. Under the correspondence principle, in the semi-classical limit, we can replace the commutator with the Poisson bracket between the phase space variables: $\left[x(t), p(0)\right] \to \left\{x(t), p(0)\right\}_{\text{PB}}$ which is equal to the phase space separation measured as $\delta x(t)/\delta x(0)$, and if that separation grows exponentially, $e^{\lambda_L t}$, the system is said to exhibit chaos, so one can expect the corresponding behavior in quantum systems to be $e^{2\lambda_L^{\text{cl.}} t}$ - where, $\lambda_L^{\text{cl.}}$ is the classical Lyapunov exponent. In many cases, OTOC has been found to be a good probe of quantum chaos like for one dimension quantum systems including billiards [88] while for other systems it may furnish a false positive [93–96] due to *e.g.* presence of a saddle point in the potential. The current understanding identifies the presence of a positive quantum Lyapunov exponent, λ_L^{OTOC}, in OTOCs as indicative of scrambling dynamics (as opposed to chaotic ones) [97]. Notably, [85] proposed a bound, now know as the *MSS bound*, on the quantum Lyapunov exponent as $\lambda_L^{\text{OTOC}}(T) \leq 2\pi T$ for a quantum system at temperature T - this bound is expected to be saturated for systems which are maximal scramblers like the SYK Model [98]. Hence, OTOCs emerge as a necessary but not sufficient condition for the dynamics to be chaotic.

4. *Quantum Complexity:* Finally, we turn to the probe of quantum chaos that's of the most relevance to this work - quantum complexity, or rather a specific notion of it - *Krylov complexity*. In simple terms, complexity quantifies the cost of performing an action or implementing a task. This is quite a flexible definition and can be adapted to a wide array of problems. We take a deep dive in the Krylov complexity in the next chapter, and briefly recount the developments in complexity leading up to it. Historically, quantum complexity was reintroduced in physics by Susskind [19, 20] in the context of black hole physics and quantum information transport/scrambling. Susskind's works proposed that the difficultly of sending information through an Einstein-Rosen bridge, aka wormhole, is related to the computational complexity of the operators used to generate the relevant signal.
Susskind envisioned it as a quantity to peer into behind-the-horizon physics [99] in general, and behind the black hole horizon, in particular, so as to be able to made advances in making a complete theory of quantum gravity. Essentially, Susskind's complexity is an alternative metric on the Hilbert space to the usual inner-product but with some notable differences: the typical inner product metric has positive curvature while complexity is negatively curved exponentially inflating the distance between any two states (hence its utility in behind-the-horizon physics). Initially, the definition of complexity adapted in physics was in terms of preparing a quantum state starting from a reference state or in terms of constructing an operator at some later time starting from the operator at a reference time. Complexity, in this context, can be understood as quantifying the cost of implementing a quantum circuit between the target state/operator and the reference state/operator. The current working definition of quantum complexity is due to Nielsen who gave a geometric interpretation to it in [21, 22]. Let us suppose that we'd like to prepare a state $|\psi_T\rangle$ from another state $|\psi_R\rangle$, then we envision a circuit connecting these two states. This circuit is implemented through a unitary $\mathcal{U}$, so that the circuit is described as, $|\psi_T\rangle = \mathcal{U}|\psi_R\rangle$. Complexity then is the minimum number of unitary gates required to realize the operator $\mathcal{U}$. In Nielsen's geometric complexity, the unitary operator $\mathcal{U}$

can be built using a decomposition along a path integral on a group manifold as follows [100],

$$\mathcal{U} = \overleftarrow{\mathcal{T}} \exp\left[i \int_0^1 ds\, G^I(s) M_I \right], \tag{2.6}$$

where, $\overleftarrow{\mathcal{T}}$ denotes the order along the path integral, M_I represent the universal gates, and $G^I(s)$ counts the number of M_I utilized at circuit time s. Clearly, there is a cost to implementing each path - this is encoded as a cost function $F(s)$ and since the complexity represents the minimum cost of implementing $\mathcal{U}$, it is imparted an ambiguity in terms of the choice of this cost function $F(s)$. Two definitions of quantum complexity in this context are most utilized,

$$\mathcal{C}_1 = \min_{G^I(s)} \int_0^1 ds \sum_I \left| G^I(s) \right|, \tag{2.7}$$

$$\mathcal{C}_2 = \min_{G^I(s)} \int_0^1 ds \sqrt{\sum_I \left[G^I(s) \right]^2}. \tag{2.8}$$

This path-optimization to compute quantum complexity is not an easy problem as it depends on the group structure as well as the ambiguity in the form of choice of an appropriate cost function. Further important developments include certain conjectures such as: complexity equals action [101], complexity equals volume [102], and complexity equals anything [103, 104].

That concludes our brief mention of a number of probes of quantum chaos. The probe that's of most importance for us is, quantum complexity. Quantum complexity was given a new guise in the form of Krylov complexity in [26] - we dedicate the next chapter to an in-depth study of Krylov complexity.

3 Theoretical Framework: Krylov Complexity

"The essence of mathematics is not to make simple things complicated, but to make complicated things simple."

- Stan Gudder

As a precursor to introducing Krylov/spread complexity and different methods of computing it, we provide an introduction to the theoretical framework underpinning Krylov/spread complexity: the Krylov subspace methods, marking the etymological origins of the Krylov complexity. The theoretical framework part of this chapter is a brief restatement of various chapters in [27] and its inclusion is intended to assist in shaping this thesis in the form of a complete, largely independent, body of work - for a suitable audience. Once the essential framework is established, we shall describe the two types of complexities that have been defined in the literature depending on the Krylov framework; provide the essential elements of the arguments that form the theme of this thesis; and finally outline a few computationally efficient ways to obtain the complexity, with the details delegated to the next chapters which demonstrate the computation. The central problem under consideration is that of studying (time) evolution of operators as well as states in quantum many-body systems and as such the following discussion will be colored accordingly - however, this is not a requirement but a choice we make since it is of significant physical interest and relevance.

Theoretical physicists typically employ two varieties of tools with the aim of describing physical phenomena and solving toy models aimed at modeling the said phenomena. The first category belongs to the tools that, roughly generalizing, have wide applicability but may not generate exact solutions to a particular problem like computing dynamic correlation functions for a system of interest. The second category of tools are, on the other hand, quite complementary to the first one: they are designed to specifically tackle a particular problem, they generally furnish exactly solutions - however, one may be circumspect in expecting them to be applicable to other systems.

A good understanding of generic and sufficiently complex physical phenomena requires bringing both categories of toolkits to bear on the problem. However, exact solutions have generally proven quite elusive but are often permeable under certain assumptions like specific states of a many-body system or some unique interaction. Particularly illuminating examples include: in the case of former, studying Rényi entropy of the ground state of a wide category of models; and quadratic (harmonic oscillator) as well as quartic (ϕ^4 theory) interactions, in the case of the latter.

The *linear response theory* establishes a connection between dynamical properties of interest in condensed-matter experiments and the calculational techniques employed to study equilibrium dynamics of the systems under study in those experiments. One avatar of the linear response theory is the *recursion method* - which frames the theoretical essence for Krylov complexity and falls into the universal category of tools discussed

above, and, consequently, has a broad range of applicability. In principle, the recursion method is limited by extrinsic factors *i.e.* by the computational power available to the method or the acumen of the scientist employing them - as such, improvements in either lead to better results.

The main task, relevant to this thesis, is of calculation of dynamical correlation functions to compute some observable (Krylov complexity) establishing a link between experiments and theory. We do this via the recursion method, the essential principle behind which is that of the *orthogonal expansion* of a specific quantity. For our purposes, this quantity shall be the auto-correlation function or the return amplitude of the type: $\langle A(t) \cdot A(0) \rangle$ - naturally, the expansion quantity is the one which comprises the time evolution aspect. In the Schrödinger picture this takes the form of the wave function, $|\psi(t)\rangle$, while for the Heisenberg picture it is the dynamical operator $A(t)$. The generator of new vectors, in the orthogonal expansion, is the Hamiltonian for the former and the *Liouvillian* for the latter. There is another key component required to execute the recursion method: the choice of the equilibrium state for which the auto-correlation function is to be computed. In the Hamiltonian representation, it is typically chosen as the ground state $|\phi_0\rangle$ of the system which is incorporated as $|\psi(0)\rangle = A\,|\phi_0\rangle$ into the problem. While for the Liouvillian representation, the same goal is achieved through a stationary density operator and the choice of the state is fixed through an inner product with respect to which the orthogonal expansion of the operator A is generated. The Liouvillian representation also affords a quick correspondence between the classical and quantum counterparts of a problem by a simple replacement of the Liouvillian operator with its classical counterpart *i.e.* replacing a commutator with a Poisson bracket transforms the Heisenberg equation into the corresponding Hamilton's equation. We shall be working with the Liouvillian representation during the course of this thesis.

3.1 The Krylov Subspace

We begin our discourse by an introduction to the Krylov subspace underpinning the construction of Krylov operator complexity as an observable for discrete quantum many-body systems. More specifically, this construction is directly applicable to regular, *i.e.* non-pathological, quantum spin-chains. We shall then extend the notion of Krylov complexity for operators to a corresponding notion of Krylov (spread) complexity for states. Lastly, we shall also give a description of the procedure to generalize the discrete notion of Krylov complexity to a continuum version - albeit with an important caveat. This chapter largely follows [27, 39, 105–109].

As stated in the previous section, the recursion technique - of which Krylov subspace method is an element - requires two elements as input: firstly, the definition of the system; and secondly, the choice of the state for which the auto-correlation function is to be computed. We shall adopt the Liouvillian representation in which the Liouvillian takes up the role of the former, while a density operator and an inner product serve to fix the latter.

Let us consider a system comprising a Hilbert space $\mathscr{H}$, with dimension $\dim(\mathscr{H}) = D$. Let the set of linear

operators that may act on $\mathscr{H}$ be denoted as $L(\mathscr{H}) \equiv \widehat{H}$ with $\dim(\widehat{H}) = D^2$. Let us assume that the Hamiltonian describing this system is denoted as H, such that $H^\dagger = H$ *i.e.* this discussion is restricted to Hermitian systems[1]. Finally, let us denote the observable of interest as $\mathcal{O} \in \widehat{H}$, which is also Hermitian so $\mathcal{O}^\dagger = \mathcal{O}$. Our aim is to characterize the behavior of the dynamical operator $\mathcal{O}$ under time evolution, $\mathcal{O}(t)$. With this setup, the Krylov space is the minimal subspace of the operator space $L(\mathscr{H})$ that comprises of the time evolved operator $\mathcal{O}(t) \forall\, t$.

Working in the Heisenberg picture, the time evolution of the operator $\mathcal{O}$ is given as,

$$\mathcal{O}(t) = e^{iHt}\mathcal{O}e^{-iHt} = \mathcal{O} + it\boldsymbol{[H,\mathcal{O}]} + \frac{(it)^2}{2!}\boldsymbol{[H,[H,\mathcal{O}]]} + \frac{(it)^3}{3!}\boldsymbol{[H,[H,[H,\mathcal{O}]]]} + \cdots = e^{i\mathscr{L}t}\mathcal{O}, \tag{3.1}$$

where $\mathcal{O} \equiv \mathcal{O}(0)$ is the short-hand notation for the operator at initial time $t = 0$. The bold terms in the above equation hint at a structure of nested commutators if one defines a *super-operator*, termed Liouvillian in literature, $\mathscr{L} \equiv [H, \cdot]$. In terms of the Liouvillian, the time evolution of the Hermitian operator $\mathcal{O}$ is given as, $\mathcal{O}(t) = e^{i\mathscr{L}t}\mathcal{O}$. That is, the time evolution of $\mathcal{O}$ is contained in the subspace generated on $L(\mathscr{H})$ by the exponentiating application of the Liouvillian on the initial operator $\mathcal{O}$ and higher-and-higher powers of $\mathscr{L}$ are associated with more-and-more nested commutators with the Hamiltonian H. Note that the above expression of $\mathcal{O}(t)$ is generically defined as the exponential map is entire on the whole complex-t plane. This is a useful representation of the time evolution of a generic Hermitian operator as it neatly organizes and orders the time evolution in terms of high powers of $\mathscr{L}$ or, equivalently, more nested commutators with H. In a sense, there is a rough (but not precise) equivalence between time evolution of $\mathcal{O}$ and powers of $\mathscr{L}$ - because, at initial times only the first few terms will contribute to the time evolution with all the others vanishing and with the evolution, more terms contribute significantly. How precisely do the terms grow and contribute determines the nature of the time evolution of $\mathcal{O}$ and assists in distinguishing generic chaotic dynamics from integrable ones.

The Krylov subspace associated with operator $\mathcal{O}$ is defined as the space spanned by the powers of Liouvillian acting on $\mathcal{O}$,

$$\mathscr{K}_\mathcal{O} \equiv \text{span}\,\{\mathscr{L}^n\mathcal{O}\}_{n=0}^{\infty} = \text{span}\{\underbrace{\mathcal{O}}_{\equiv\mathscr{L}^0\mathcal{O}}, \underbrace{[H,\mathcal{O}]}_{\equiv\mathscr{L}\mathcal{O}}, \underbrace{[H,[H,\mathcal{O}]]}_{\equiv\mathscr{L}^2\mathcal{O}}, \cdots\}. \tag{3.2}$$

The dimension of the Krylov subspace is denoted as $\dim(\mathscr{K}_\mathcal{O}) = K$ and it can be computed as the cardinality of the maximal set of linearly independent elements of the general form $\mathscr{L}^n\mathcal{O}$. More explicitly, let us work in the energy eigenbasis $|\omega_{ab}) \equiv |E_a\rangle\langle E_b|$ on $\widehat{H}$. The operator under study can be expanded in this basis as, $\mathcal{O} = \sum_{a,b}\mathcal{O}_{a,b}|E_a\rangle\langle E_b|$. Each application of the Liouvillian can now be computed as,

$$\mathscr{L}^n\mathcal{O} = \delta_{n0}\sum_{a=1}^{D}\mathcal{O}_{aa}\,|\omega_{aa}) + \sum_{\substack{a,b=1\\a\neq b}}^{D}\mathcal{O}_{ab}\,\omega_{ab}^n\,|\omega_{ab})\,, \tag{3.3}$$

[1] for a corresponding discussion on non-Hermitian systems see [110–112].

with the definition of phases given as $\omega_{ab} = E_a - E_b$. Of course, this means that $\omega_{aa} = E_a - E_a = 0, \forall\ a = 1, \dots, D$. The phases ω_{ab} constituting the eigenvalues of the operator $\mathscr{L}$ on the $\{|\omega_{ab}) ;\ a, b = 1, \cdots, D\}$ basis with coefficients $\{\mathcal{O}_{ab};\ a, b = 1, \cdots, D\}$ can all be neatly arranged in the form of a square Vandermonde matrix,

$$\begin{bmatrix} \mathcal{O} \\ \mathscr{L}\mathcal{O} \\ \mathscr{L}^2\mathcal{O} \\ . \\ . \\ . \end{bmatrix} = \underbrace{\begin{bmatrix} \mathcal{O}_{11} & \mathcal{O}_{12} & . & . & . & \mathcal{O}_{DD} \\ \omega_{11}\mathcal{O}_{11} & \omega_{12}\mathcal{O}_{12} & . & . & . & \omega_{DD}\mathcal{O}_{DD} \\ \omega_{11}^2\mathcal{O}_{11} & \omega_{12}^2\mathcal{O}_{12} & . & . & . & \omega_{DD}^2\mathcal{O}_{DD} \\ . & . & . & . & . & . \\ . & . & . & . & . & . \\ . & . & . & . & . & . \end{bmatrix}}_{D^2 \text{ columns}}$$

$$= \left[\begin{array}{ccc|ccc} 1 & \cdots & 1 & 1 & \cdots & 1 \\ 0 & \cdots & 0 & \omega_{12} & \cdots & \omega_{D-1\,D} \\ 0 & \cdots & 0 & \omega_{12}^2 & \cdots & \omega_{D-1\,D}^2 \\ \vdots & \vdots & \vdots & \vdots & \vdots & \vdots \\ \vdots & \vdots & \vdots & \vdots & \vdots & \vdots \\ \vdots & \vdots & \vdots & \vdots & \vdots & \vdots \end{array}\right] \times \begin{bmatrix} \mathcal{O}_{11} & & & & & \\ & \ddots & & & & \\ & & \mathcal{O}_{DD} & & & \\ & & & \mathcal{O}_{12} & & \\ & & & & \ddots & \\ & & & & & \mathcal{O}_{D-1\,D} \end{bmatrix}. \tag{3.4}$$

Let us unpack this matrix to understand the cardinality of the Krylov subspace, which will reveal whether it is useful to compute the Krylov subspace to study the time evolution of an operator: if K, the Krylov subspace, dimension is roughly the same as D^2, the dimension of the Hilbert space then there isn't much utility to computing the Krylov subspace as we've just exchanged a difficult problem with another difficult problem. The Krylov dimension shall shed light on the integrable or chaotic dynamics of the system - while the structure of the Liouvillian shall lead to a significant reduction in the complexity of the problem. The Vandermonde matrix (3.4) has exactly D^2 columns, corresponding to the dimensionality of the Hilbert space. The cardinality of the Krylov subspace is dictated by the rank of the Vandermonde matrix, which is computed by considering its determinant,

$$\Delta(\omega_{ab}) \prod_{i,j=1}^{D} \mathcal{O}_{ij}, \tag{3.5}$$

with $\Delta(\omega_{ab})$ being the Vandermonde determinant of the ω_{ab} in the matrix. Clearly, the determinant vanishes if any of the phase ω_{ab} is zero, or if any of the matrix elements $\mathcal{O}_{ab}$ is vanishing - both leading to a reduction in the dimension of the Krylov subspace due to the removal of the corresponding column from (3.4) to count the maximal rank of the Vandermonde matrix. Hence, we can conclude that the Krylov subspace dimension K will be equal to the number of distinct phases (with non-vanishing matrix elements in (3.4)). Of course, the trivially zero phase $\omega_{aa} = 0$ has D degeneracy as the indices of the phases take D values - this provides an upper bound to the Krylov dimension as: $D^2 - D + 1$, since there are total D^2 columns and D of them correspond to a single independent column. The lower bound is naturally 1, which corresponds to the case of no time-evolution of the operator $\mathcal{O}$. So, the Krylov subspace dimension has a range,

$$\boxed{1 \leq K \leq D^2 - D + 1.} \tag{3.6}$$

The Krylov subspace vectors can be further redefined by encorporating the matrix elements of $\mathcal{O}$, the operator under study, into them:

$$|\mathcal{K}_\omega) \equiv \sum_{(a,b)\in\mathbb{I}} \mathcal{O}_{ab}\,|\omega_{ab})\,, \tag{3.7}$$

this indicates that the basis elements are characterized by the phases ω_{ab}, which are also the eigenvalues of the $\mathscr{L}$ in the Krylov subspace. Thus, the Krylov subspace associated with the operator $\mathcal{O}$ is now represented as,

$$\boxed{\mathcal{K}_\mathcal{O} = \text{span}\left\{|\mathcal{K}_\omega)\,, \omega \in \sigma(\mathscr{L})\right\},} \tag{3.8}$$

with $\sigma(\mathscr{L})$ being the spectrum of $\mathscr{L}$. The Krylov subspace dimension, K, is now equal to the number of non-vanishing $|\mathcal{K}_\omega)$. If the system under study has no degeneracies or symmetries then K will be maximally equal to $K = D^2 - D + 1$. Consequently, for integrable systems (with an extensive number of conserved quantities) we should expect a significant subtraction from the cardinality of the Krylov subspace leading to a reduction in the complexity to solve the problem, while for chaotic systems the cardinality is near or at the upper bound.

3.2 Lanczos Algorithm to Krylov Basis

It is apparent that the Krylov subspace $\left\{|\mathcal{K}_\omega)\right\}$ is not orthonormal, and hence does not constitute a basis. Orthonormal bases are easier to work with and make many physical properties explicitly manifest in their formulation so we'd like to orthonormalize the Krylov basis. A straightforward approach to this would be to consider the *Lanczos* algorithm [113], which is an adaptation of the Gram-Schmidt orthogonalization procedure to the case of operators. We begin with the knowledge of the system as specified via its Hamiltonian, and a generic non-pathological Hermitian dynamical operator $\mathcal{O}(t)$. As mentioned previously, an additional input in the form of the choice of inner product is required to be able to define the Krylov subspace associated with $\mathcal{O}$. Typical choices of the inner product involve, the Frobenius product and the Wightman inner product. We shall use the Frobenius product for this discussion: $(\mathscr{A}|\mathscr{B}) = \frac{1}{D}\text{Tr}\left[\mathscr{A}^\dagger, \mathscr{B}\right]$, such that $||\mathscr{A}|| = \sqrt{\frac{1}{D}\text{Tr}\left[\mathscr{A}^\dagger, \mathscr{A}\right]}$. We chalk out the corresponding Lanczos algorithm below:

(a) choose $b_0 = 0$ and $|\mathcal{O}_{-1}) = 0$;

(b) $\mathcal{O}_0 = \frac{\mathcal{O}}{||\mathcal{O}||}$;

(c) for $n \geq 1$, $|\mathscr{A}_n\big) = \mathscr{L}\,|\mathcal{O}_{n-1}\big) - b_{n-1}\,|\mathcal{O}_{n-2}\big)$;

(d) choose $b_n = \sqrt{\big(\mathscr{A}_n|\mathscr{A}_n\big)}$;

(e) if $b_n = 0$ abort; otherwise set $|\mathcal{O}_n\big) = \frac{1}{b_n}\,|\mathscr{A}_n\big)$.

This implementation of the Lanczos algorithm will generate two objects: first an orthonormal set $\left\{\mathcal{O}_n\right\}_{n=0}^{K-1}$; and second, the set of Lanczos coefficients $\left\{b_n\right\}$. Every Lanczos step serves to produce an element in the algorithm that is orthogonal to all the previous $|\mathcal{O}_m\big)$ for $m < n$. This basis has "rank" K and hence for $n < K$

we can state with certainty that $|\mathscr{A}_n) \neq 0$. As $\{\mathcal{O}_n\}_{n=0}^{K-1}$ is orthonormal, the algorithm shall generate a $|\mathscr{A}_K)$ which will be orthogonal to each of the elements of a complete basis and hence $|\mathscr{A}_K)$ will vanish, and likewise will b_K. So the terminating condition for the Lanczos algorithm is the vanishing of all directions, and is reflected as such in the last step of the algorithm. It is worthwhile to note that the complete dynamical information of the system, in respect of the operator under consideration, is contained within the Lanczos coefficients. Furthermore, it is clear that the Krylov basis is *ordered* according to the number of the nested commutators in each term *i.e.* basis elements with a higher label correspond to more nested commutators with Hamiltonian, and hence the average position on the Krylov basis is an indicator of the time-evolved operator.

The most crucial part, however, is the following. The Liouvillian, in the Krylov basis, assumes a tridiagonal form. This is particularly nice as it leads to a significant reduction in the complexity of the task to obtain the time evolved operator and, in fact, it is this tridiagonal property of the Liouvillian that renders the transformation from the familiar Hamiltonian representation to the Liouvillian representation non-trivial.

$$\left(\mathcal{O}_m|\mathscr{L}|\mathcal{O}_n\right) = \begin{pmatrix} 0 & b_1 & 0 & 0 & \cdots & 0 \\ b_1 & 0 & b_2 & 0 & \cdots & 0 \\ 0 & b_2 & 0 & b_3 & \cdots & 0 \\ \vdots & \ddots & \ddots & \ddots & \vdots & \\ \vdots & & & \ddots & 0 & b_{K-1} \\ 0 & 0 & 0 & \cdots & b_{K-1} & 0 \end{pmatrix}. \tag{3.9}$$

As a result of its construction the eigenvalues of the above matrix are non-degenerate. Unfortunately, the algorithm, as discussed here, is prone to numerical instabilities and the numerics may derail quickly. The accumulation of errors leads to the basis elements not really being orthonormal to each other. Fortunately, there are known formal techniques like Full Orthogonalization and Partial Re-Orthogonalization [31–34] designed to assist the numerics overcome the numerical instabilities besides more informal tricks as described in App.(E). A final remark would be towards the diagonal elements, they identically vanish for all operator Krylov complexities, however, for state complexities they constitute another independent set of Lanczos coefficients denoted as $\{a_n; n = 0, \ldots, K\}$ the origin of which is explained in more detail in the Ch.3.3. Briefly, we can see that the diagonal elements for the operator complexity vanish as the corresponding phases would be of the form ω_{aa} and as a result of vanish. We shall briefly return to this in the next section.

3.3 Krylov Complexity for Operators

The Lanczos process results in two outputs: the Krylov basis and the Lanczos coefficients. The problem under study is that of the time-evolution of a generic Hermitian dynamical operator. The time evolved operator can be expanded in the Krylov basis as follows,

$$\boxed{|\mathcal{O}(t)) = \sum_{n=0}^{K-1} i^n \, \phi_n(t) \, |\mathcal{O}_n)\,,} \tag{3.10}$$

where i^n serves to make each term explicitly Hermitian, while $\phi_n(t)$ are the coefficients containing the dynamical information of the operator, and hence are also known as the *complexity wavefunctions*[1]. Employing the Heisenberg time-evolution equation: $\frac{d}{dt}\mathcal{O}(t) = -i\,[H, \mathcal{O}(t)]$ we find a differential recurrence relation for the complexity wavefunctions,

$$\boxed{\dot{\phi}_n(t) = b_n\phi_{n-1}(t) - b_{n+1}\phi_{n+1}(t),} \tag{3.11}$$

as expected owing to the tridiagonal structure of the Liouvillian in the Krylov basis. Interestingly, we note that recurrence relation hints at a nearest-neighbor hopping behavior in the complexity wavefunction space - the Lanczos coefficients are interpreted as the hopping amplitudes for the initial operator $\mathcal{O}(t)$ exploring the Krylov basis chain such that the complexity wavefunctions are the wavepackets hitch-hiking along. With the boundary condition $\phi_n(0) = \delta_{n0}$ this gives the time evolution of the dynamical operator - this condition is merely stating that all the support initially is at the initial operator $\mathcal{O}(0)$. Naturally, we expect that $\sum_{n=0}^{K-1} \left|\phi_n(t)\right|^2 = 1 \forall t$, *i.e.* the sum of the probabilities - which correspond to observables - of the complexity wavefunctions are preserved under time-evolution of the initial operator and remain fixed to 1.

We are now in an ideal position to finally define the Krylov complexity for operators as the average position of the dynamical operator under consideration on the Krylov basis chain. As is typical in quantum mechanics we define the average position of a wavefunction as,

$$\boxed{C_K(t) = K_c(t) = \sum_{n=0}^{K-1} n\left|\phi_n(t)\right|^2.} \tag{3.12}$$

So, in essence, the task of computing the Krylov complexity for a generic Hermitian operator in a system with unitary Hamiltonian boils down to solving for the complexity wavefunctions or, equivalently, the Lanczos coefficients in (3.11) and, then, the time evolution of the operator, at a specific time, is understood via the Krylov complexity as the average position on the Krylov chain at that time. As noted previously, this is a sensible definition due to the Krylov basis being naturally ordered in respect of the nested commutators via construction - if one keeps in mind that the more nested commutators correspond to more *complex* state of the system / more evolved state of the system. In a sense, the Krylov complexity is a probe of the time-dependent profiles of the complexity wavefunctions. Naturally, one cannot expect the average position on a chain to be greater than the length of the chain. So the Krylov complexity is bounded by the Krylov subspace dimension with a saturation time, for generic chaotic systems, proportional to an exponential in its entropy, e^{2S}. Finally, we tabulate expected behavior of Krylov complexity, according to OGH, for different classes of dynamical systems depending on the behavior of the Lanczos coefficients, b_n in Table 1.

3.4 Krylov Complexity for States

[1] The $\phi_n(t)$*s*, and by extension the Krylov complexity, are a way to re-express part of the information available in the Lanczos coefficients and, in particular, Krylov complexity is a more physically accessible and intuitive shape of the Lanczos coefficients.

Dynamics	Chaotic (d > 1)	Chaotic (d = 1)	Integrable	Unknown	Unknown	Bounded
b_n	αn	$\alpha n / \log n$	αn^{δ}	$\alpha n^{\delta} (\log n)^{\pm}$	$\alpha \log n$	b
$K_c(t)$	$e^{2\alpha t}$	$e^{\sqrt{4\alpha t}}$	$(2\alpha t)^{\gamma}$	$(2\alpha t)^{\gamma} \log^{\pm\gamma}(2\alpha t)$	$2\alpha t \log(2\alpha t)$	$2bt$

Table 1: Lanczos coefficient b_n for different classes of dynamical systems in the thermodynamic limit and the (operator) Krylov complexity as a function of time with leading contributions. α and b are dimensionful constants with dimensions of energy, while $\gamma = \frac{1}{1-\delta}$, $0 < \delta < 1$. This compilation is adapted from [114].

This section is dedicated to chalking-out the notion of Krylov complexity that we actually use in the course of this thesis: Krylov complexity adapted to the study of quantum-states, also known as Krylov spread complexity or, simply, *spread complexity*. Etymological origins of the term indicate towards the "spread" of a quantum state through the Krylov basis or the Hilbert space - naturally, this can be used for the operator Krylov complexity as well but practically, in literature, the term "spread complexity" is reserved for the Krylov complexity for states, while the term "Krylov complexity" is slightly more ambiguous but typically refers to the operator Krylov complexity. The discussion in this subchapter is a recounting of the discussion in [106] and [109] and is included, again, for the purposes of self-containment.

The central problem under consideration is that of the evolution of some arbitrary quantum state under an arbitrary unitary transformation. This can be thought of as a circuit from the initial state $|\Psi_0\rangle$, through circuit parameter s, to the final state $|\Psi(s)\rangle$, and this transformation is effected through a unitary operation as follows,

$$|\Psi(s)\rangle = e^{-isH}|\Psi_0\rangle\,. \tag{3.13}$$

In the circuit analogy, we shall choose to denote the state $|\Psi_0\rangle$ as the reference state and $|\Psi(s)\rangle$ as the target state of a circuit with Hamiltonian, H. The circuit parameter s traverses the circuit from the reference state ($s = 0$) to the target state ($s = 1$). [106] introduced a notion of Krylov complexity for states by considering the spread of the target state $|\Psi(s)\rangle$ through the Hilbert space. More precisely, one can quantify the spread of target state by expanding it in some basis, $\mathscr{B} = \{|B_n\rangle, n = 0, 1, 2, \cdots\}$ wherein $|B_0\rangle = |\Psi_0\rangle$, is the reference state. Quite similar to Nielsen's circuit complexity, we can define a cost-function that measures the weighted average distribution of the target state across the elements of the chosen basis $\mathscr{B}$,

$$C_{\mathscr{B}}(s) = \sum_n n |\langle \Psi(s)|B_n\rangle|^2, \tag{3.14}$$

and we ask for it to be minimized over all choices of basis $\mathscr{B}$. Now, we define the spread complexity as the same as cost-function $C_{\mathscr{B}}(s)$ with the property that the choice of $\mathscr{B}$ should minimize the cost function,

$$\mathscr{C}(s) = \min_{\mathscr{B}} C_{\mathscr{B}}(s). \tag{3.15}$$

This furnishes the spread complexity for a state characterized in the circuit through the parameter s, such that the spread complexity for the target state is given by choosing $s = 1$ *i.e.* the spread complexity of the target state is just $\mathscr{C}(s = 1)$.

It was shown in [106] that it is actually the Krylov basis that minimizes the cost function (3.14). The Krylov basis $\{|K_n\rangle\}$ comes out as a result of some kind of Gram-Schmidt procedure on the states $|\mathcal{O}_n\rangle = H^n|\Psi_0\rangle$ - with the specific algorithm to perform it depending on the system *e.g.* for Hermitian systems the Lanczos algorithm serves this purpose as discussed earlier in this chapter. Other properties of the Krylov basis remain the same as that for the operator Krylov complexity - with a notable addition, the circuit Hamiltonian is again tri-diagonal except that the diagonal terms are no longer vanishing,

$$\boxed{H|K_n\rangle = a_n|K_n\rangle + b_n|K_{n-1}\rangle + b_{n+1}|K_{n+1}\rangle.} \tag{3.16}$$

So for spread complexity there are two sets of Lanczos coefficients $\{a_n\}$ and $\{b_n\}$, while the elements of the former identically vanish for operator Krylov complexity. These coefficients are an output of the Gram-Schmidt orthogonalization procedure, along with the Krylov basis, and can also be generated by the moments of the return amplitude of the reference state, also known as the survival or Loschmidt amplitude [115] and expressed as,

$$S(s) \equiv \langle\Psi(s)|\Psi(0)\rangle = \langle\Psi_0|e^{isH}|\Psi_0\rangle. \tag{3.17}$$

As the task at hand is to quantify the spread of the target state through some basis, we express the target state in terms of the Krylov basis,

$$|\Psi(s)\rangle = \sum_n \psi_n(s)|K_n\rangle\,, \tag{3.18}$$

and, by construction, the corresponding Lanczos coefficients participate in the following discrete recurrence relation,

$$\boxed{i\partial_s\psi_n(s) = a_n\psi_n(s) + b_n\psi_{n-1}(s) + b_{n+1}\psi_{n+1}(s),} \tag{3.19}$$

where $\psi_n(t)$ are the complexity wavefunctions introduced earlier in this chapter. One can, hence, solve for the complexity wavefunctions with the knowledge of the two sets of the Lanczos coefficients as well as the initial condition $\psi_n(0) = \delta_{n0}$ and express the spread complexity in terms of these complexity wavefunctions:

$$\mathscr{C}(s) = \sum_n n|\psi_n(s)|^2. \tag{3.20}$$

This definition, while similar to the operator Krylov complexity definition, is distinct as it adapts the notion of the operator Krylov complexity defined in [26] to states (see also [35, 64, 105, 108, 114, 116–132]). Furthermore, for the operator Krylov complexity definition one needs to make an arbitrary choice of mapping operators to states: $\mathcal{O} \to |\mathcal{O}\rangle$), this is achieved in a number of ways, including the Gelfland-Naimark-Segal (GNS) construction [133] and Choi-Jamiolkowski map (both of which we demonstrate further in this chapter), or simply expanding the operator in the phase basis $|\omega_{ab}\rangle$ as in the Ch.3.3. We now define a "complexity operator" which proves useful as we shall see in Ch.4,

$$\boxed{\widehat{K} = \sum_n n|K_n\rangle\langle K_n|, \qquad \mathscr{C}(s) \equiv \langle\Psi(s)|\widehat{K}|\Psi(s)\rangle.} \tag{3.21}$$

We shall work with (3.20) and (3.21) as effective definitions of the spread complexity for the remainder of this thesis. As a final remark, similar to [109], we extend the above definitions to continuum limit and free

theories to explore the nature of results in the thermodynamics limit. The circuit states in the next chapter on Kitaev chain shall have a decomposed product form over momentum modes and we shall compute the spread complexity of the circuit with respect to each momentum mode - then, exactly as for Nielsen's circuit complexity, sum over them or integrate over them to obtain results in the thermodynamic limit. [1].

3.5 Unifying Krylov Complexities for Operators and States

We've presented two, very similar but as-of-yet distinct, notions of the Krylov complexity: one, of the operators that act on the Hilbert space $\mathcal{O} \in L(\mathscr{H})$; and two, of the states that constitute that Hilbert space $\{|\Psi\rangle\} \in \mathscr{H}$. As these notions are similar, one gets an intuitive notion of a sort of coarse equivalence between the two notions. A natural curiosity would be to explore if there is a more precise relation between these notions and, if so, the implications of such a relation. It turns out that there, indeed, is a relation between these two notions and a unified framework can be developed for them as demonstrated in [107]. We provide a brief summarized account of the same here.

We begin by, rather arbitrarily, introducing an operator that we label *label operator*. Our premise is that of a quantum system whose time-evolution dynamics is described by a time-independent Hermitian Hamiltonian with eigenstates given as $\{|\Psi_a\rangle\,; a = 1, 2, \ldots, D\}$ and corresponding eigenvalues as E_a where D is the dimension of the Hilbert space $\mathscr{H}$. Let us consider a Hermitian operator on this Hilbert space $\mathcal{O} : \mathscr{H} \mapsto \mathscr{H}$, and it is possible to construct an orthonormal ordered basis corresponding with any state $|\psi\rangle$ in the Hilbert space $\mathscr{H}$ with th aim of computing the spread complexity of this state's evolution under $\mathcal{O}$. The first element of this basis, assumed to be normalized, can be chosen as the state $|\psi\rangle$. The other elements can be generated recursively as described in the Ch.3.3 using a Gram-Schmidt procedure which generates both the basis, which is quickly identified as the Krylov basis and denote simply as $\{|n\rangle\}\,; n = 0, 1, \ldots, K-1$, and the Lanczos coefficients - with K being the dimension of the Krylov subspace. This has already been covered previously.

Now, since the basis is an ordered one any element of this basis can be identified with a number and this can be represented as a label operator[2],

$$l = \sum_{n=0}^{K-1} c_n \, |n\rangle \langle n| \,, \tag{3.22}$$

[1] We note that, for generic states, demonstrating that this procedure is, in principle, the same as the canonical Krylov complexity definition in position space or the definition starting from the return amplitude is not apparent and we leave the study of this facet to future works independent of this thesis. We thank an anonymous referee of [1] for bringing this aspect to our attention.

[2] The label operator can be identified as the Krylov complexity operator in (3.21) - up to an appropriate choice of the basis *i.e.* one should make the choice of Krylov basis rather than an arbitrary basis. The procedure to make this choice is explained in detail in [107] but, essentially, boils down to choosing the same (Hermitian) seed operator for Gram-Schmidt procedure as the one that we'd like to evolve the circuit with. To our knowledge, it hasn't been explored in the literature if this remains true for non-Hermitian cases but, apriori, it should.

where c_n are arbitrary coefficients encoding the "number" or label uniquely identifying the element of the basis. As this is an ordered basis, we should insist that $c_n > c_m$ if $n > m$ *i.e.* the coefficients c_n are monotonically increasing with increasing n. We might as well choose them as $c_n = n$ since this is the simplest monotonically increasing function of n. As we saw in Ch.3.3 the Krylov vectors $\{|n\rangle\}$ complete a basis over the Krylov subspace $\mathscr{K}$ and hence any state in $\mathscr{K}$ can be expressed in terms of this basis,

$$|\phi\rangle = \sum_n \phi_n |n\rangle, \quad \text{with} \quad \sum_{n=0}^{K-1} |\phi_n|^2 = 1. \tag{3.23}$$

Interestingly, computing the expectation value of the label operator l in this arbitrary state $|\phi\rangle$ expanded in the Krylov basis $|n\rangle$,

$$\langle \phi \,|\, l \,|\, \phi \rangle = \mathrm{Tr}\left[l \cdot \rho_\phi\right] = \sum_{n=0}^{K-1} n \ |\phi_n|^2, \tag{3.24}$$

is exactly the same as the spread complexity, with $\rho_\phi = |\phi\rangle\langle\phi|$ interpreted as the density matrix corresponding to the state $|\phi\rangle$. Correspondingly, we can write down an expression for the spread complexity[1] of the circuit evolution, generated through a unitary e^{iHs} of some arbitrary target state $|\psi(s)\rangle$ in terms of the circuit parameter s as,

$$\boxed{\mathscr{C}(s) = \sum_{n=0}^{K-1} n \ |\psi_n(s)|^2 = \mathrm{Tr}\left[l \cdot \rho_\psi(s)\right],} \tag{3.25}$$

where $\rho_\psi(s) = |\psi(s)\rangle\langle\psi(s)|$ is the density matrix corresponding to the circuit target state $|\psi(s)\rangle$.

Having established the label operator notation and having expressed the spread complexity in terms of the same, we are now in a position to turn our attention to the operator Krylov complexity and, more specifically, towards a uniform description of both flavors of Krylov complexities. This unification, unsurprisingly, comes through the label operator representation of operator complexity - which, unfortunately, isn't as straight forward as for the spread complexity case. To this end, let us note again a remark from the introduction to Ch.3. There are two main ingredients required to implement the recursion method which, in the Liouvillian representation, are: one, a stationary density operator; and two, an inner product. The label operator is quickly identified to serve in the stead of the former, while for the latter a different prescription is provided here in which the inner product arises naturally. We shall employ the channel-state map [134], as an alternative to the typically used GNS construction, to map an operator to a state in the doubled Hilbert space, and then essentially deploy the same label operator procedure that we did for the spread complexity. The channel-state map is also known as Choi-Jamiolkowski map in literature [135].

[1] Technically, the $\mathscr{C}(s)$ only gives a spreading number and it is equivalent to the complexity when the choice of the Hermitian operator (among all possible ones) minimizes the spreading number, in the same vein as the cost-function equivalence to spread complexity subject to a minimization of all possible bases discussed in Ch.3.4. It is not straightforward to make such a specific choice, however, if the operator which generates the unitary transformation is the same as the one which serves as the seed operator for the Gram-Schmidt procedure, then it can be seen that spreading number minimizes.

Let us work in the same setup described previously: a quantum system whose dynamics are elucidated through a Hamiltonian H with eigenstate-eigenvalue pairs given as $\left(\left\{|E_a\rangle\right\}, E_a\right); a = 1, \ldots, D$, where D is the dimension of the Hilbert space $\mathscr{H}$. We consider an arbitrary operator on the Hilbert space $\mathcal{O} : \mathscr{H} \mapsto \mathscr{H}$ and a basis that spans $\mathscr{H}$ denoted as $\{|i\rangle; i = 1, 2, \ldots, D\}$. As this basis spans $\mathscr{H}$, the operator $\mathcal{O}$ can be expanded in this basis with matrix elements, $\mathcal{O}_{ij} = \langle i \,|\, \mathcal{O} \,|\, j\rangle$. The task at hand is to map this operator to a state $\mathcal{O} \mapsto |\psi_{\mathcal{O}}\rangle$[1]. This is where the Choi-Jamiolkowski map comes in:

$$\boxed{|\psi_{\mathcal{O}}\rangle = \sum_{i,j=1}^{D} \rho_{ij} \, |i\rangle \otimes |j\rangle \equiv \sum_{i,j=1}^{D} \rho_{ij} \, |i, j\rangle \,.} \tag{3.26}$$

The state $|\psi_{\mathcal{O}}\rangle$ lives in the auxiliary doubled Hilbert space $\mathscr{H}_d \equiv \mathscr{H} \otimes \mathscr{H}$. The P_{ij} density matrix elements are proportional to the matrix elements of $\mathcal{O}$ subject to their probabilities being conserved *i.e.* $\sum_{i,j} \left|\rho_{ij}\right|^2$, and, consequently, the proportionality factor is just a normalization,

$$\rho_{ij} = \frac{\mathcal{O}_{ij}}{\sqrt{\sum_{i',j'} \mathcal{O}_{i'j'} \mathcal{O}_{i'j'}}}. \tag{3.27}$$

As remarked before, this comes equipped with an inner product which satisfies the second requirement of implement the recursion method. The inner product is,

$$\mathcal{O}_1 \cdot \mathcal{O}_2 \equiv \left\langle \psi_{\mathcal{O}_1} \,\middle|\, \psi_{\mathcal{O}_2} \right\rangle. \tag{3.28}$$

It is now straightforward to adapt the label operator notation for the doubled Hilbert space $\mathscr{H}_d$ and we delegate the details to [107] and simply provide the results,

$$\mathscr{C}_{\mathcal{O}}(s) = \mathrm{Tr}\left[l \cdot \rho_{\mathcal{O}}(s)\right], \tag{3.29}$$

where, $\rho_{\mathcal{O}}(s) = |\psi_{\mathcal{O}}(s)\rangle \langle \psi_{\mathcal{O}}(s)|$ - with s being the circuit parameter. We, again, remark that technically $\mathscr{C}_{\mathcal{O}}(s)$ is only a spreading number which is identified as the Krylov complexity if one chooses to evolve the circuit with the same operator as the seed operator that goes into the Gram-Schmidt process.

Finally, it is instructive to elucidate the case of the time-evolution via Hamiltonian in the Choi-Jamiolkowski doubled Hilbert space setup for operator complexity. The setup is to study the growth of a Hermitian operator under time-evolution as prescribed by the Hamiltonian of the system : $\mathcal{O}(t) = e^{iHt} \mathcal{O} e^{-iHt}$. Of course, we should use the energy eigenstates for the Choi-Jamiolkowski map for which the state associated with a Hermitian operator $\mathcal{O}$ is written in a similar vein as (3.26),

$$|\psi_{\mathcal{O}}\rangle = \sum_{a,b}^{D} \rho_{ab} \, |E_a, E_b\rangle \,, \tag{3.30}$$

[1] As discussed earlier in the chapter, an input of the recursion method is this map - for operators *i.e.* even when one computes operator Krylov complexity, one works with states. When computing Krylov complexity for states, this choice of operator to state map is not required.

with D being the dimension of the Hilbert space and ρ_{ab} being the normalized matrix elements (3.27) of the operator under study in the energy basis. Naturally, the time evolution of the state $|\psi_{\mathcal{O}}\rangle$ is encoded in the matrix elements ρ_{ab} and is expressed as (in the Heisenberg/Liouvillian picture),

$$\rho_{ab}(t) = e^{i(E_a - E_b)t}\rho_{ab}, \tag{3.31}$$

such that ρ_{ab} are the matrix elements at $t = 0$. This indicates that the form of the state in the doubled space $\mathcal{H}_d$ is,

$$|\psi_{\mathcal{O}}(t)\rangle = e^{iH_- t}|\psi_{\mathcal{O}}\rangle, \tag{3.32}$$

such that $H_- = H \otimes \mathbb{1} - \mathbb{1} \otimes H$. As discussed, if the basis construction via Gram-Schmidt is performed using this H_- operator then we can be assured that the spreading number (or cost-function) is indeed the Krylov complexity. Following the prescription outline above, we can write down the Krylov complexity as,

$$\mathcal{C}(t) = \mathrm{Tr}\left[l \cdot \rho_{\mathcal{O}}(t)\right] = \sum_{n=0}^{K} n\,|\mathcal{O}_n(t)|^2, \tag{3.33}$$

where $\mathcal{O}_n(t) = \sum_{a,b}\rho_{ab}(t)\,\langle n, n \,|\, E_a, E_b\rangle$ and K is the dimension of the Krylov basis. In summary, through the unified framework we can study the Heisenberg evolution of an operator using the same procedure as for the spread complexity, albeit in the doubled Hilbert space and with the Hamiltonian H_-. Additionally, evolution through H_- vanishes the $\{a_n\}$ set of Lanczos coefficients. However, what's really interesting here is the following hidden symmetry. For a doubled system with dynamics generated through H_- in the $\mathcal{H}_d$ space, $H_+ = H \otimes \mathbb{1} + \mathbb{1} \otimes H$ is a symmetry as $[H_+, H_-] = 0$. Hence, the state $|\psi_{\mathcal{O}}\rangle$ is an eigenstate of the H_+ operator with its eigenvalue interpreted as the average energy: $H_+|\psi_{\mathcal{O}}\rangle = (E_a + E_b)|\psi_{\mathcal{O}}\rangle$. As evolution through H_- cannot mix different energy sectors, the complexity splits into a sum of complexities for each individual energy sector - this provides a partial justification to the remark at the end of Ch.3.4. In fact, it is this particular behavior of energy-sector separation that leads to the diagonal elements $\mathcal{O}_{aa}$ vanish or, equivalently, the Liouvillian matrix for operators in the Krylov basis has vanishing ($a_n = 0, \forall n$). Naturally, one can envisage an operator which, under Choi-Jamiolkowski, maps to the following diagonal state,

$$|\psi_{\mathcal{O}}\rangle = \sum_a \rho_a\,|E_a, E_a\rangle\,. \tag{3.34}$$

Clearly, this state exhibits trivial dynamics under evolution through H_- but more interestingly, the dynamics of these states are governed through the H_+ operator! With a choice of,

$$\rho_a = \frac{e^{-\frac{\beta E_a}{2}}}{\sqrt{\sum_a e^{-\beta E_a}}}, \tag{3.35}$$

the state $|\psi_{\mathcal{O}}\rangle$ becomes the very well-known Thermofield Double (TFD) state. This role reversal of $H_+ \longleftrightarrow H_-$ has its origins in the assumption that the energy eigenstates that constitute the doubled Hilbert space are also eigenstates of the time-reversal operator. This assumption may be true for many systems, however, it is not

so generically. In fact, we've just seen an example of the famous AdS/CFT duality [136] in action. On one hand, the TFD states arise by respecting the time-reversal symmetry of the basis eigenstates (the boundary perspective); while on the other hand, the second method does not respect the time-reversal symmetry (the bulk perspective) and the TFD state arises organically through evolution with H_+ which can be thought of as the bulk Hamiltonian. This concludes our discussion on the unification of the two notions of the Krylov complexity.

3.6 Continuum Krylov Complexity

TFD states are a widely used tool to study various models in the context of the bulk-boundary correspondence. Naturally, most of their utility is towards studying continuum or field theories. Additionally, a good portion of physics is described by field theories. So, it is imperative to develop a continuum notion of Krylov complexity for field theories if it is to be used to study a wide array of phenomena. As a final remark on the theoretical framework sculpting Krylov complexity, we demonstrate the procedure to extend the definitions of Krylov complexity developed in this chapter for, mostly, quantum-mechanical discrete setups to the continuum or field theory ones. Our discussion largely follows [108], however, a similar procedure is outlined in [39].

We'll adapt the same approach as [108] and discuss the formulation of Krylov complexity in free theories for operators rather than the unified framework. The unified framework is easily identified in this setup and, additionally, a reader of this thesis can seamlessly extend their study to [108] for a more intricate and detailed account. An important observation is that in both the state and operator Krylov complexities we calculate the complexity for a state. This is an obvious choice for the former, but for the latter it takes the form of a map from the operator to a corresponding state: we've already demonstrated that this can be achieved through the GNS construction (which was implicitly used in Ch.3.3) or the Choi-Jamiolkowski map. We start by briefly chalking out the GNS construction.

The GNS construction[1] maps operator evolution to a more conventional quantum state evolution, and assists in providing an extension of the notion of operator growth to QFT. It essentially expresses the operator space algebra in terms of elements of a Hilbert space, $\mathscr{H}_{\text{GNS}}$. The Liouvillian, then, acts as a regular Hermitian operator on the $\mathscr{H}_{\text{GNS}}$ space if the corresponding Hamiltonian is Hermitian. More precisely, the GNS construction represents a state on a *-algebra over $\mathbb{C}$ which at the onset takes a mere algebraic definition as a non-degenerate positive linear function $\rho : \mathscr{A} \to \mathbb{C}$, by a vector $|\psi\rangle \in \mathscr{H}$, a complex Hilbert space, as the matrix element of A with $|\psi\rangle$,

$$\rho(A) = \langle \psi \,|\, A \,|\, \psi \rangle := \langle \psi, \pi(A)\psi \rangle \,, \tag{3.36}$$

with respect to some *-representation $\pi : \mathscr{A} \to \text{End}(\mathscr{H})$. Essentially, one can understand $\rho(A) = |A)$ *i.e.* ρ defines the map from the operator A to the state $|A)$. A matrix element in the space $\mathscr{H}_{\text{GNS}}$ produces a

[1] There is an illustrative ncatlab article on GNS construction.

complex element in $\mathscr{H}$. So that, $|\mathcal{O}) = \left\langle \psi \,\middle|\, \widehat{\mathcal{O}} \,\middle|\, \psi \right\rangle$. Expanding in energy basis we get,

$$\begin{aligned} |\mathcal{O}) = \left\langle \psi \,\middle|\, \widehat{\mathcal{O}} \,\middle|\, \psi \right\rangle = \sum_{ij} \langle \psi \,|\, E_i \rangle \left\langle E_i \,\middle|\, \widehat{\mathcal{O}} \,\middle|\, E_j \right\rangle \langle E_j \,|\, \psi \rangle = \sum_{ij} \underbrace{\left\langle E_i \,\middle|\, \widehat{\mathcal{O}} \,\middle|\, E_j \right\rangle}_{\mathcal{O}_{ij}} |E_i\rangle \langle E_j| \underbrace{\langle \psi \,|\, \psi \rangle}_{=1} \\ |\mathcal{O}) = \sum_{ij} \mathcal{O}_{ij} |E_i\rangle \langle E_j| \,. \end{aligned} \tag{3.37}$$

Likewise, we can compute the action of the Liouvillian on the state corresponding to the operator $\mathcal{O}$,

$$\begin{aligned} \mathscr{L}|\mathcal{O}) = |\mathscr{L}\mathcal{O}) &= \sum_{ij} \left\langle E_i \,\middle|\, \mathscr{L}\mathcal{O} \,\middle|\, E_j \right\rangle |E_i\rangle \langle E_j| = \sum_{ij} \left\langle E_i \,\middle|\, (H\mathcal{O} - \mathcal{O}H) \,\middle|\, E_j \right\rangle |E_i\rangle \langle E_j| \\ &= \sum_{ij} \left(E_i - E_j\right) \left\langle E_i \,\middle|\, \mathcal{O} \,\middle|\, E_j \right\rangle |E_i\rangle \langle E_j| \,, \end{aligned} \tag{3.38}$$

exactly as obtained in (3.3). Now, we had set out with a goal to come up with a continuum description of the above setup while keeping the spectrum discrete (but with a possibility to relax this condition). It is difficult to get a continuum representation for the quantity $\left\langle E_i \,\middle|\, \mathcal{O} \,\middle|\, E_j \right\rangle$ so we define new state variable *i.e.* energy & express $E_{i/j}$ in terms of an *average-energy* variable, E, such that $E_j = E - \frac{\omega}{2}$ and $E_i = E + \frac{\omega}{2}$ with $\omega = E_i - E_j$.

Ideally, we want to write something that goes as $\sim \int dE\, \omega \, \langle E|\mathcal{O}|E\rangle \, |E\rangle \langle E|$ since this lies more in line with what one can easily calculate and use. Substituting values and identifying $\left\langle E + \frac{\omega}{2} \,\middle|\, \mathcal{O} \,\middle|\, E - \frac{\omega}{2} \right\rangle \equiv \mathcal{O}(E, \omega)$, we obtain:

$$\int dE\, \omega\, \mathcal{O}(E, \omega) \left| E + \frac{\omega}{2} \right\rangle \left\langle E - \frac{\omega}{2} \right| . \tag{3.39}$$

Generically, $|E\rangle$ is not an energy eigenstate of the Hamiltonian H. Additionally, we don't know how many energy states lie between E_i and E_j so we need to introduce a density function to count the number of intermediate states. We interpret this as a *spectral measure*, $\rho(E, \omega)$, since it deals with the spectrum and it measures the number of energy states. This gives,

$$\int dE \int d\omega\, \rho(E, \omega)\, \omega\, \mathcal{O}(E, \omega) \left| E + \frac{\omega}{2} \right\rangle \left\langle E - \frac{\omega}{2} \right| . \tag{3.40}$$

We can determine a generic form of the spectral measure $\rho(E, \omega)$ by the following constraints:

- $\because E$ is the average of E_i and $E_j \implies \rho(E, \omega) \propto \delta\left(E - \frac{E_i + E_j}{2}\right)$
- the equi-spaced distance between E and $E_{i/j}$ is denoted as $\frac{\omega}{2} \implies \rho(E, \omega) \propto \delta\left(\frac{\omega}{2} - (E_i - E)\right)$ $\times\, \delta\left(\frac{\omega}{2} - \left(E - E_j\right)\right)$, however, we can add the two requirements : $E_i - E = \frac{\omega}{2}$ and $E - E_j = \frac{\omega}{2}$ to get $E_i - E_j = \omega$ so as to reduce the above product of delta functions to a single delta function : $\delta\left(\omega - E_i + E_j\right)$
- since this spectral measure exists for all pairs of (i, j) we need to have a $\sum_{ij}$
- to avoid over-counting we can choose $i > j$ in the summation (or something equivalent)

$$\boxed{\rho(E,\omega) = \sum_{i>j} \delta\left(E - \frac{E_i + E_j}{2}\right)\delta\left(\omega - E_i + E_j\right).} \tag{3.41}$$

We can easily re-scale so that E doesn't take negative values without loss of generality so the integral on E will run $0 \to \infty$. Limits on the ω integral :

$$\begin{aligned} E \pm \frac{\omega}{2} &= E_{\substack{i \\ j}} \\ \implies \omega = -2E + 2E_i \quad &\text{and} \quad \omega = 2E - 2E_j, \end{aligned} \tag{3.42}$$

since both E_i and E_j can take a minimum value of 0 as per our convention, we have the limits of the integral on $\omega : -2E \to 2E$. Hence, $\mathscr{L}|\mathcal{O})$ is,

$$\mathscr{L}|\mathcal{O}) = \int_0^\infty dE \int_{-2E}^{2E} d\omega\, \rho(E,\omega)\, \omega\, \mathcal{O}(E,\omega) \left|E + \frac{\omega}{2}\right\rangle \left\langle E - \frac{\omega}{2}\right|, \tag{3.43}$$

with $\rho(E,\omega) = \sum_{i>j} \delta\left(E - \frac{E_i+E_j}{2}\right)\delta\left(\omega - E_i + E_j\right)$ and $\mathcal{O}(E,\omega) = \left\langle E + \frac{\omega}{2} \,\middle|\, \mathcal{O} \,\middle|\, E - \frac{\omega}{2}\right\rangle$. While this notation is typically used when making a continuous approximation to some spectrum, that's not the case here as the spectrum continues being discrete. Importantly, $\mathscr{L}$ only sees the energy difference, ω, of the state associated to the operator $\mathcal{O}(E,\omega)$ and, hence, does not mix sectors that differ in average energy E. Furthermore, one can see the action of $\mathscr{L}$ on $|\mathcal{O})$, which gives terms proportional to $E_i - E_j$ arising from $\left\langle E_i \,\middle|\, H\mathcal{O} - \mathcal{O}H \,\middle|\, E_j\right\rangle$, and note that if one wants to construct an average energy operator with "eigenvalue" $E \equiv \frac{E_i+E_j}{2}$ it is possible to define an operator on $\mathscr{H}_{GNS}$ (which is a super-operator for $\mathscr{H}$), $\mathscr{E} = \frac{1}{2}\{H, \cdot\}$, such that it gives rise to terms proportional to $\frac{E_i+E_j}{2}$ arising from $\left\langle E_i \,\middle|\, \frac{H\mathcal{O}+\mathcal{O}H}{2} \,\middle|\, E_j\right\rangle$. The average energy operator $\mathscr{E}$ corresponds to the H_+ operator in the unified framework discussed in the previous section and, consequently, constitutes a symmetry of the $\mathscr{L}$, $[\mathscr{E}, \mathscr{L}] = 0$. So, the average energy E is a conserved charge for $\mathscr{L}$ as demonstrated below.

$$\begin{aligned} [\mathscr{E}, \mathscr{L}]\,|\mathcal{O}) &= |\,[\mathscr{E}, \mathscr{L}]\,\mathcal{O}) \\ &\sim \left\langle E_i \,\middle|\, \mathscr{E}\mathscr{L}\mathcal{O} - \mathscr{L}\mathscr{E}\mathcal{O} \,\middle|\, E_j\right\rangle \\ &\sim \left\langle E_i \,\middle|\, \mathscr{E}\,(H\mathcal{O} - \mathcal{O}H) - \mathscr{L}\,(H\mathcal{O} + \mathcal{O}H) \,\middle|\, E_j\right\rangle \\ &\sim \left\langle E_i \,\middle|\, \cancel{HH\mathcal{O}} + \cancel{H\mathcal{O}H} - \cancel{H\mathcal{O}H} - \cancel{\mathcal{O}HH} - \cancel{HH\mathcal{O}} + \cancel{H\mathcal{O}H} - \cancel{H\mathcal{O}H} + \cancel{\mathcal{O}HH} \,\middle|\, E_j\right\rangle \to 0. \end{aligned} \tag{3.44}$$

Iterative applications of $\mathscr{L}$ generate time evolution and the growth of an operator throughout the system which makes the operator more "complex". Since E is a conserved charge for $\mathscr{L}$, this evolution generated through $\mathscr{L}$ is restricted to each fixed-E sector *i.e.* applications of $\mathscr{L}$ cannot take the system from one energy sector to another. We need to take this fact into account in the definition of complexity basis and the corresponding cost function or spread number (both of which reduce to Krylov complexity, as described previously), otherwise the chaotic signatures may be veiled as in the case when a Hamiltonian is paired with conserved charges and chaotic signatures do not reflect on the usually reliable observables like level repulsion.

More seriously, if the complexity measure is blind to the presence of symmetry sectors it may yield some false-positives as observed in [121], wherein, a - false - exponential growth was observed for even free and integrable theories. To our knowledge, there are two solutions to this issue as presented in [108] and [39]. The latter proposes to compactify the space to suppress the exponential contributions to Krylov complexity arising exclusively from continuous momenta. We refer an interested reader to browse the relevant paper to see the intricacies involved. The former solution, however, is presented here in some detail.

Recognizing that the issue arises from a mixing of different average-energy sectors, a natural way to fix the undesirable exponential contributions is to consider orthonormalizations within every average-energy sector. This is straightforward to implement using the "microcanonical" inner product, as compared to the "canonical" inner product used in [121],

$$(A|B)_E = \int_{-2E}^{2E} d\omega \rho(E,\omega) A^*(E,\omega) B(E,\omega). \tag{3.45}$$

As an example, a thermal inner product with the state selected as a thermal density matrix is connected to the above microcanonical inner product via a Laplace transform,

$$\mathrm{Tr}\left[\rho^{\frac{1}{2}} A^\dagger \rho^{\frac{1}{2}} B\right] = \int_0^\infty dE\, e^{-\beta E} (A|B)_E. \tag{3.46}$$

Likewise, if adhering to the micro-canonical orthonormalization as a solution, then, for each conserved charge of the Liouvillian the same microcanonical orthonormalization technique should be utilized which amounts to constructing a Krylov basis, corresponding to each charge, sourced using the microcanonical inner-product. This distinguishes the quantum chaotic signatures from the aspects generated through the conserved charges, and, importantly, avoids false-positive signatures. Using canonical inner product, the exponential signature of chaos is an artefact of Liouvillian being restricted to a symmetry sector and hence the canonical inner product furnishing a false-positive. This growth is indicative of the ever-increasing contributions from the sectors of ever-increasing average-energy as we explore the tails of the relevant thermal distribution and it is expected to be universal for all ∞-dimensional theories.

Now, one can construct the Krylov basis keeping in mind the change of inner product to get orthonormal bases for each E, $\mathscr{B}_K^E$, by applying the Gram-Schmidt procedure to the linear operator basis $\left\{\mathscr{L}^n|\mathcal{O})_E\right\}_{n=0}^{D-1}$ - where $|\mathcal{O})_E$ is the usual GNS-state associated with $\mathcal{O}$ as an operator, $|\mathcal{O})$, without the integral over E *i.e.* $|\mathcal{O})_E$ = fixed average energy sector $|\mathcal{O})$,

$$\mathscr{B}_K^E = \left\{ |\mathcal{O}_{E,n}) = \mathcal{N}(E)^{-\frac{1}{2}} \int_{-2E}^{2E} d\omega\, \rho(E,\omega)\, \mathcal{O}(E,\omega)\, P_n^E(\omega) \left|E+\frac{\omega}{2}\right\rangle \left\langle E-\frac{\omega}{2}\right| \right\}_{n=0}^{D_E-1}, \tag{3.47}$$

where, $P_n^E(\omega)$ is a polynomial of degree n, $D_E = \dim\left[\mathscr{H}_{GNS}^E\right] \sim e^{2S(E)}$ and $\mathscr{N}(E)$ serves to normalize the polynomials P_n^E defined as,

$$\mathscr{N}(E) = \int_{-2E}^{2E} d\omega\, \rho(E,\omega)\ |\mathcal{O}(E,\omega)|^2 . \tag{3.48}$$

Successive terms in the Krylov basis are generated through increasing powers of $\mathscr{L}$. Calculating $\mathscr{L}^2|\mathcal{O})$,

$$\mathscr{L}^2|\mathcal{O}) = \sum_{ij} \left\langle E_i \middle| \mathscr{L}^2\mathcal{O} \middle| E_j \right\rangle |E_i\rangle\langle E_j| = \sum_{ij} \left\langle E_i \middle| (HH\mathcal{O} - 2H\mathcal{O}H + \mathcal{O}HH) \middle| E_j \right\rangle |E_i\rangle\langle E_j| \tag{3.49}$$

$$= \sum_{ij} \left(E_i^2 + E_j^2 - 2E_iE_j\right) \left\langle E_i \middle| \mathcal{O} \middle| E_j \right\rangle |E_i\rangle\langle E_j| = \sum_{ij} \omega^2 \left\langle E_i \middle| \mathcal{O} \middle| E_j \right\rangle |E_i\rangle\langle E_j| . \tag{3.50}$$

Likewise, one can verify that,

$$\mathscr{L}^n|\mathcal{O}) = \sum_{ij} \omega^n \left\langle E_i \middle| \mathcal{O} \middle| E_j \right\rangle |E_i\rangle\langle E_j| . \tag{3.51}$$

This gives, in the continuum notation,

$$\mathscr{L}^n|\mathcal{O})_E = \int_{-2E}^{2E} d\omega\, \omega^n\, \rho(E,\omega)\, \mathcal{O}(E,\omega) \left|E + \frac{\omega}{2}\right\rangle \left\langle E - \frac{\omega}{2}\right| , \tag{3.52}$$

applying Gram-Schmidt process to the above $\left\{\mathscr{L}^n|\mathcal{O})_E;\ \forall\, n\right\}$ will give the desired orthonormal basis $\mathscr{B}_K^E$ for each energy sector.

Let us now delve more rigorously into the structure of the Krylov subspace generated through the Gram-Schmidt on $\left\{\mathscr{L}^n|\mathcal{O})_E;\ \forall\, n\right\}$ as outlined in the Lanczos algorithm described earlier in the chapter. Using (3.52) the initial seed-operator's corresponding GNS-state, $|\mathcal{O})_E$, is given as,

$$|\mathcal{O})_E = \int_{-2E}^{2E} d\omega\, \rho(E,\omega)\, \mathcal{O}(E,\omega)\ \left|E + \frac{\omega}{2}\right\rangle \left\langle E - \frac{\omega}{2}\right| , \tag{3.53}$$

such that the inner product is defined as,

$${}_E(\mathcal{O}|\mathcal{O})_E \equiv \int_{-2E}^{2E} d\omega\, \rho(E,\omega)\, \mathcal{O}^*(E,\omega)\mathcal{O}(E,\omega) = \int_{-2E}^{2E} d\omega\, \rho(E,\omega)\ |\mathcal{O}(E,\omega)|^2 = \mathscr{N}(E), \tag{3.54}$$

as noted previously. We can also define $|\mathcal{O})_E$ with a $\sqrt{\rho(E,\omega)}$ and the microcanonical inner product as,

$${}_E(A|B)_E = |A)_E^\dagger \times |B)_E, \tag{3.55}$$

rather than the one defined in [108]. In the notation that the authors of [108] have adapted, the microcanonical inner product $(A|B)_E$ requires one to discard $\rho(E,\omega)$ and $\left|E+\frac{\omega}{2}\right\rangle\left\langle E-\frac{\omega}{2}\right|$ of $|A)_E$ and $|B)_E$ and just use the contribution of $\mathscr{L}^n\cdot\mathcal{O}(E,\omega)$ coming from them, as the construction takes care of the former terms. Hence, the normalized seed-operator GNS-state is,

$$|\mathcal{O}_0)_E=\frac{1}{\sqrt{\mathcal{N}(E)}}\int_{-2E}^{2E}d\omega\,\rho(E,\omega)\,\mathcal{O}(E,\omega)\,\left|E+\frac{\omega}{2}\right\rangle\left\langle E-\frac{\omega}{2}\right|, \tag{3.56}$$

and likewise we can re-express actions of $\mathscr{L}$ on the GNS-state $|\mathcal{O})_E$ into a normalized (though not orthogonal) form,

$$\boxed{\mathscr{L}^n|\mathcal{O})_E=\frac{1}{\sqrt{\mathcal{N}(E)}}\int_{-2E}^{2E}d\omega\,\omega^n\,\rho(E,\omega)\,\mathcal{O}(E,\omega)\,\left|E+\frac{\omega}{2}\right\rangle\left\langle E-\frac{\omega}{2}\right|,} \tag{3.57}$$

Let's consider the overlap of the seed operator state with itself after a single Liouvillian action on it,

$$_E(\mathcal{O}_0,\mathscr{L}\mathcal{O}_0)_E=\int_{-2E}^{2E}d\omega\,\rho(E,\omega)\,\mathcal{O}^*(E,\omega)\,\omega\,\mathcal{O}(E,\omega)\to 0, \tag{3.58}$$

because the integrand is odd in ω whereas the interval/measure is even. $|\mathcal{O}(E,\omega)|^2$ is even in ω due to the modulus and $\rho(E,\omega)$ is even in ω due to its definition. Similarly, this gets rid of the diagonal terms of the tridiagonal matrix $_E(\mathcal{O}_m|\mathscr{L}|\mathcal{O}_n)_E$,

$$\boxed{_E(\mathcal{O}_n|\mathscr{L}\mathcal{O}_n)_E\sim\int_{-2E}^{2E}d\omega\,\omega^{2n+1}\to 0.} \tag{3.59}$$

Now, $A_1=\mathscr{L}\mathcal{O}_0-(\mathcal{O}_0,\mathscr{L}\mathcal{O}_0)\mathcal{O}_0=\mathscr{L}\mathcal{O}_0$, and the associated GNS state,

$$|A_1)_E=\frac{1}{\sqrt{\mathcal{N}(E)}}\int_{-2E}^{2E}d\omega\,\rho(E,\omega)\,\mathcal{O}(E,\omega)\,\omega\,\left|E+\frac{\omega}{2}\right\rangle\left\langle E-\frac{\omega}{2}\right|, \tag{3.60}$$

and the corresponding (first) Lanczos coefficient,

$$b_1=\sqrt{||A_1||}=\sqrt{_E(\mathscr{L}\mathcal{O}_0|\mathscr{L}\mathcal{O}_0)_E}=\sqrt{\frac{1}{\mathcal{N}(E)}\int_{-2E}^{2E}d\omega\,\rho(E,\omega)\,\omega^2\,\,|\mathcal{O}(E,\omega)|^2}\equiv b_1^E, \tag{3.61}$$

with,

$$\mathcal{O}_1=\frac{A_1}{b_1}=|\mathcal{O}_1)_E=\frac{1}{\sqrt{\mathcal{N}(E)}}\int_{-2E}^{2E}d\omega\,\rho(E,\omega)\,\mathcal{O}(E,\omega)\,\left[\frac{\omega}{b_1}\right]\left|E+\frac{\omega}{2}\right\rangle\left\langle E-\frac{\omega}{2}\right|, \tag{3.62}$$

where, $b_1 \equiv b_1^E$ is independent of ω. Then, $A_2 = \mathscr{L}\mathcal{O}_1 - b_1\mathcal{O}_0 = \frac{\mathscr{L}^2\mathcal{O}_0}{b_1} - \frac{b_1^2\mathcal{O}_0}{b_1}$,

$$|A_2)_E = \frac{1}{\sqrt{\mathcal{N}(E)}} \int_{-2E}^{2E} d\omega\, \rho(E,\omega)\mathcal{O}(E,\omega) \left[\frac{\omega^2 - b_1^2}{b_1}\right] \left|E + \frac{\omega}{2}\right\rangle \left\langle E - \frac{\omega}{2}\right|, \tag{3.63}$$

and the corresponding (second) Lanczos coefficient,

$$b_2 = \sqrt{||A_2||_E} = \sqrt{\frac{1}{\mathcal{N}(E)} \int_{-2E}^{2E} d\omega\, \rho(E,\omega) \left[\frac{\omega^2 - b_1^2}{b_1}\right]^2 |\mathcal{O}(E,\omega)|^2}, \tag{3.64}$$

with,

$$\mathcal{O}_2 = \frac{A_2}{b_2} = |\mathcal{O}_2)_E = \frac{1}{\sqrt{\mathcal{N}(E)}} \int_{-2E}^{2E} d\omega\, \rho(E,\omega)\mathcal{O}(E,\omega) \left[\frac{\omega^2 - b_1^2}{b_2 b_1}\right] \left|E + \frac{\omega}{2}\right\rangle \left\langle E - \frac{\omega}{2}\right|, \tag{3.65}$$

It is apparent that the elements of the set $\{\mathcal{O}_n; \forall\, n\}$ are orthonormal. Based on visual cues, we can asset that the GNS-state is nothing but a re-expression of the specific combination of the various powers of ω and the Lanczos coefficients. More formally, we can cast this into an elucidating form that conveniently converts integral equations to algebraic ones,

$$\boxed{\mathscr{B}_K^E = \left\{ |\mathcal{O}_{E,n}) = \mathcal{N}(E)^{-\frac{1}{2}} \int_{-2E}^{2E} d\omega\, \rho(E,\omega)\, \mathcal{O}(E,\omega)\, P_n^E(\omega) \left|E + \frac{\omega}{2}\right\rangle \left\langle E - \frac{\omega}{2}\right| \right\}_{n=0}^{D_E - 1}.} \tag{3.66}$$

Here, $\{P_n^E(\omega)\}$ is a sequence of orthogonal polynomials which follow the well known second order recurrence relation,

$$\boxed{\omega\, P_n^E(\omega) = b_{n+1}^E\, P_{n+1}^E(\omega) + b_n^E\, P_{n-1}^E(\omega).} \tag{3.67}$$

The first few elements are given by : $P_0^E(\omega) = 1, P_1^E(\omega) = \frac{\omega}{b_1}$ and the recurrence relation gives $P_2^E(\omega) = \frac{\omega^2 - b_1^2}{b_2 b_1}$ which agrees with the calculation above. For greater details on the connection of orthogonal polynomials with Krylov complexity, see [131]. P_n^E form a sequence of orthogonal polynomials with respect to a measure μ_E determined by the orthonormality condition with the microcanonical inner product,

$$\int_{-2E}^{2E} \underbrace{\mathcal{N}(E)^{-1}\rho(E,\omega)\, |\mathcal{O}(E,\omega)|^2\, d\omega}_{\equiv d\mu_E(\omega)}\, P_n^E(\omega)\, P_m^E(\omega) = \delta_{nm}. \tag{3.68}$$

The measure is normalized *i.e.* $\int_{-2E}^{2E} d\mu_E(\omega) = 1$. This measure will be referred to as *operator-weighted spectral measure* to bring attention to the fact that it is a re-scaling of the associated spectral measure, $\rho(E,\omega)$,

with the operator wavefunction, $|\mathcal{O}(E,\omega)|^2$. The time evolved operator $\mathcal{O}(t) = e^{-iHt}\,\mathcal{O}\,e^{-iHt}$ can be expressed in the Krylov basis as follows,

$$\boxed{|\mathcal{O}(t)) = \int_0^\infty dE\,\mathcal{N}(E)^{\frac{1}{2}} \sum_{n=0}^{D-1} \phi_{E,n}(t)\, i^n |\mathcal{O}_{E,n}).} \tag{3.69}$$

The terms after the $\sum$ are the regular terms that one uses while expanding an operator in the relevant Krylov basis. However, the relevant Krylov basis here happens to correspond to a particular energy sector only, so we need to integrate over all the available energy sectors (since no energy sector is special). The $\mathcal{N}(E)^{\frac{1}{2}}$ just ensures that $\sum_n \left|\phi_{E,n}(t)\right|^2 = 1$, and we identify $\phi_{E,n}(t)$ as the complexity wavefunctions restricted to a particular energy sector E. This is an easy check by considering $(\mathcal{O}(t)|\mathcal{O}(t))$ without having $\mathcal{N}(E)^{\frac{1}{2}}$ in the definition of $|\mathcal{O}(t))$.

$$\begin{aligned}(\mathcal{O}(t)|\mathcal{O}(t)) &= \int_0^\infty dE \int_0^\infty dE' \sum_{m,n=0}^{D-1} i^n\,(-i)^m\,\phi^*_{E',m}(t)\,\phi_{E,n}(t)\,\underbrace{(\mathcal{O}_{E',m}|\mathcal{O}_{E,n})}_{\delta_{E,E'}\times(\mathcal{O}_{E,m}|\mathcal{O}_{E,n})} \\ &= \int_0^\infty dE \sum_{m,n=0}^{D} i^n(-i)^m\,\phi^*_{E,m}(t)\,\phi_{E,n}(t)\,(\mathcal{O}_{E,m}|\mathcal{O}_{E,n}).\end{aligned} \tag{3.70}$$

And,

$$(\mathcal{O}_{E,m}|\mathcal{O}_{E,n})_E = \frac{1}{\mathcal{N}(E)} \int_{-2E}^{2E} d\omega\,\rho(E,\omega)\;|\mathcal{O}(E,\omega)|^2\;\underbrace{P^{*E}_m(\omega)}_{=P^E_m(\omega)}\,P^E_n(\omega). \tag{3.71}$$

$\{P^E_n(\omega);\,\forall\, n\}$ are orthogonal polynomials with respect to measure $d\mu_E(\omega) = \mathcal{N}(E)^{-1}\rho(E,\omega)\,|\mathcal{O}(E,\omega)|^2\,d\omega$. This gives,

$${}_E(\mathcal{O}_{E,m}|\mathcal{O}_{E,n})_E = \int_{-2E}^{2E} d\mu\,P^E_m(\omega)P^E_n(\omega) = \delta_{nm}. \tag{3.72}$$

Upon substituting back we get,

$$\begin{aligned}(\mathcal{O}(t)|\mathcal{O}(t)) &= \int_0^\infty dE \sum_{m,n=0}^{D-1} i^n(-i)^m\,\phi^*_{E,m}(t)\,\phi_{E,n}(t)\,(\mathcal{O}_{E,m}|\mathcal{O}_{E,n}) \\ &= \int_0^\infty dE \sum_{n=0}^{D-1} \left|\phi_{E,n}(t)\right|^2.\end{aligned} \tag{3.73}$$

We would like it if $(\mathcal{O}(t)|\mathcal{O}(t)) = 1$. This is easily implemented with the inclusion of $\sqrt{\mathcal{N}(E)}$ in the definition of $|\mathcal{O}(t))$, which would have given us,

$$(\mathcal{O}(t)|\mathcal{O}(t)) = \int_0^\infty dE\,\mathcal{N}(E) \sum_{n=0}^{D-1} \left|\phi_{E,n}(t)\right|^2 := 1, \tag{3.74}$$

and now we can choose $\sum_{n=0}^{D} \left|\phi_{E,n}(t)\right|^2 = 1$, giving us,

$$1 = \int_0^\infty dE\, \mathcal{N}(E), \tag{3.75}$$

which is a perfectly reasonable normalization condition. Had we not included $\sqrt{\mathcal{N}(E)}$ in the definition of $|\mathcal{O}(t))$ and still chosen $\sum_{n=0}^{D-1} \left|\phi_{E,n}(t)\right|^2 = 1$ then we would have obtained $1 = \int_0^\infty dE$ - which doesn't make any sense. We ought to note that the microcanonical inner product has been defined only for the fixed-energy time-independent operator GNS-states *i.e.* for $|\mathcal{O}_{E,n})$ and not for time dependent states, $|\mathcal{O}(t))$. The inner product on time dependent states $|\mathcal{O}(t))$ works as a regular inner product. We also have the boundary condition : $\phi_{E,n}(t) = \delta_{n,0} \forall E \in [0,\infty)$ which ensures that at time $t = 0$ we start with the desired initial operator *i.e.* $\mathcal{O}(0) = \mathcal{O}_0$ or $|\mathcal{O}(0)) = \int_0^\infty dE \sqrt{\mathcal{N}(E)}\, |\mathcal{O}_{E,0}) \forall\, E \in [0,\infty)$. This can be explicitly verified by calculating $|\mathcal{O}(t))\big|_{t=0}$ and setting it equal to $\int_0^\infty dE \int_{-2E}^{2E} d\omega\, \rho(E,\omega)\, \mathcal{O}(E,\omega)\ \left|E + \frac{\omega}{2}\right\rangle \left\langle E - \frac{\omega}{2}\right|$.

With regards to computing Krylov complexity, the Liouvillian again assumes a tridiagonal form in the Krylov basis for a fixed energy sector due to the following recurrence relations.

$$\mathscr{L} = \begin{pmatrix} 0 & b_1^E & 0 & 0 & \cdots \\ b_1^E & 0 & b_2^E & 0 & \cdots \\ 0 & b_2^E & 0 & b_3^E & \cdots \\ 0 & 0 & b_3^E & 0 & \cdots \\ \vdots & \vdots & \vdots & \vdots & \ddots \end{pmatrix}. \tag{3.76}$$

And correspondingly, the complexity wavefunction recurrence relations go by,

$$\dot{\phi}_{E,n}(t) = b_{n+1}^E \phi_{E,n+1} - b_n^E \phi_{E,n-1}(t), \tag{3.77}$$

which can be solved for $\phi_{E,n}(t)$ in each energy sector and be used to compute the corresponding Krylov complexity.

As an illustrative example, we consider the Krylov complexity corresponding to a thermal field theory. The time-evolved two-point function at canonical temperature β for a generic thermal field theory is given as,

$$\mathrm{Tr}\left[e^{-\frac{\beta H}{2}}\, \mathcal{O}(0)\, e^{-\frac{\beta H}{2}}\, \mathcal{O}(t)\right] = \int_0^\infty dE\, e^{-\beta E}{}_E\left(\mathcal{O}(0)|\mathcal{O}(t)\right)_E. \tag{3.78}$$

We need to use the microcanonical inner product definition to calculate ${}_E(\mathcal{O}(0)|\mathcal{O}(t))_E$ but at fixed energy. So, we can use $|\mathcal{O}(t))_E = \mathcal{N}(E)^{\frac{1}{2}} \sum_{n=0}^{D-1} \phi_{E,n}(t)\, i^n\, |\mathcal{O}_{E,n})$, which is just the expansion of $|\mathcal{O}(t))$ in the Krylov basis but at fixed E so there is no integration over E. So,

$$\begin{aligned} {}_E(\mathcal{O}(\tilde{t})|\mathcal{O}(t))_E &= \left[\sqrt{\mathcal{N}(E)} \sum_{m=0}^{D-1} \phi_{E,m}^*(\tilde{t})(-i)^m (\mathcal{O}_{E,m}|\right]\left[\sqrt{\mathcal{N}(E)} \sum_{n=0}^{D-1} \phi_{E,n}(t)\, i^n\, |\mathcal{O}_{E,n})\right] \\ &= \mathcal{N}(E) \sum_{m,n=0}^{D-1} \phi_{E,m}^*(\tilde{t}) \phi_{E,n}(t)\ (-i)^m\, i^n\, (\mathcal{O}_{E,m}|\mathcal{O}_{E,n}). \end{aligned} \tag{3.79}$$

Using $(\mathcal{O}_{E,n}|\mathcal{O}_{E,m}) = \delta_{nm}$, $\phi_{E,n}(0) = \delta_{n0}$ and taking $\tilde{t} = 0$ we get,

$$_E(\mathcal{O}(\tilde{t})|\mathcal{O}(t))_E = \mathcal{N}(E)\sum_{n=0}^{D-1}\phi^*_{E,n}(0)\phi_{E,n}(t)(i\times -i)^n = \mathcal{N}(E)\sum_{n=0}^{D-1}\delta_{n0}\,\phi_{E,n}(t) = \mathcal{N}(E)\,\phi_{E,0}(t). \tag{3.80}$$

The thermal two-point function now becomes,

$$\mathrm{Tr}\left[e^{-\frac{\beta H}{2}}\mathcal{O}(0)e^{-\frac{\beta H}{2}}\mathcal{O}(t)\right] = \mathcal{N}(E)\int_0^\infty dE\, e^{-\beta E}\phi_{E,0}(t). \tag{3.81}$$

In any fixed average energy sector E, we can now present a definition of the Krylov complexity of the time evolved operator as,

$$\boxed{C_E\left[\mathcal{O}(t)\right] = \sum_{n=0}^{D_E-1} n\left|\phi_{E,n}(t)\right|^2.} \tag{3.82}$$

Generically, our object of interest is not the Krylov complexity restricted to a fixed energy sector, but rather that of the full time-evolved operator $\mathcal{O}(t)$ as an excitation over the thermal state $e^{-\beta H}$. Since the different average energy sectors follow a thermal distribution, the thermal K-complexity of $\mathcal{O}(t)$ is defined by the formula,

$$\boxed{C_{\text{th}}\left[\mathcal{O}(t)\right] = \frac{\int_0^\infty dE\, e^{-\beta E}\,\mathcal{N}(E)\,C_E(t)}{\int_0^\infty dE\, e^{-\beta E}\mathcal{N}(E)}.} \tag{3.83}$$

With this, we conclude our discourse on the theoretical foundations of Krylov complexity.

3.7 Computational Approaches to Krylov Complexity

Having established the two notions of Krylov complexity, a unifying framework, and a continuum description for them we'd like to turn our attention to computing the Krylov operator/spread complexity in specific, hopefully great, examples to establish the soundness of the motivated proposal of this thesis. To that end, we make note of a few computational approaches to computing the relevant Krylov complexity. After rigorously delving into the framework supporting Krylov complexity, we actually turn to the task of *not* using that same framework. It might seem counter-intuitive at first, but there is a very straightforward reason to do so, which is that the full Krylov subspace method including the Lanczos algorithm etc is often rather cumbersome to perform, if not outright impractical. There are, however, some tricks-of-the-trade in an ever growing dictionary that make the computation of Krylov complexity much more approachable and, in the right setup, even completely analytically tractable. Hence, in this section, we compile a brief mention of the computational approaches to Krylov complexity, besides the usual Krylov subspace method which we have already demonstrated in full glory to develop the framework, with the detailed demonstrations deferred to later chapters or literature, as appropriate. An overview of some tricks that can be utilized to compute Krylov complexity numerically with minimal resources (basically, an everyday notebook computer) is provided in

App.(E).

1. *Coherent States*

   Let us assume that a quantum system is described by a Hamiltonian H which constitutes some Lie algebra $\mathfrak{a}$ e.g. $\mathfrak{su}(2,\mathbb{C})$ of a symmetry group *i.e.* $H \in \mathfrak{a}$. As is usual for physics, presence of symmetry lends to a simplification in the analytical solution of the relevant problem. The Krylov complexity conveniently follows this rule-of-thumb observation. It was realized in [35] and [106] that the computation for Krylov complexity is significantly less complex, for a researcher, if $H \in \mathfrak{a}$.

   More specifically, the generalized coherent states corresponding to the symmetry group constitute the Krylov basis! So, in these cases, much of the machinery that has been developed in this chapter to generate the Krylov basis can be conveniently skipped by simply identifying, if it exists, the symmetry algebra to which the Hamiltonian belongs and constructing the generalized coherent states with respect to the corresponding symmetry group. The unitary generalized displacement operator obtained through the exponential action of the elements of $\mathfrak{a}$ serves to generate all the coherent states, with assistance from the Baker-Campbell-Hausdorff formulae, from the lowest-weight state (or any other weight state, as desired). In this sense, the unitary time evolution effected through the Hamiltonian is generating trajectories in the coherent state manifold by expressing the circuit states in terms of the coherent basis. This approach has been used in the Chs.4 and 5 - with the procedure made explicit in the former.

2. *Moments Method*

   Another way to interpret Krylov complexity is as a repackaging of the information contained in the survival/return amplitude of an initial reference state *i.e.* the probability amplitude for the reference state to persist upon time-evolution. In this method, the computation involves generating the Lanczos coefficients through the moments of the return amplitude via a Hankel transformation and solving (3.19) to successively or simultaneously generate the complexity wavefunctions, whose weighted probabilities upon summation equal to the Krylov complexity.

   Importantly, this method can be used in conjunction to the coherent state expression of the circuit *i.e.* first, the circuit states are rewritten in terms of the generalized coherent state basis (which is also the Krylov basis); and then, the circuit which acts as a 2-pt function equivalent to the return amplitude can be used as an input to the moments method quickly generating the Lanczos coefficients. Thereafter, complexity can be computed by solving for the complexity wavefunctions in (3.19).

   Even more importantly, the moments approach lends itself very well to making approximations to the Krylov complexity. There are well established techniques across literature to expand generic 2-pt functions at various orders. This can serve to obtain approximate results for Krylov complexity analytically, as well as to assist in establishing the accuracy of numerical results. An example of the same was seen in, [108] and [107]. The former computed the Krylov complexity in a 2D JT Gravity theory up to first order in expansion and merely observed a growing profile. It was conjectured that including corrections will furnish the expected plateau. The latter, then, demonstrated the same - although, as

a byproduct[1]. This method is further explored in App.(E).

3. *Toda chain*

   This method is closely related to the recursion method and was first implemented in the context of Krylov subspace methods in [137], with the first application to computing Krylov complexity appearing in [138]. The Toda chain assists in extracting the Lanczos coefficients and hence serves as an alternative to the moments method, though suffers from similar numerical instabilities as it. There is no particular computational advantage to using the Toda chain method to our knowledge and it is briefly mentioned for the sake of a compilation of known computational methods associated with the Krylov subspace methods. The details of implementing Toda chain to complete Krylov complexity are provided in [137, 138].

3.8 The Proposal

We have now developed an appropriate background in Krylov complexity, and its computation. The proposal we made at the beginning of this thesis was the robust utility of Krylov complexity to detect quantum phase transitions and, of course, we need to test this proposal. Before moving ahead to the hypothesis-testing phase, we take a step back and understand the merit of our hypothesis *i.e.* since we now have a mathematical grounding in Krylov complexity, are there any arguments we can make *a priori* that would be able to justify the resources that shall be devoted to computing Krylov complexity for various models. We present two efforts in this direction below, and identify two classes of quantum phase transitions that Krylov complexity can identify.

1. *Topological Phase Transitions*

   We remarked earlier in Ch.2.3 that Nielsen provided a geometric interpretation to circuit complexity in [21, 22]. This was further extended in [139], with the identification of circuit complexity as the minimal geodesic length of a Riemannian geometry on the space of unitary operators. This geometry is endowed as a result of the cost function $F(H(t))$, since an arbitrary unitary acn be generated through a time-dependent Hamiltonian. Now, a topological phase transitions, by its very definition, is accompanied by a change in the underlying geometry and hence a change in geometry consequently leads to a change in the minimal geodesic length and, hence, the complexity. So, circuit complexity is expected to show signatures of topological phase transitions. Likewise, a geometric interpretation to Krylov complexity was introduced in [35] as a quantity proportional to volume of a specific geometry. This implies that across topological phase boundaries the geometry, and the associated topological invariant, changes - thereby leaving characteristic signatures on the Krylov complexity.

[1] We had been computing the same concurrently when the results in [107] appeared on the preprint arXiv, admittedly, in a nicer setup.

2. *Dynamical Phase Transitions*

We observed in Ch.3.1 that the operator evolution dynamics, in the Heisenberg representation, can be effected through an operator called the Liouvillian operator. We further noted that in the energy eigenbasis, the spectrum of the Liouvillian is just the differences of energy eigenvalues *i.e.* $\sigma(\mathscr{L}) = \{\omega_{mn}\ ;\ m, n \in 1, \cdots, D\}$ with D being the dimension of the corresponding Hilbert space. Furthermore, the energy eigenbasis encodes and is sensitive to a system's symmetries. This means that an operator with a spectrum consisting of the corresponding eigenvalues would similarly encode those same symmetries. Since, distinct phases of matter correspond to distinct flavors of symmetries - one expects Krylov basis (generated through $\mathscr{L}$), and any suitable observable constructed in that basis, to be sensitive to dynamical phase transitions and the other phase transitions that correspond to a change in symmetries. There are, however, subtleties in the interplay of symmetry and the ability of Krylov complexity to unveil chaos as discussed in relation to the incorrect results obtained in [121]. These subtleties may extend to Krylov complexity's ability to unveil phase transitions as well - which is an open direction of research and, to our knowledge, has not been explored.

4 Application I : Kitaev Chain

"What we observe is not nature itself, but nature exposed to our method of questioning."
- Werner Heisenberg

Now that we've established the framework formalizing the structure defining Krylov/spread complexity and having good motivation that the proposal is sound - as well as meritorious - we'd like to turn our attention to finding suitable examples to test out the proposal, colloquially known as 'toy models' in physics. Toy models come with various properties with their defining characteristic being their ability to 'model' *i.e.* simulate a phenomenon or system - while, ideally, being significantly easier to solve compared to their parent aspect. Exceptional toy models are those that elucidate physics beyond the phenomena they model - the most-widely known example being the harmonic oscillator. We bring the Krylov subspace toolkit to a similarly exceptional toy model - the Kitaev chain and compute spread complexity in this model [1]. The spread complexity shows characteristic behavior across topological phase transitions.

4.1 The Model and Properties

Kitaev chain is a quantum wire model of tight-binding one-dimensional chain of spinless electrons together with a superconducting interaction. It was introduced by Alexei Kitaev [36] in 2001 as an attempt at building a stable quantum memory by way of constructing degrees of freedom safe from decoherence. Kitaev chain exhibits these degrees of freedom: uncoupled Majorana fermions or Majorana edge modes. Etymologically, the former indicates the fact that generically Majorana fermions occur as bounded pairs in toy models while the latter signifies that the uncoupled Majorana fermions occur on edges or defects *i.e.* not throughout the bulk. There has been no experimental confirmation of existence of Majorana fermions, at least not one that's conclusive and widely agreed to - though it has often been claimed in literature [140–145]. Having decoherence protected degrees of freedom is advantageous for various quantum-technological applications, including quantum computers.

The Kitaev chain Hamiltonian H_K is given as,

$$H_K \equiv H_K(J,\mu,\Delta) = \sum_{j=1}^{L-1}\Bigg[\underbrace{-\frac{J}{2}\left(c_j^\dagger c_{j+1} + c_{j+1}^\dagger c_j\right)}_{\text{hopping terms}} \underbrace{-\mu\left(c_j^\dagger c_j - \frac{1}{2}\right)}_{\text{chemical potential}} \underbrace{+\frac{\Delta}{2}\left(c_j^\dagger c_{j+1}^\dagger + c_{j+1} c_j\right)}_{\text{p-wave superconducting term}}\Bigg], \tag{4.1}$$

with L denoting the lattice sites in the quantum wire and $c_j^\dagger / c_j$ at site j the spinless fermionic creation/annihilation operators defined via the algebra $\left\{c_j^\dagger, c_k\right\} = \delta_{jk}$.

The structure of H_K is motivated by the following arguments. An arbitrary quadratic Hamiltonian can be expressed via the following generic form,

$$H = \frac{i}{4}\sum_{m,n} A_{mn}\gamma_m\gamma_n\,, \qquad A^*_{mn} = A_{mn} = -A_{nm}, \tag{4.2}$$

with γ_l, the Majoranas, being specific linear combinations of normal modes of fermionic creation and annihilation operators.

The ground state of this generic quadratic Hamiltonian can be recast as pairs of Majorana fermions. A few Majorana operators which are localized to defects / boundary remain free while all the others are paired with an energy gap. For the unpaired Majorana modes to occur it is necessary for two conditions to be met:

- the $U(1)$ symmetry associated with the conservation of electric charge, $c_j \mapsto e^{i\phi}c_j$, needs to be reduced to a $\mathbb{Z}_2$ symmetry, $c_j \mapsto -c_j$. In fact, if a single Majorana operator is to be localized it must not mix with other operators upon a symmetry transformation making it natural to consider superconducting systems - with the specific mechanics of superconductivity not being particularly important; and,
- the electron spectrum must strongly depend on the spin.

The Hamiltonian is composed of three terms : a tight-binding adjacent-only hopping term with strength J, a chemical potential term with strength μ, and a p-wave superconducting term with gap Δ - which in general is complex but the argument can be absorbed into the fermionic operators : $c_j \to e^{i\frac{1}{2}\arg\Delta}c_j$ to furnish a $\Delta > 0$. The choice of a positive or negative Δ results in the scale factor $e^{i\frac{1}{2}\arg\Delta} = \pm 1$ or $\pm i$. As a result, all three parameters for the Kitaev chain model can be taken as real valued. Gap-closing in the quasiparticle spectrum indicates a topological phase transition, which in the continuum limit $L >> 1$, translates to a topologically non-trivial phase for $\left|\frac{\mu}{J}\right| < 1$ with degenerate ground state and topologically trivial phase for $\left|\frac{\mu}{J}\right| > 1$ with unique ground state (regardless of the boundary conditions) such that the transition occurs at $\left|\frac{\mu}{J}\right| = 1$. There are exactly two topological phases in the $\left(\frac{\Delta}{J} - \frac{\mu}{J}\right)$ plane, distinguished through $\Delta = 0$, since the winding number of the topological phase is determined through the sign of Δ which we choose as a real positive parameter.

We also note the connections of Kitaev chain model to other widely-used toy models [146–148]:

- for appropriate choices of J, Δ the Kitaev chain is connected to the transverse-field Ising model via a Jordan-Wigner (JW) transformation;
- with $\Delta = 0$, along with the Jordan-Wigner transformation, the Kitaev chain maps to the isotropic limit of the XY model.

We briefly demonstrate the above two connections. To that end, note that these models only involved quadratic (at most) nearest-neighbor interactions and hence, the corresponding JW transformation con-

necting spin-$\frac{1}{2}$ fermions to spin operators are useful to note [148],

$$\begin{aligned} c_j^\dagger c_j &= \frac{1}{2}\left(1+\sigma_j^z\right) \\ c_{j+1}^\dagger c_j &= \sigma_{j+1}^+ \sigma_j^- \\ c_{j+1}^\dagger c_j^\dagger &= -\sigma_{j+1}^+ \sigma_j^+, \end{aligned} \tag{4.3}$$

where $c_j^\dagger / c_j$ are the fermionic creation-annihilation operators and σ^i are the three Pauli matrices for $i \in \{x, y, z\}$. The above JW transformations can now be substituted in (4.1), to obtain the following:

$$\begin{aligned} H_K^{\mathrm{JW}} &= -\frac{J}{2}\sum_j \left\{\sigma_j^+\sigma_{j+1}^- + \sigma_{j+1}^+\sigma_j^-\right\} - \mu \sum_j \left\{\frac{\mathbb{1} + \sigma_j^z}{2} - \frac{\mathbb{1}}{2}\right\} + \frac{\Delta}{2}\sum_j \left\{-\sigma_j^+\sigma_{j+1}^+ - \sigma_j^-\sigma_{j+1}^-\right\} \\ &= \frac{J}{8}\sum_j \left\{\sigma_j^x\sigma_{j+1}^x - \cancel{i\sigma_j^x\sigma_{j+1}^y} + \cancel{i\sigma_j^y\sigma_{j+1}^x} + \sigma_j^y\sigma_{j+1}^y + \sigma_{j+1}^x\sigma_j^x - \cancel{i\sigma_{j+1}^x\sigma_j^y} + \cancel{i\sigma_{j+1}^y\sigma_j^x} + \sigma_{j+1}^y\sigma_j^y\right\} \\ &\quad - \mu\sum_j \frac{\sigma_j^z}{2} \\ &\quad - \frac{\Delta}{8}\left\{\sigma_j^x\sigma_{j+1}^x + \cancel{i\sigma_j^x\sigma_{j+1}^y} + \cancel{i\sigma_j^y\sigma_{j+1}^x} - \sigma_j^y\sigma_{j+1}^y + \sigma_j^x\sigma_{j+1}^x - \cancel{i\sigma_j^x\sigma_{j+1}^y} - \cancel{i\sigma_j^y\sigma_{j+1}^x} - \sigma_j^y\sigma_{j+1}^y\right\} \\ &= -\frac{J}{4}\sum_j \left\{\sigma_j^x\sigma_{j+1}^x + \sigma_j^y\sigma_{j+1}^y\right\} - \mu\sum_j\left\{\frac{\sigma_j^z}{2}\right\} - \frac{\Delta}{4}\sum_j\left\{\sigma_j^x\sigma_{j+1}^x - \sigma_j^y\sigma_{j+1}^y\right\}. \end{aligned} \tag{4.4}$$

The spin operators are expressed as $S^i = \frac{\sigma^i}{2}$ for $i \in \{x, y, z\}$, leading to the following Jordan-Wigner transformed Kitaev Hamiltonian,

$$\boxed{H_K^{\mathrm{JW}} = -J\sum_j \left\{S_j^x S_{j+1}^x + S_j^y S_{j+1}^y\right\} - \mu\sum_j S_j^z - \Delta\sum_j\left\{S_j^x S_{j+1}^x - S_j^y S_{j+1}^y\right\}.} \tag{4.5}$$

Clearly, choosing $\Delta = 0$ leads to the transverse field Ising equation if one interprets μ as the magnetic field strength $\hbar$,

$$H_K^{\mathrm{JW}}\Big|_{\Delta=0,\ \mu=\hbar} = -J\sum_j \left\{S_j^x S_{j+1}^x + S_j^y S_{j+1}^y\right\} - \hbar\sum_j S_j^z = H_{\mathrm{Ising}}. \tag{4.6}$$

Likewise, parameterizing $\Delta = \gamma J$ and again identifying μ as the magnetic field strength $\hbar$ leads to,

$$H_K^{\mathrm{JW}}\Big|_{\Delta=\gamma J,\ \mu=\hbar} = -J\sum_j \left\{(1+\gamma)S_j^x S_{j+1}^x + (1-\gamma)S_j^y S_{j+1}^y\right\} - \hbar\sum_j S_j^z = H_{\mathrm{XY}}, \tag{4.7}$$

the anisotropic XY model, and with a choice of $\gamma = \pm 1$ this reduces to the isotropic XY model.

We should stress that JW transformations are generically (highly) non-local, and as such transform the properties of a model (and consequently the physics) drastically. Such correspondences are more mathematical

than physical correspondences [148], and enable building duality webs that help solve various models along with establishing some classification among the myriad of models. The Ising and XY models, themselves dual to other models like the Coulomb gas model and SOS models [149], are found to describe aspects of a wide range of physics from thin films and crystal growth to superconductivity and exhibit rich phenomena like vortices, Kosterlitz Thouless (KT) phase transitions [150,151] that constitute the contemporary studies of quantum matter. This highlights the ubiquity of the Kitaev chain and the primary reason for consideration under this work.

4.2 Majorana Modes in Kitaev chain

Having argued that the Kitaev chain hosts unpaired Majorana modes, let us take a closer look and explicitly uncover the presence of unpaired Majorana modes. A Majorana mode or fermion, by definition, is its own anti-particle and hence can be represented by an operator γ_k in quantum state k such that $\gamma_k = \gamma_k^\dagger$ *i.e.* the operators creating and annihilating Majorana fermions are same! One choice of the convention to describe these in terms of conventional (Dirac) fermionic operators, $c^\dagger$ and c, is as follows,

$$c^\dagger = \frac{\gamma_1 + i\gamma_2}{2}, \qquad c = \frac{\gamma_1 - i\gamma_2}{2}. \tag{4.8}$$

Note that there are two Majoranas associated to each fermionic operator localized at each lattice site. Following the algebra defining Dirac fermionic operators, $\left\{c_l^\dagger, c_m\right\} = \delta_{lm}$, it is readily established that,

$$\begin{aligned} \gamma_k^2 &= 1, \\ \left[\gamma_l, \gamma_m\right] &= 2\delta_{lm}. \end{aligned} \tag{4.9}$$

Let us define the following Majorana operators for sites $n = 1, 2, ..., N$,

$$\gamma_{2n-1} = c_n + c_n^\dagger, \quad \text{and} \quad \gamma_{2n} = i\left(c_n - c_n^\dagger\right). \tag{4.10}$$

Expressing the Kitaev chain Hamiltonian in terms of these Majoranas and rescaling the chemical potential we obtain,

$$\boxed{H_K(J, 2\mu, \Delta; \gamma) = i\sum_{n=1}^{N-1}\left[J_x\,\gamma_{2n}\gamma_{2n+1} - J_y\,\gamma_{2n-1}\gamma_{2n+2}\right] + i\sum_{n=1}^{N}\mu\,\gamma_{2n-1}\gamma_{2n},} \tag{4.11}$$

with $J_x = \frac{1}{2}(t - \Delta)$ and $J_y = \frac{1}{2}(t + \Delta)$. Let us explore the parameter space of this Hamiltonian to uncover some unpaired Majoranas:

- Case I : $t = \Delta$ and $\mu = 0 \mapsto J_x = 0$ and $J_y = t$ such that $H = -i\sum_{n=1}^{N-1}\left[t\,\gamma_{2n-1}\gamma_{2n+2}\right]$; and,
- Case II : $t = -\Delta$ and $\mu = 0 \mapsto J_y = 0$ and $J_x = t$ such that $H = i\sum_{n=1}^{N-1}\left[t\,\gamma_{2n}\gamma_{2n+1}\right]$.

In the former case, the even Majorana at the left end and the odd Majorana at the right end have decoupled from the chain. Likewise, for the latter case the opposite holds true. These are the unpaired Majoranas we

argued were present in the Kitaev chain [1]. These modes are, etymologically, also known as Majorana Zero Modes and are present due to the degenerate nature of the ground state. Furthermore, these Majorana Zero Modes are localized at the boundary of the chain and hence are also termed as edge modes. Another point of note is that, strikingly, the presence of unpaired Majoranas is not an artefact of specific choice of parameters, but rather is a genuine phenomenon of Kitaev chain. These unpaired modes persist as long as the bulk gap remains finite due to a phenomenon known as Symmetry Protected Topological Phases.

4.3 Spread Complexity

Having studied the Kitaev chain model in some detail, examined its phase structure, and uncovered unpaired Majoranas we are now in an ideal position to test whether spread complexity shows distinguishing behavior across Topological Phase Transitions of Kitaev chain at $\left|\frac{\mu}{J}\right| = 1$. To that effect let us use the formalism identified in Ch.3.

4.3.1 Step I: BdG Procedure

The BdG, for Bogoliubov-de-Gennes, procedure essentially boils down to expressing the Hamiltonian in terms of the normal modes of the fermionic Dirac creation and annihilation operators as a way to easily diagonalize it. To this effect, let's obtain these normal modes by considering Fourier Transformations of the ladder operators,

$$a_k = \frac{1}{\sqrt{L}} \sum_{j=1}^{L} c_j e^{+ikj}, \quad a_k^\dagger = \frac{1}{\sqrt{L}} \sum_{j'=1}^{L} c_{j'}^\dagger e^{-ikj'}. \tag{4.12}$$

To express the Hamiltonian in terms of these normal modes, a_k and $a_k^\dagger$, it is necessary to understand their commutation (or anti-commutation) properties to uncover the associated algebra behind these definitions. Since these are normal modes of fermionic operators, we analyze the anti-commuting properties. As expected this furnishes the usual fermionic relations,

$$\begin{aligned} \left\{a_k, a_{k'}^\dagger\right\} &= \frac{1}{L} \sum_{j,j'=1}^{L} e^{i(kj-k'j')} \left\{c_j, c_{j'}^\dagger\right\} \\ &= \frac{1}{L} \sum_{j,j'=1}^{L} e^{i(kj-k'j')} \delta_{j,j'} \\ &= \frac{1}{L} \sum_{j=1}^{L} e^{i(k-k')j} = \delta_{k,k'}. \end{aligned} \tag{4.13}$$

[1] For a nice visualization of the presence of Majoranas via Python see the blog post that this part follows.

Summarily,

$$\begin{aligned}\left\{a_k, a_{k'}^\dagger\right\} &= \delta_{k,k'},\\ \left\{a_k, a_{k'}\right\} &= 0,\\ \left\{a_k^\dagger, a_{k'}^\dagger\right\} &= 0.\end{aligned} \tag{4.14}$$

We will now recast the H_K in terms of $\left\{a_k, a_k^\dagger;\ \forall\ k\right\}$. To that purpose, we will need the inverse Fourier transforms,

$$c_j = \frac{1}{\sqrt{L}} \sum_{k\in \mathrm{BZ}} e^{-ikj} a_k\,, \quad c_j^\dagger = \frac{1}{\sqrt{L}} \sum_{k'\in \mathrm{BZ}} e^{+ik'j} a_{k'}^\dagger. \tag{4.15}$$

Let's see how the hopping terms are expressed in terms of these normal modes,

$$\begin{aligned}\sum_{j=1}^{L} c_{j+1}^\dagger c_j + c_j^\dagger c_{j+1} &= \frac{1}{L}\sum_{j=1}^{L}\left[\sum_{k,k'\in \mathrm{BZ}} e^{ik'(j+1)-ikj} a_{k'}^\dagger a_k + \sum_{k,k'\in \mathrm{BZ}} e^{ik'j-ik(j+1)} a_{k'}^\dagger a_k\right]\\ &= \frac{1}{L}\sum_{j=1}^{L}\sum_{k,k'\in \mathrm{BZ}}\left[e^{ik'(j+1)-ikj} + e^{ik'j-ik(j+1)}\right] a_{k'} a_k\\ &= \sum_{k,k'\in \mathrm{BZ}}\left(\frac{1}{L}\sum_{j=1}^{L} e^{i(k'-k)j}\right)\left[e^{ik'} + e^{-ik}\right] a_{k'}^\dagger a_k\\ &= \sum_{k,k'\in \mathrm{BZ}} \delta_{k,k'}\left(e^{ik'} + e^{-ik}\right) a_{k'}^\dagger a_k\\ &= 2\sum_{k\in \mathrm{BZ}} \cos(k)\, a_k^\dagger a_k\\ &= 2\sum_{\substack{k\in \mathrm{BZ}\\ k>0}} \cos(k)\left(a_k^\dagger a_k + a_{-k}^\dagger a_{-k}\right).\end{aligned} \tag{4.16}$$

So we have the transformation of the hopping terms,

$$\sum_{j=1}^{L} c_{j+1}^\dagger c_j + c_j^\dagger c_{j+1} = 2\sum_{\substack{k\in \mathrm{BZ}\\ k>0}} \cos(k)\left(a_k^\dagger a_k + a_{-k}^\dagger a_{-k}\right). \tag{4.17}$$

It can be observed that the hopping in physical space translates, pun intended, to just creating degrees of freedom in positive and negative momentum states - as expected. Similarly, the superconducting terms should just pair up degrees of freedom with positive and negative momentum so as to form Cooper pairs. This is easily verified.

$$\sum_{j=1}^{L} c_j^\dagger c_{j+1}^\dagger + c_{j+1} c_j = \frac{1}{L}\sum_{j=1}^{L}\sum_{k,k'\in \mathrm{BZ}}\left[e^{ikj+ik'(j+1)} a_k^\dagger a_{k'}^\dagger + e^{-ik'(j+1)-ikj} a_{k'} a_k\right]$$

$$
\begin{aligned}
&= \sum_{k,k'\in \mathrm{BZ}} \left[\left(\frac{1}{L} \sum_{j=1}^{L} e^{i(k+k')j} \right) e^{ik'} a_k^\dagger a_{k'}^\dagger + \left(\frac{1}{L} \sum_{j=1}^{L} e^{-i(k+k')j} \right) e^{-ik'} a_{k'} a_k \right] \\
&= \sum_{k,k'\in \mathrm{BZ}} \left[\delta_{k,-k'} e^{ik'} a_k^\dagger a_{k'}^\dagger + \delta_{k,-k'} e^{-ik'} a_{k'} a_k \right] \\
&= \sum_{k\in \mathrm{BZ}} \left[e^{-ik} a_k^\dagger a_{-k}^\dagger + e^{ik} a_{-k} a_k \right] \\
&= \sum_{\substack{k\in \mathrm{BZ} \\ k>0}} \left[\left(e^{-ik} - e^{ik} \right) a_k^\dagger a_{-k}^\dagger + \left(e^{ik} - e^{-ik} \right) a_{-k} a_k \right] \\
&= \sum_{\substack{k\in \mathrm{BZ} \\ k>0}} \left[2i \sin(k)\, a_{-k} a_k - 2i \sin(k)\, a_k^\dagger a_{-k}^\dagger \right] \\
&= 2i \sum_{\substack{k\in \mathrm{BZ} \\ k>0}} \sin(k) \left(a_{-k} a_k - a_k^\dagger a_{-k}^\dagger \right).
\end{aligned} \tag{4.18}
$$

Hence, the transformation of the superconducting terms is given as,

$$
\sum_{j=1}^{L} c_j^\dagger c_{j+1}^\dagger + c_{j+1} c_j = 2i \sum_{\substack{k\in \mathrm{BZ} \\ k>0}} \sin(k) \left(a_{-k} a_k - a_k^\dagger a_{-k}^\dagger \right). \tag{4.19}
$$

Finally, let's compute the chemical potential terms' transformation, which keeps track of the number of fermions in the system with the factor of negative half re-scaling the ground state energy to make the Hamiltonian gap-less at $(J, \Delta) = (0, 0)$, so isn't expected to furnish terms different from the ones obtained above,

$$
\begin{aligned}
\sum_{j=1}^{L} c_j^\dagger c_j &= \frac{1}{L} \sum_{j=1}^{L} \sum_{k,k'\in \mathrm{BZ}} e^{i(k'-k)j} a_{k'}^\dagger a_k \\
&= \sum_{k,k'\in \mathrm{BZ}} \left(\frac{1}{L} \sum_{1}^{L} e^{i(k'-k)} j \right) a_{k'}^\dagger a_k \\
&= \sum_{k,k'\in \mathrm{BZ}} \delta_{k,k'} a_{k'}^\dagger a_k \\
&= \sum_{k\in \mathrm{BZ}} a_k^\dagger a_k = \sum_{\substack{k\in \mathrm{BZ} \\ k>0}} \left(a_k^\dagger a_k + a_{-k}^\dagger a_{-k} \right).
\end{aligned} \tag{4.20}
$$

Hence, the transformation is given as,

$$
\sum_{j=1}^{L} c_j^\dagger c_j = \sum_{\substack{k\in \mathrm{BZ} \\ k>0}} \left(a_k^\dagger a_k + a_{-k}^\dagger a_{-k} \right). \tag{4.21}
$$

We can now put the above transformations together and observe that the Hamiltonian is diagonalized in terms of the normal modes of the fermionic operators,

$$H_K = \sum_{\substack{k\in \mathrm{BZ}\\ k>0}} \left[-J\cos(k)\left(a_k^\dagger a_k + a_{-k}^\dagger a_{-k}\right) - \mu\left(a_k^\dagger a_k + a_{-k}^\dagger a_{-k} - \frac{1}{2}\right) + i\Delta\sin(k)\left(a_{-k}a_k - a_k^\dagger a_{-k}^\dagger\right)\right], \tag{4.22}$$

$$H_K = \left[-\frac{\mu}{2} - \sum_{\substack{k\in \mathrm{BZ}\\ k>0}} J\cos(k)\right] + \sum_{\substack{k\in \mathrm{BZ}\\ k>0}} \underbrace{\begin{pmatrix} a_k^\dagger & a_{-k}\end{pmatrix}}_{\chi_k^\dagger} \underbrace{\begin{pmatrix} -J\cos(k)-\mu & -i\Delta\sin(k) \\ i\Delta\sin(k) & J\cos(k)+\mu\end{pmatrix}}_{H_{\mathrm{BdG}}(J,\Delta,\mu)} \underbrace{\begin{pmatrix} a_k \\ a_{-k}^\dagger\end{pmatrix}}_{\chi_k}. \tag{4.23}$$

The 2×2 matrix $H_{\mathrm{BdG}}(J,\mu,\Delta)$, hereafter referred simply as H_{BdG}, looks suspiciously like an element of the Lie algebra $\mathfrak{su}(2)$. Let's test these suspicions. H_{BdG} would be an element of $\mathfrak{su}(2)$ if we can find $a,b,c,d\in\mathbb{C}$ such that,

$$\begin{aligned}\begin{pmatrix} -J\cos(k)-\mu & -i\Delta\sin(k) \\ i\Delta\sin(k) & J\cos(k)+\mu\end{pmatrix} &= a\mathbb{I}_{2\times 2} + b\sigma_x + c\sigma_y + d\sigma_z \\ &= a\begin{pmatrix}1&0\\0&1\end{pmatrix} + b\begin{pmatrix}0&1\\1&0\end{pmatrix} + c\begin{pmatrix}0&-i\\i&0\end{pmatrix} + d\begin{pmatrix}1&0\\0&-1\end{pmatrix}.\end{aligned} \tag{4.24}$$

If we choose, $a=0, b=0, c=\Delta\sin(k), d=-J\cos(k)-\mu$, then the above is satisfied. We can further express H_{BdG} as,

$$H_{\mathrm{BdG}} = \vec{P}\cdot\vec{\sigma}, \tag{4.25}$$

where $P^T = \begin{pmatrix}0 & \Delta\sin(k) & -J\cos(k)-\mu\end{pmatrix}$. So, the BdG diagonalized Kitaev chain Hamiltonian is,

$$H_K = -\frac{\mu}{2} - \sum_{\substack{k\in \mathrm{BZ}\\ k>0}} J\cos(k) + \sum_{\substack{k\in \mathrm{BZ}\\ k>0}} \chi_k^\dagger\left(\vec{P}\cdot\vec{\sigma}\right)\chi_k. \tag{4.26}$$

4.3.2 Step II: Recasting H_{BdG} as an element of $\mathfrak{su}(2,\mathbb{C})$ algebra

Furthermore, it was demonstrated in [106] that if a Hamiltonian is of the generic form of (A.1) then the computation of spread complexity is further simplified beyond the coherent state simplification introduced earlier in the text,

$$H = -\sum_k \left[2R_3 J_0^{(k)} + iR_1\left(J_+^{(k)} - J_-^{(k)}\right)\right]. \tag{4.27}$$

For such a specific Hamiltonian the ground state can be written as (see App.(A) for a detailed derivation),

$$|\Omega\rangle = \prod_{k>0} \mathcal{N}_k e^{-i\tan\left(\frac{\phi_k}{2}\right)\left(J_+^{(k)}+J_-^{(-k)}\right)} \left|\frac{1}{2},-\frac{1}{2}\right\rangle_k, \tag{4.28}$$

if $J_0^{(k)}, J_\pm^{(k)}$ are the generators of an $\mathfrak{su}(2,\mathbb{C})$ algebra. The Hamiltonian we have looks like, from (4.22),

$$H_K = \sum_{\substack{k\in \mathrm{BZ}\\ k>0}} \left[\left(-J\cos(k) - \mu\right)\left(a_k^\dagger a_k + a_{-k}^\dagger a_{-k}\right) - \frac{\mu}{2} + i\Delta \sin(k)\left(a_{-k}a_k - a_k^\dagger a_{-k}^\dagger\right)\right]. \tag{4.29}$$

If we make a particular choice of,

$$\begin{aligned} R_1 &= \Delta\sin(k), \quad R_3 = \left[J\cos(k) + \mu\right], \\ J_0^{(k)} &= \frac{1}{2}\left(a_k^\dagger a_k + a_{-k}^\dagger a_{-k}\right), \quad J_+^{(k)} = a_k^\dagger a_{-k}^\dagger, \text{ and } J_-^{(k)} = a_{-k}a_k, \end{aligned} \tag{4.30}$$

then it is easy to realize that the operators $J_{\pm/0}^{(k)}$ form a $\mathfrak{su}(2,\mathbb{C})$ algebra,

$$\begin{aligned} \left[J_0^{(k)}, J_+^{(k)}\right] &= \frac{1}{2}\left(\left[a_k^\dagger a_k, a_k^\dagger a_{-k}^\dagger\right] + \left[a_{-k}^\dagger a_{-k}, a_k^\dagger a_{-k}^\dagger\right]\right) \\ &= \frac{1}{2}\Bigg(a_k^\dagger \underbrace{a_k a_k^\dagger}_{\substack{\text{use}\\ \text{identity}}} a_{-k}^\dagger - \underbrace{a_k^\dagger a_{-k}^\dagger}_{\text{swap}} a_k^\dagger a_k + a_{-k}^\dagger a_{-k} \underbrace{a_k^\dagger a_{-k}^\dagger}_{\substack{\text{swap +}\\ \text{identity}}} - a_k^\dagger \underbrace{a_{-k}^\dagger a_{-k}^\dagger}_{\cancelto{0}{}} a_{-k}\Bigg) \\ &= \frac{1}{2}\left[a_k^\dagger\left(1 - a_k^\dagger a_k\right)a_{-k}^\dagger + a_{-k}^\dagger \underbrace{a_k^\dagger a_k^\dagger a_k}_{\cancelto{0}{}} - a_{-k}^\dagger\left(1 - a_{-k}^\dagger a_{-k}\right)a_k^\dagger\right] \\ &= \frac{1}{2}\left[a_k^\dagger a_{-k}^\dagger - \underbrace{a_k^\dagger a_k^\dagger}_{\cancelto{0}{}} a_k a_{-k}^\dagger + \underbrace{a_{-k}^\dagger a_{-k}^\dagger}_{\cancelto{0}{}} a_{-k}a_k^\dagger - a_{-k}^\dagger a_k^\dagger\right] = \frac{1}{2}\times 2a_k^\dagger a_{-k}^\dagger = a_k^\dagger a_{-k}^\dagger = J_+^{(k)}, \end{aligned} \tag{4.31}$$

and similarly. So we have,

$$\left[J_0^{(k)}, J_\pm^{(k)}\right] = \pm J_\pm^{(k)}, \quad \left[J_+^{(k)}, J_-^{(k)}\right] = 2J_0^{(k)}, \tag{4.32}$$

thereby ensuring that $J_0^{(k)}, J_\pm^{(k)}$ satisfy a $\mathfrak{su}(2,\mathbb{C})$ algebra. One can further simplify the ground state of the Kitaev chain Hamiltonian expressed as an element of $\mathfrak{su}(2,\mathbb{C})$ algebra using Baker-Campbell-Hausdorff formulae and the fact that coherent states, by definition, are eigenstates of the annihilation operator and hence the action of operators J_-^k on the lowest-weight state $\left|\frac{1}{2}, -\frac{1}{2}\right\rangle_k$ will be trivial upto some appropriate normalization factors,

$$\boxed{|\Omega\rangle = \prod_{k>0} \sin\left|\frac{\phi_k}{2}\right| \exp\left[e^{-i\psi_k}\cot\left(\frac{\phi_k}{2}\right)J_+^{(k)}\right]\left|\frac{1}{2}, -\frac{1}{2}\right\rangle_k,} \tag{4.33}$$

wherein the above we've introduced the following notation short-hands,

$$\boxed{\begin{aligned} R(k) &= \left|\vec{R}(k)\right| = \left|\left(\Delta\sin(k), 0, \left[J\cos(k)\right] + \mu\right)\right|, \\ \phi_k &= \arctan\left[\frac{|\Delta|\sin(k)}{\mu + J\cos(k)}\right] \ (\text{for } k > 0), \\ \psi_k &= \frac{\pi}{2} - \arg\Delta = \frac{\pi}{2} \ (\text{for } \Delta > 0). \end{aligned}} \tag{4.34}$$

It must be noted that throughout the discussion on Kitaev chain we've made a choice of convention to facilitate visual clarity of expressions: the momentum states represented through k are actually represented through k_n *i.e.* the momentum states have modes - corresponding to lattice sites 1 to L. The way to see this is to calculate the values of k_n - which come through requiring that the fermionic Dirac operators $c_j/c_j^\dagger$ follow appropriate commutation properties as well as imposing desired boundary conditions. The most general boundary condition for a chain with L sites can be expressed through the condition,

$$c_{L+1} = e^{i\phi}\, c_1, \tag{4.35}$$

with ϕ encapsulating the generic twist between the operator at $(L+1)^{\text{th}}$ site and the first site - as such, periodic boundary condition corresponds to $e^{i\phi} = 1$ and anti-periodic boundary condition corresponds to $e^{i\phi} = -1$, respectively capturing whether the $(L+1)^{\text{th}}$ operator is completely in-phase with the first one or completely out-of-phase. The generic twisted boundary condition corresponds to the momenta,

$$k_n = \frac{2\pi}{L}\left(-\left\lfloor\frac{L-1}{2}\right\rfloor + n + \frac{\phi}{2\pi}\right); \quad n = 0, 1, \ldots, L-1. \tag{4.36}$$

4.3.3 Step III: Choosing the circuit and computing spread complexity

It has been established previously that the eigenstates of the Kitaev chain can be expressed in terms of the $SU(2)$ spin-coherent states. We now have all the mathematical machinery needed to compute the spread complexity for any desired circuit connecting two any two states of the Kitaev chain Hamiltonian. We pick three different circuits and compute the spread complexity for the same. We observe that spread complexity captures the transitions of Kitaev chain in-and-out of the topologically non-trivial phase via all three considered circuits - in fact, it can be naturally understood to capture them for all circuits - of, conservatively, the Kitaev chain and the associated toy models, demonstrating the robustness of utility of spread complexity to diagnose these transitions. We shall make a choice of considering even L and anti-periodic boundary conditions to compute spread complexity - unless stated otherwise. Specific computation of spread complexity for the three circuits is deferred to App.(C). For all three circuits we make a choice of using the ground state of the Kitaev chain as the target state and distinguish the circuits by the choice of different, natural, reference states. We note that the spread complexity is symmetric under the exchange of the target and reference states. We choose s as the circuit parameter that captures a flow from the reference state ($s = 0$) to the target state ($s = 1$).

Let us put Baker-Campbell-Hausdorff formulae to utility and express the target ground state (4.33), of all three circuits we consider, into a more convenient form as,

$$\begin{aligned}
|\Omega(s=1)\rangle &= \bigotimes_{k>0} |\Omega_k(s=1)\rangle, \\
|\Omega_k(s=1)\rangle &= \exp\left[\frac{\pi-\varphi_k}{2} e^{-i\left(\frac{\pi}{2}-\arg\Delta\right)} J_+^{(k)} - \frac{\pi-\varphi_k}{2} e^{i\left(\frac{\pi}{2}-\arg\Delta\right)} J_-^{(k)}\right] \left|\frac{1}{2}, -\frac{1}{2}\right\rangle_k \\
&= \exp\left[-i\frac{\pi-\varphi_k}{2}\left(e^{i\arg\Delta} J_+^{(k)} + e^{-i\arg\Delta} J_-^{(k)}\right)\right] \left|\frac{1}{2}, -\frac{1}{2}\right\rangle_k .
\end{aligned} \tag{4.37}$$

4.4 Results

Circuit A:

For the first circuit we choose the following as the reference state,

$$|\Omega_k(s=0)\rangle = \left|\frac{1}{2}, \text{sgn}\left(\mu + J\cos k\right)\cdot\frac{1}{2}\right\rangle_k . \tag{4.38}$$

As mentioned previously, this is one of the "natural" choices of a reference state as it is the ground state of the mass part of the Kitaev chain Hamiltonian *i.e.* the free fermionic Hamiltonian with $\Delta = 0$ given by,

$$H_M = -\sum_{k>0} 2R_3 J_0^{(k)} = -\sum_{k>0} 2|R_3|\left(\text{sgn}\, R_3 \cdot J_0^{(k)}\right), \tag{4.39}$$

where $R_3 = \mu + J\cos k$ as per (4.34) and in the second part of the above equation, the Hamiltonian has been re-expressed in a form that makes the ground state manifest. We may note (4.38)'s equivalence with,

$$|\Omega_k(s=0)\rangle = \exp\left[-i\frac{\pi}{2}\Theta\left(\mu + J\cos k\right)\cdot\left(J_+^{(k)} + J_-^{(k)}\right)\right]\left|\frac{1}{2}, -\frac{1}{2}\right\rangle_k , \tag{4.40}$$

wherein Θ is the step function on $R_3 = \mu + J\cos(k)$.

We can now express the circuit from reference state (4.40) to the target state (4.37) in terms of the circuit parameter s,

$$|\Omega_k(s)\rangle = \exp\left[-is\left(\frac{\pi-\varphi_k}{2}\,\text{sgn}\,\Delta - \frac{\pi}{2}\Theta\left(\mu + J\cos k\right)\right)\left(J_+^{(k)} + J_-^{(k)}\right)\right]|\Omega_k(s=0)\rangle. \tag{4.41}$$

The spread complexity is then computed to be,

$$\begin{aligned}\mathscr{C}_k(s=0\mapsto 1; 1\mapsto 0) &= \sin^2\left(\theta_k - \frac{\pi}{2}\Theta\left(\mu + J\cos k\right)\right) = \frac{1}{2}\left(1 + \text{sgn}\left(\mu + J\cos k\right)\cdot\cos 2\theta_k\right)\\ &= \frac{1}{2}\left(1 - \text{sgn}\left(\mu + J\cos k\right)\cdot\cos\varphi_k\right)\\ &= \frac{1}{2}\left(1 - \frac{|\mu + J\cos(k)|}{\sqrt{(\mu + J\cos(k))^2 + \Delta^2\sin^2(k)}}\right).\end{aligned} \tag{4.42}$$

Naturally, the tensor product (over momentum modes) structure of the ground state in (4.37) results in the above being the circuit complexity corresponding to a particular choice of momentum mode k_n. So to obtain the total spread complexity for the circuit we need to count the contributions from each k_n - which take discrete values for finite L. In the continuum limit, $L >> 1$, this gives the spread complexity for the Circuit A,

$$C(J,\mu,\Delta) = \frac{1}{L}\sum_{n>0} C_{k_n}(s=0\mapsto 1) \to \frac{1}{\pi}\int_0^\pi dk C_k(s=0\mapsto 1). \tag{4.43}$$

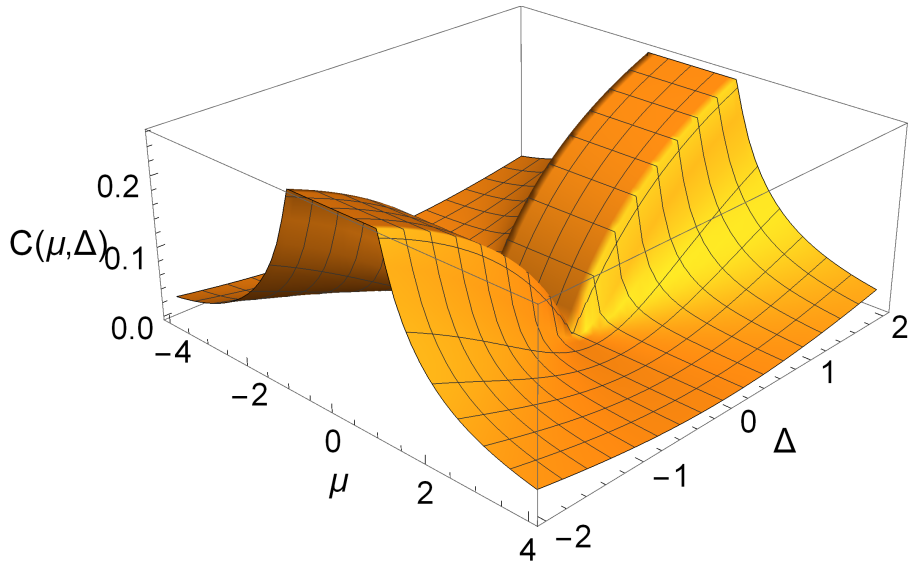

Figure 2: The (continuum limit) spread complexity for the circuit connecting the free fermion ground state to the Kitaev chain ground state. With $J = 1$, $|\mu| < 1$ regime represents the topologically non-trivial phase through which the spread complexity remains constant with its value fixed by Δ.

We did not manage to find a closed-form analytic expression for the complexity for generic values of μ in the continuum limit but it can be seen that the complexity in the topologically non-trivial phase is represented by,

$$C(J, |\mu| < |J|, \Delta) = \frac{1}{2} - \frac{1}{\pi}\int_0^{\frac{\pi}{2}} \sin(\varphi_k)\tan^{-1}\left(\frac{\tan(\varphi_k)}{|\Delta|}\right)d\varphi_k, \tag{4.44}$$

a μ-independent expression. So in the continuum limit, at least qualitatively, we concur with the results obtained, concurrently, in [109] where the spread complexity of the same circuit was observed to be a constant through the topological phase. Consequently, we conclude the correlation between spread complexity and topological phase transitions, and demonstrate the same in Fig.(2).

As a comparison with the results in [109], we plot the spread complexity as a function of Δ in Fig.(3a). As expected, the spread complexity assumes a constant value in the topologically non-trivial phase - a value which depends on Δ. At finite L, one can see a number of perturbations from this constant value in the topological phase in terms of a rough pasting of a number of distinct arcs as μ is varied through the topological phase, as in Fig.(3b) - indicating that the spread complexity indeed not captured completely without the continuum limit. Increasing l, increases the number of arcs but with fuzzier cusps resulting in a smoother profile which in the continuum limit goes to a constant value characterizing the topological phase being captured by the spread complexity.

Another point of note is the profile of spread complexity as $\Delta \to 0$. (4.42) indicates that the spread com-

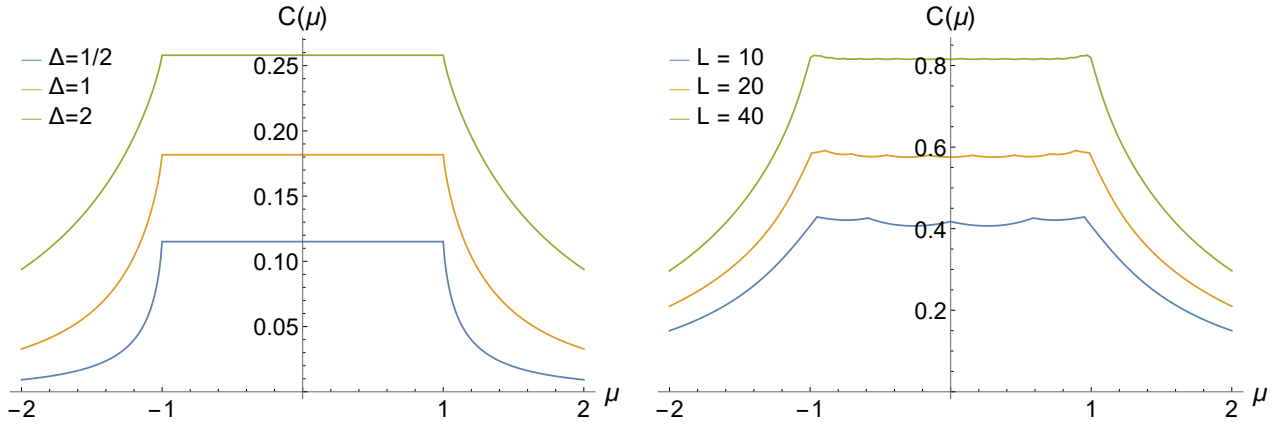

(a) (b)

Figure 3: Spread complexity as a function of μ with $J = 1$ and $\Delta = 2$ for Circuit A. The y-axis has been factored by $\sqrt{L}$ for a better outlook and clarity in the plot. (a) corresponds to the continuum case while (b) corresponds to the discrete case. The arc segments in the latter represent deviation of results from the true values due to finite L. As L is increased the cusps become less and less sharply defined eventually smoothing in the continuum limit.

plexity vanishes as $\Delta \to 0$ but remains continuous at $\Delta = 0$. In this case, with only mass terms *i.e.* the superconducting interaction off, the topologically-relevant phase boundaries are captured via the first derivative $\frac{\partial C(J,\mu,\Delta)}{\partial \Delta}$, as $\Delta \to 0$. More precisely, when $|\mu| > |J|$ (*i.e.* the topologically trivial phase) the first derivative approaches zero as $\Delta \to 0$ while for $|\mu| < |J|$ (*i.e.* the topologically non-trivial phase) the first derivative approaches a constant value. As a function of Δ, spread over the positive and negative values, the spread complexity displays cusp-like behavior in the topological phase at $\Delta = 0$. Even though we don't have a physical explanation of this behavior at the moment we note the striking resemblance with the behavior of the order parameter of a conventional second order phase transition. This behavior is neatly captured in Fig.(4) where we plot the derivative of spread complexity for a couple of values of μ near the phase boundaries.

Circuit B:

The spread complexity of the Circuit A displays a plateauing behavior in the topological phase - as it did for the SSH model considered in [109]. A feature, perhaps undesirable, of the circuit A, is that the reference state (4.38) is μ-dependent. Consequently, one may ask whether it is possible to choose a reference state, independent of Δ and μ, for spread complexity to furnish a plateauing behavior in the topological phase? It, indeed, is. Let us choose the reference state to be,

$$|\Omega_k(s=0)\rangle = \exp\left[\frac{\pi}{4}e^{-i\frac{\pi}{2}}J_+^{(k)} - \frac{\pi}{4}e^{+i\frac{\pi}{2}}J_-^{(k)}\right]\left|\frac{1}{2},-\frac{1}{2}\right\rangle_k . \tag{4.45}$$

This state may be seen as the ground state of the superconducting part of the Kitaev chain Hamiltonian *i.e.* the cooper-pair ground state. With this choice, the reference state to target state circuit, as a function of circuit parameter s, forms the second circuit of this work and is expressed as,

$$|\Omega_k(s)\rangle = \exp\left[-i\cdot s\cdot\left(\operatorname{sgn}\Delta\cdot\frac{\pi-\varphi_k}{2}-\frac{\pi}{4}\right)\left(J_+^{(k)}+J_-^{(k)}\right)\right]|\Omega_k(s=0)\rangle, \tag{4.46}$$

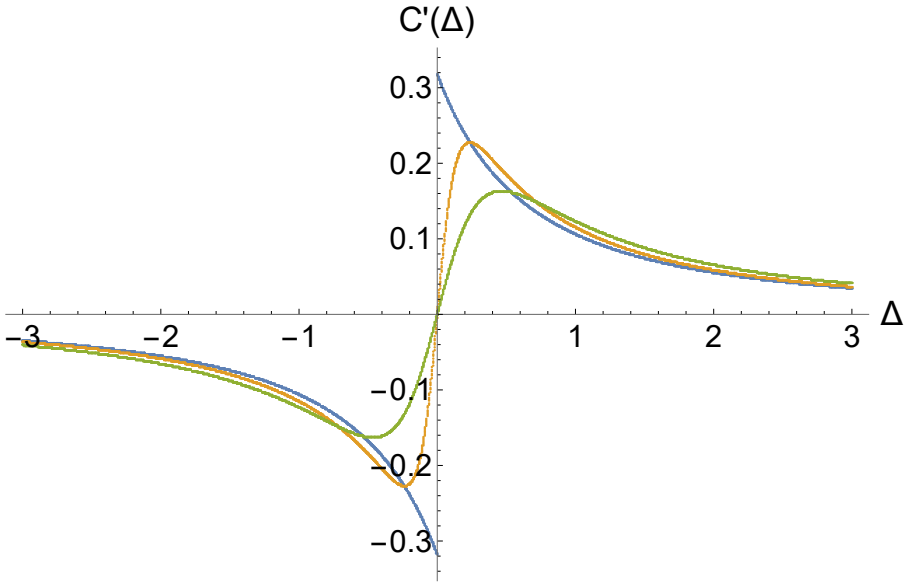

Figure 4: The derivative of spread complexity with respect to Δ in the continuum limit for the Circuit A with $J = 1$. The blue line corresponds to $\mu = 0.98$, the orange $\mu = 1.02$, and the green $\mu = 1.1$. Across the topological-phase boundary at $|\mu| = 1$, the derivative displays a striking discontinuity capturing the phase transition into and out of the topological phase.

and the corresponding spread complexity is computed as,

$$\mathscr{C}_k(s=1) = \sin^2\left(\operatorname{sgn}\Delta\cdot\frac{\pi-\varphi_k}{2}-\frac{\pi}{4}\right) = \frac{1}{2}\left(1-\frac{\Delta\sin k}{\sqrt{(\mu+J\cos(k))^2+\Delta^2\sin^2(k)}}\right). \tag{4.47}$$

In the topological phase *i.e.* $|\mu| < |J|$, we observe that the total spread complexity is given by, after integrating by parts,

$$\mathscr{C}(J,|\mu|<|J|,\Delta) = \frac{1-\operatorname{sgn}\Delta}{2}+\frac{1}{\pi}\int_0^{\pi/2} d\varphi_k\cos\varphi_k\tan^{-1}\frac{\tan\varphi_k}{\Delta}, \tag{4.48}$$

an expression independent of μ - exactly what we set out to do at the beginning of this section. This integral can be evaluated analytically in a closed form as,

$$\mathscr{C}(J,|\mu|<|J|,\Delta) = \frac{1}{2}-\frac{1}{\pi}\frac{\Delta\tan^{-1}\sqrt{\Delta^2-1}}{\sqrt{\Delta^2-1}}. \tag{4.49}$$

This spread complexity is plotted as a function of μ for various choices of Δ in Fig.(5) as a visual aid to understand the behavior better. The plateauing behavior that we expected is distinguished in this figure. As mentioned in the previous chapter, inside the spread complexity inside the topological phase *i.e.* $\mathscr{C}(J,|\mu|<|J|,\Delta)$ is a Δ-dependent constant and this is what we explore in Fig.(6) and observe the change in the height of the plateau as a function of Δ. The red bullets on this figure correspond with the plateau value observed in [109]

for the SSH model , with $\Delta = -1$. At these points the numerator and denominator of (4.49) approach zero, and the value can be computed by considering the limit $\Delta^2 \to 1$.

Just as for circuit A, the derivatives of spread complexity demarcate characteristic behavior in the topologically non-trivial phase and it can be seen that,

$$\pi \frac{d}{d\Delta} \mathscr{C}(J, |\mu| < |J|, \Delta) = \frac{1}{1-\Delta^2} + \frac{\tan^{-1}\left(\sqrt{\Delta^2-1}\right)}{(\Delta^2-1)^{3/2}}, \tag{4.50}$$

is continuous everywhere, including $|\Delta| = 1$. However, for this circuit it is the second derivative that captures characteristic signatures of topological phase boundaries as it is continuous at $|\Delta| = 1$ but diverges at $\Delta = 0$,

$$\because \pi \frac{d^2}{d\Delta^2} \mathscr{C}(J, |\mu| < |J|, \Delta) = \frac{2\Delta^2+1}{\Delta\,(\Delta^2-1)^2} - \frac{3\Delta \tan^{-1}\left(\sqrt{\Delta^2-1}\right)}{(\Delta^2-1)^{5/2}} \sim \Delta^{-1}, \tag{4.51}$$

as $\Delta \to 0$. This divergence of the second derivative is again remarkable and resembles a conventional third order phase transition and mandates further investigation that we defer to future studies.

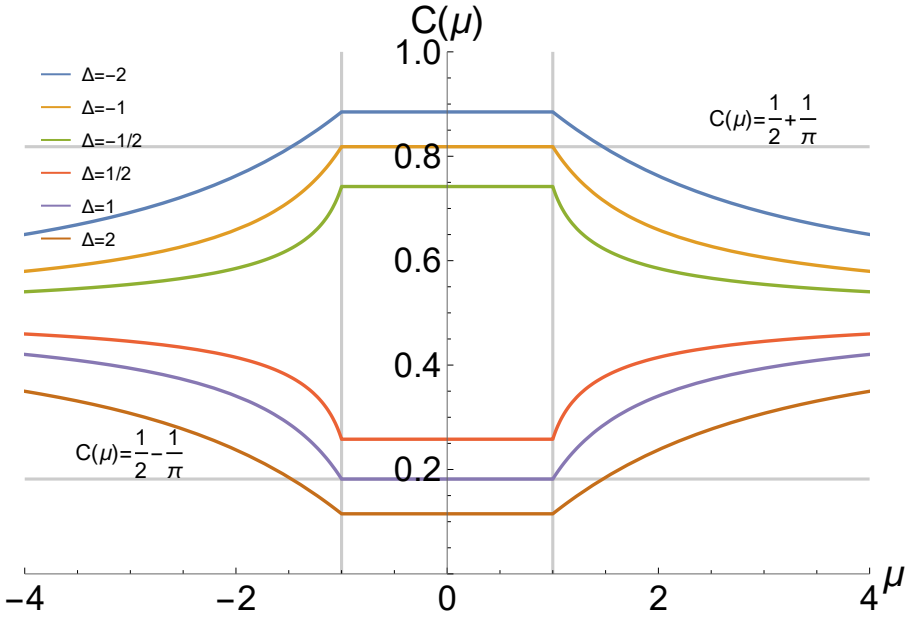

Figure 5: Complexity $\mathscr{C}(s = 1; \mu, \Delta)$ visualized as a function of μ for various choices of fixed Δs for the circuit B. Between the pair of vertical lines ($\mu = \pm 1$), spread complexity is free of μ as we envisioned at the onset. The pair of horizontal lines visualize the analytical results of $\mathscr{C}(|\mu| < 1, \Delta = \pm 1)$. For $|\mu| \to \infty$, the spread complexities corresponding to different Δs approach the horizontal line $\mathscr{C} = 1/2$.

Circuit C:

We shall consider one more circuit, one connection the full Kitaev chain ground state to the connecting the fermionic vacuum state - which we term as circuit C. With a lack of fermions, the fermionic vacuum

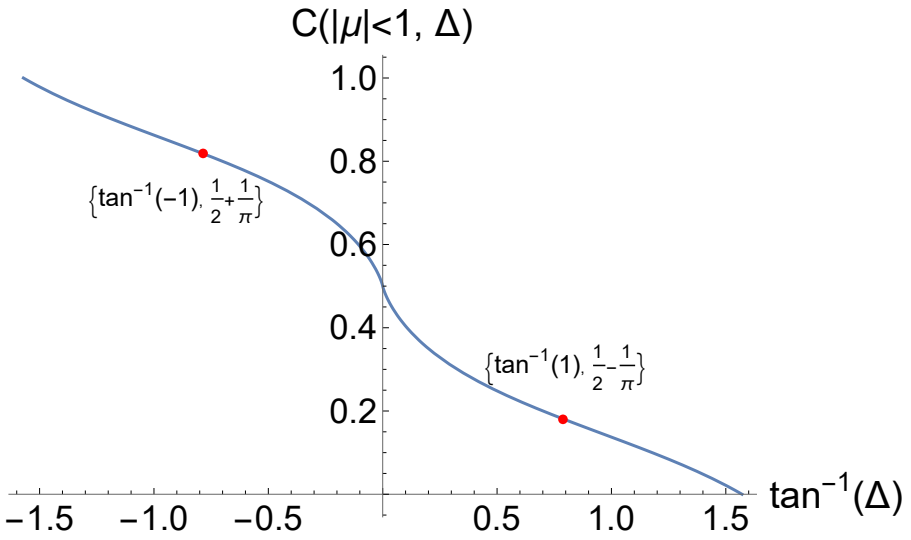

Figure 6: Complexity $\mathscr{C}(s = o \mapsto 1; J = 1, |\mu| < 1, \Delta)$ as a function of Δ for the circuit B. The two red dots demarcate the analytical results we obtained for the cases of $\mathscr{C}(s = 0 \mapsto 1; J = 1, |\mu| < 1, \Delta = \pm 1)$, respectively, *i.e.* for the topological phase.

state is in a sense the most natural choice of state characterizing the system. As demonstrated previously in Ch.4.3.2 the Kitaev chain Hamiltonian is part of an **su(2)** algebra and as a result the vacuum state, in the $SU(2)$ representation, is the momenta tensor product of the lowest-weight spin-$\frac{1}{2}$ states. The circuit can be expressed as follows for each momentum mode k with a circuit parameter s,

$$|\Omega_k(s)\rangle = \exp\left[s \cdot \left(\frac{\pi - \varphi_k}{2} e^{-i\left(\frac{\pi}{2} - \arg\Delta\right)} J_+^{(k)} - \frac{\pi - \varphi_k}{2} e^{i\left(\frac{\pi}{2} - \arg\Delta\right)} J_-^{(k)}\right)\right] \left|\frac{1}{2}, -\frac{1}{2}\right\rangle_k , \tag{4.52}$$

again employing Baker-Campbell-Hausdorff formulae to re-express (4.33). We compute the spread complexity to be,

$$\mathscr{C}_k(s = 0 \mapsto 1) = \sin^2 \frac{\pi - \varphi_k}{2} = \frac{1}{2}\left(1 + \frac{\mu + J\cos(k)}{\sqrt{(\mu + J\cos(k))^2 + \Delta^2 \sin^2(k)}}\right). \tag{4.53}$$

Our analysis from the cases of circuits A and B indicates that it would be useful to compute the derivative of spread complexity with respect to μ,

$$\frac{\partial}{\partial \mu}\mathscr{C}_k(s = 0 \mapsto 1) = \frac{\Delta^2 \sin^2(k)}{2((\mu + J\cos(k))^2 + \Delta^2 \sin^2(k))^{\frac{3}{2}}}. \tag{4.54}$$

Of course, to obtain the total complexity we should sum over the discrete values of k and take the continuum limit. In Fig.(7a), the continuum spread complexity is displayed as a function of μ. Interestingly, we observe a monotonic increase in the spread complexity for the parameter space probed. There is a distinctive absence of the plateauing effect through the topological phase observed for the previous cases. We note

that this is not an artefact of finite L as these results are in the continuum limit. However, as we're aware of the topological boundaries we correlate the aberrant behavior displayed around these boundaries to spread complexity capturing the phase transition in a sense. To sharpen this notion we turn again to the derivative of spread complexity and observe a divergence in the derivative, as demonstrated via Fig.(7b). Furthermore, we can ascribe the divergence at $\mu = -1$ to low momentum modes while the divergence at $\mu = 1$ to the high ones as seen through,

$$\begin{aligned} \frac{\partial}{\partial\mu}\mathscr{C}_k(s=0\mapsto 1)\Big|_{\mu=1} &= \frac{1}{2|\Delta|k} + \mathcal{O}(k), \\ \frac{\partial}{\partial\mu}\mathscr{C}_k(s=0\mapsto 1)\Big|_{\mu=-1} &= \frac{1}{2|\Delta|(k-\pi)} + \mathcal{O}(k-\pi). \end{aligned} \tag{4.55}$$

We observe that for some value of $k \in [0, \pi]$, there always exists a pole in the parameter space associated with $|\mu| < 1$ which leads to a divergence of the continuum integral. Consequently, even though the plateauing effect between the phase boundaries is absent, we conclude that the spread complexity still distinguishes the topological phase - and its derivative sharpens this understanding.

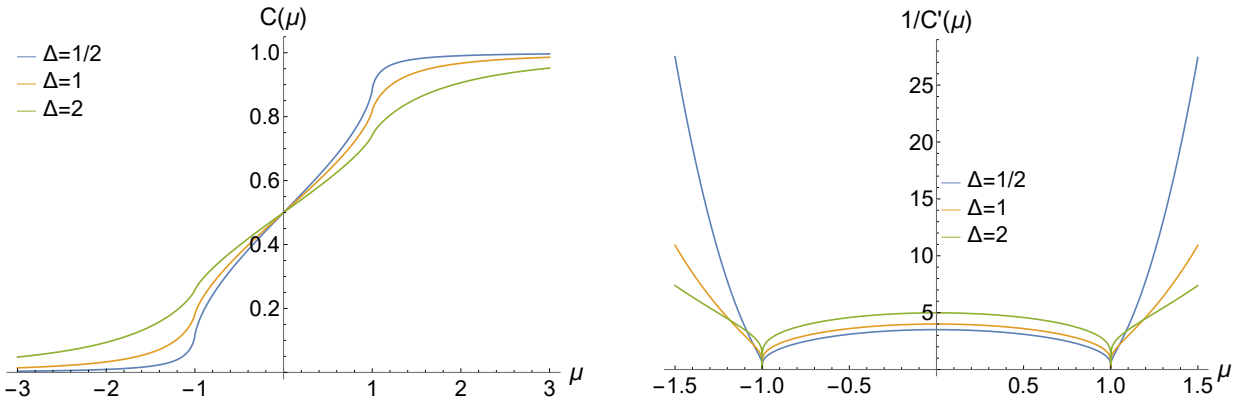

(a) (b)

Figure 7: a) The spread complexity for the circuit C with $J = 1$. A monotonic increase is observed with varying μ monotonically - along with a distinct lack of plateauing effect in the topological phase. b) With $\Delta = \frac{1}{2}$ and $J = 1$, we visualize the inverse of the derivative of continuum spread complexity with varying μ. At the phase boundaries, this can be seen to approach zero indicating a divergence in the derivative of the spread complexity and characterizes the phase transition.

To build a complete dictionary for future studies, it is prudent to consider the behavior in spread complexity as well as its derivative/s at finite L. At finite L, the profile of the spread complexity is similar to Fig.(7a), as expected. This indicates a mere change in the numerical value of the spread complexity but in the behavior characterizing the system. We do expect the derivative to exhibit more dramatic changes due to the presence of divergence in the continuum limit. We observe that the derivative retains its finiteness - but is now accompanied by a sharp change in the sign of the second derivative. This sharp change intensifies as L is increased

- eventually, introducing a divergence in the continuum limit of $L \gg 1$. We further demonstrate the robustness of spread complexity in capturing the phase transition by an alternative approach via the behavior around $\Delta = 0$. Using (4.53) we obtain,

$$\begin{aligned} \frac{\partial^2}{\partial \Delta^2} C_k(s = 0 \mapsto 1)\Big|_{\mu=1,\Delta=0} &= \frac{1}{2}\cot^2\left(\frac{k}{2}\right), \\ \frac{\partial^2}{\partial \Delta^2} C_k(s = 0 \mapsto 1)\Big|_{\mu=-1,\Delta=0} &= -\frac{1}{2}\tan^2\left(\frac{k}{2}\right). \end{aligned} \tag{4.56}$$

When continuum contributions are accounted for via the integral over $k \in [0, \pi]$ it can be seen that for $|\mu| > 1$ regime the second derivative remains finite and on the other hand for $|\mu| \leq 1$ the integral is divergent. A pole is present in the second derivative for $k \in [0, \pi]$, leading to a diverging integral exactly as happens for circuit A. We note again that the discourse in this chapter followed by assuming even L and anti-periodic boundary conditions. For a discussion surrounding odd L and periodic boundary conditions we refer the interested reader to App.(B).

5 Application II: Coupled Bateman Oscillator

"The career of a young theoretical physicist consists of treating the harmonic oscillator in ever-increasing levels of abstraction."

- Sidney Coleman

As we remarked earlier, toy models are to theoretical physicists what laboratories are to the experimental ones - they are the arena upon which theoretical physicists perform their Gedankenexperiments, or thought experiments, to describe certain natural phenomena, to predict certain others, and - more generally - to learn principles of nature. And there is perhaps no greater toy model than the harmonic oscillator - which physicists and engineers have brought to utility to describe a wide array of natural phenomena: from violins, clocks, and radio circuits to quantum fields. Even with such ubiquitous applications, the fact remains that harmonic oscillator is a highly idealized system and a simple way to make it more realistic is to consider it being coupled to a source that drives or dampens its oscillations. This source itself can also be modeled as a harmonic oscillator itself - which drives or is driven by the other oscillator. Such a simple system has a rich phase structure owing to the intricacies associated with the parameters of this system - more specifically, this system has a PT-symmetric phase and two phases which are not PT−-symmetric. Along the theme of this thesis we may ask if Krylov complexity is able to detect phase transitions in and out of the PT-symmetric phase in the coupled-damped-harmonic-oscillator system. If so, then the ubiquity of the harmonic oscillator implies that Krylov complexity is a great candidate to investigate the phase structure of a wide variety of systems and one may forgo apriori justification to utilize Krylov complexity for studying the phase structure of some particular model/system under consideration. Some aspects of our numerical implementation for computing Krylov complexity for this chapter are presented in E. We note the preprint communication of a similar body of work [152] studying Krylov complexity in PT-symmetric systems after our work [2] was communicated to the same preprint, arXiv.

5.1 The Model and Properties

We describe the coupled Bateman oscillator model and discuss its properties, phases transitions etc in this chapter which borrows heavily from a similar discussion in [37]. We start by considering the equations of motion of a simple damped harmonic oscillator with unit mass, damping factor γ, and natural frequency ω, and an equilibrium displacement $x(t)$,

$$\ddot{x}(t) + 2\gamma\dot{x}(t) + \omega^2 x(t) = 0. \tag{5.1}$$

This is a damped system and the energy is not conserved such that the dynamics is non-unitary. This leads to a Lagrangian density that is explicitly time-dependent. We would like to quantize this system and traditional quantization techniques, path integral quantization and second/canonical quantization, require that the Lagrangian density be not explicitly dependent on time. This presents a conundrum which was tackled by

Bateman in [153]. Bateman introduced an auxiliary oscillator which complements the damped oscillations via driven oscillations. This auxiliary driven oscillator together with the original damped oscillator constitute a *composite*, but not coupled, system. Remarkably, Bateman showed that the Lagrangian for such a composite system is in-fact not dependent on time and thus this composite system is a unitarity-preserving system. The equation of motion for the auxiliary system is given as,

$$\ddot{y}(t) - 2\gamma\dot{y}(t) + \omega^2 y(t) = 0. \tag{5.2}$$

The composite system, with both oscillators at unit mass, is then represented by the Lagrangian,

$$\boxed{L = \dot{x}\dot{y} + \gamma(x\dot{y} - \dot{x}y) - \omega^2 xy.} \tag{5.3}$$

The composite nature of the system is reflected in at least three aspects:

- their Euler-Lagrange equations of motion are obtained by complimentary coordinates *i.e.* extremizing (5.3) with respect to $x(t)$ coordinate gives the equation of motion for the y (auxiliary) oscillator while extremizing it with respect to $y(t)$ coordinate gives the same for the x (primary) oscillator (reminiscent of the JT gravity action);
- the energy lost by the primary oscillator exactly equals the energy gained by the auxiliary one - however, the source/sink of the energy for auxiliary/primary oscillator remains arbitrary lending a composite nature to this system rather than a coupled one;
- the two equations of motions, .(5.1) and (5.2), are connected through a time-reversal transformation which implies that bilinear forms like the Hamiltonian are time-independent, consequently one can infer the unitarity-preserving nature of the composite system.

We can use the standard method of employing Legendre transformations to obtain the Hamiltonian for the Bateman composite oscillator system. The momenta conjugate to the two oscillator coordinates x and y are,

$$\begin{aligned} p_x &\equiv \frac{\partial L}{\partial \dot{x}} = \dot{y} - \gamma y, \\ p_y &\equiv \frac{\partial L}{\partial \dot{y}} = \dot{x} + \gamma x, \end{aligned} \tag{5.4}$$

giving a Hamiltonian,

$$\boxed{H_B = p_x\dot{x} + p_y\dot{y} - L = p_x p_y + \gamma(yp_y - xp_x) + \varkappa xy \equiv H_0 + H_1,} \tag{5.5}$$

with definitions, $\varkappa \equiv \omega^2 - \gamma^2$, $H_0 \equiv p_x p_y + \varkappa xy$ and $H_1 \equiv \gamma(yp_y - xp_x)$. The quantization procedure is now apparent and we impose that the conjugate coordinate and momenta pairs for both oscillators follow the canonical Heisenberg algebra,

$$[x, p_x] = [y, p_y] = i\hbar, \tag{5.6}$$

and that commutators between coordinates/momenta belonging to different variables vanish since this is a composite system with independent oscillators. Using (5.4), we can also express the non-vanishing commutators of the Bateman oscillator system as,

$$[x, \dot{y}] = [y, \dot{x}] = i\hbar. \tag{5.7}$$

For completeness, we discuss some more properties of the system and discuss the solutions. One way to solve the Bateman problem is to shift to the Fock basis by constructing creating and annihilation operators from the coordinate-momentum operators. Assuming $\varkappa > 0$ to avoid complex frequencies,

$$\begin{aligned} a_x &= \frac{1}{\sqrt{2\hbar\sqrt{\varkappa}}}\left(p_x - i\sqrt{\varkappa}x\right), \quad a_y = \frac{1}{\sqrt{2\hbar\sqrt{\varkappa}}}\left(p_y - i\sqrt{\varkappa}y\right), \\ a_x^\dagger &= \frac{1}{\sqrt{2\hbar\sqrt{\varkappa}}}\left(p_x + i\sqrt{\varkappa}x\right), \quad a_y^\dagger = \frac{1}{\sqrt{2\hbar\sqrt{\varkappa}}}\left(p_y + i\sqrt{\varkappa}y\right). \end{aligned} \tag{5.8}$$

This fulfills the usual commutation relations,

$$\left[a_x, a_x^\dagger\right] = \left[a_y, a_y^\dagger\right] = 1, \tag{5.9}$$

$$\left[a_x, a_y\right] = \left[a_x^\dagger, a_y^\dagger\right] = 0. \tag{5.10}$$

We can define a "free" Hamiltonian in the sense that there is no damping *i.e.* $\gamma \to 0$,

$$H_0 = \hbar\sqrt{\varkappa}\left(a_x^\dagger a_y + a_y^\dagger a_x\right). \tag{5.11}$$

It is instructive to define composite operators,

$$\begin{aligned} A &\equiv \frac{a_x + a_y}{\sqrt{2}} \quad \text{and} \quad B \equiv \frac{a_x - a_y}{\sqrt{2}}, \\ A^\dagger &\equiv \frac{a_x^\dagger + a_y^\dagger}{\sqrt{2}} \quad \text{and} \quad B^\dagger \equiv \frac{a_x^\dagger - a_y^\dagger}{\sqrt{2}}, \end{aligned} \tag{5.12}$$

that satisfy the same commutation algebra that $(a_x, a_x^\dagger)$ and $(a_y, a_y^\dagger)$ do, and expressing the free Hamiltonian H_0 in terms of these composite operators,

$$\boxed{H_0 = \hbar\sqrt{\varkappa}\left(A^\dagger A - B^\dagger B\right).} \tag{5.13}$$

We can now attribute the terms that contribute to the full Hamiltonian in the finite γ limit as a perturbation on the free Hamiltonian,

$$\boxed{H_1 = i\hbar\gamma\left(A^\dagger B^\dagger - AB\right).} \tag{5.14}$$

We make the following observations and comments:

1. The operators $A^\dagger A$ and $B^\dagger B$ have non-negative integral eigenvalues and can be interpreted as number operators. Hence, H_0 eigenstates given in terms of Fock basis as $|n_A, n_B\rangle$ with corresponding eigenvalues as $\hbar\varkappa\,(n_A - n_B)$. Furthermore, as only the difference in A and B oscillator "occupation numbers" determines the eigenvalues, there is a large symmetry class of states associated with the same eigenvalue: all states $|n_A + p, n_B + p\rangle$ with $p \in \mathbb{Z}$, have the same eigenvalue as $|n_A, n_B\rangle$.

2. In the free Hamiltonian limit, *i.e.* $\lim_{\gamma\to 0} H_B \mapsto H_0$, the states annihilated by the operator B are exactly the eigenstates of the un-damped harmonic oscillator. So, in terms of these new operators, $\left(A, A^\dagger\right)$ and $\left(B, B^\dagger\right)$, the eigenstates of H_0 are given by $B\left|\psi\right\rangle = 0$.
3. Clearly the free Hamiltonian and the perturbation on it, .(5.13) and (5.14) respectively, commute *i.e.* $\left[H_0, H_1\right] = 0$. Turning on γ in the full Hamiltonian H_B has the effect of producing states : $|n_A, 0\rangle \mapsto |n_A + n_B, n_B\rangle$. This serves to indirectly identify the sink into which the energy from the damped oscillator is going - it goes into the other oscillator to produce particles in the auxiliary oscillator. However, we stress that this is an indirect inference only *i.e.* the system is still a composite system rather than a coupled one.
4. Finally, we note the following three dynamical regimes depending on the sign of $\varkappa$,
   - $\varkappa > 0$: under-damped regime, corresponds to the most physical regime with $\omega^2 > \gamma^2$ *i.e.* the natural frequencies of the system can compensate for the damping and can facilitate interesting dynamics;
   - $\varkappa < 0$: over-damped regime, with $\omega^2 < \gamma^2$ the system is strongly damped and we do not observe features that call for a careful study; and,
   - $\varkappa = 0$: critically-damped regime, with $\omega^2 = \gamma^2$ the system's natural frequencies are in sync with the damping and again, there doesn't seem to be any interesting dynamical phenomenon.

We move on to the explore the algebraic structure of the Hamiltonian, if it exists. Upon definining the following operators it can be seen that the Hamiltonian belongs to a Lie algebra,

$$\begin{aligned} X &\equiv \frac{1}{2}\left(A^\dagger B^\dagger + AB\right), \\ Y &\equiv \frac{i}{2}\left(A^\dagger B^\dagger - AB\right), \\ Z &\equiv \frac{1}{2}\left(A^\dagger A + BB^\dagger\right), \end{aligned} \tag{5.15}$$

with commutation relations,

$$\begin{aligned} [X, Y] &= iZ, \\ [Z, Y] &= iX, \\ [X, Z] &= iY, \end{aligned} \tag{5.16}$$

which corresponds to the non-compact $\mathfrak{su}(1,1)$ Lie algebra. To have more physical insight into this algebra we can further express it as,

$$L_+ = X + Y, \quad L_- = X - Y, \quad L_0 = Z, \tag{5.17}$$

that satisfy,

$$\left[L_-, L_+\right] = 2L_0, \quad \left[L_0, L_\pm\right] = 0. \tag{5.18}$$

We observe the connections of this algebra and the Bateman oscillator Hamiltonian:

1. $H_1 = i\hbar\gamma Y$, *i.e.* the perturbation Hamiltonian is the same as an element of $\mathfrak{su}(1,1)$ algebra - upto some natural constants and a rescaling by the damping factor ;
2. the free Hamiltonian can be associated with the Casimir element of $\mathfrak{su}(1,1)$,

$$Z^2 - X^2 - Y^2 = h_0^2 - \frac{1}{4}, \tag{5.19}$$

   with $2\hbar\sqrt{\varkappa}h_0 = H_0$; and,
3. since the Casimir element commutes with all the other elements of the algebra, so does H_0.

Summarily, the full Bateman composite system Hamiltonian is the sum of a (rescaled) element of an $\mathfrak{su}(1,1)$ algebra and (a simple function of) the Casimir element of the same $\mathfrak{su}(1,1)$ algebra.

5.2 Interactions and *PT* symmetry

In this section we turn our attention to the primary aspect related to the theme of this thesis: that of the phase structure and transition between various phases. In the previous subchapter we insisted on interpreting the Bateman oscillator system as a *composite* one rather than a coupled one and argued the validity of this interpretation. We also argued that the energy sink for the primary oscillator is arbitrary and likewise the energy source for the auxiliary oscillator is arbitrary - in a manner that there is an overall balance of energy loss and gain. Consequently, phase-space flows for the Bateman oscillator system are preserve volume. However, one may in fact make the energy source/sink more explicit by coupling the two oscillators thereby giving a truly coupled system rather a composite one. What, then, happens to the volume-preserving nature of the phase space flows? Nothing! The system retains its conservative properties,

$$\begin{aligned} \ddot{x} + 2\gamma\dot{x} + \omega^2 x + F_1(x,y) &= 0, \\ \ddot{y} - 2\gamma\dot{y} + \omega^2 y + F_2(x,y) &= 0, \end{aligned} \tag{5.20}$$

with $F_1(x,y)$ and $F_2(x,y)$ being arbitrary functions of the coordinates of the two oscillators. Of course, the case of $F_1(x,y) = 0 = F_2(x,y)$ corresponds to the standard Bateman composite system, as opposed to the coupled system for non-vanishing $F_1(x,y)$ and $F_2(x.y)$. The latter additionally possesses the property of being symmetric under a combination of PT-transformation [37],

$$\mathsf{P} : x \to -y, \quad y \to -x, \quad p_x \to -p_y, \quad p_y \to -p_x, \tag{5.21}$$

$$\mathsf{T} : x \to x, \quad y \to y, \quad p_x \to -p_x, \quad p_y \to -p_y. \tag{5.22}$$

It can be seen that the action of parity operator is to exchange the roles of the two oscillators: the driven becomes the damped and vice-versa. On the other hand, the time-reversal operator has no such nice interpretation and performs its usual job. The Bateman oscillator is not symmetric individually under either of P or T transformations - however, it is symmetric under the joint PT-transformation [37] and a characteristic feature of such systems is that they undergo phase transitions. In [2] we consider a simple choice of the coupling functions: $F_1(x,y) = \epsilon = F_2(x,y)$ with $\epsilon \in \mathbb{R}$ *i.e.* a linear coupling between the two oscillators. This immediately provides a linear source or sink, respectively, to the auxiliary or primary oscillators,

thereby lifting the ambiguity associated with energy exchanges. One can now easily intuit the phase transitions accompanying the dynamics depending on ϵ. The equilibrium state for the linearly coupled Bateman oscillators would simple be a phase with an ϵ that can sustain indefinite energy exchange between the two oscillators - with the source becoming sink after exhausting its energy and the process repeating in reverse for an indefinite duration. This would require an ϵ which is neither too small nor too large as in either of these cases the oscillators are either not connected strongly enough or are connected too strongly such that the energy flow is uni-directional with the system never reaching equilibrium. We may define a couple of threshold values for the coupling ϵ between which the system equilibriates and outside this region it doesn't. It is instructive to look at classical solutions to understand the basic phase structure and transitions. As usual for oscillator problems, we work with wave-solution ansatz: $x = x_0 e^{i\lambda t}$ and $y = y_0 e^{i\lambda t}$. If this ansatz is to be a solution of the coupled Bateman problem, (5.20) with $F_1(x, y) = \epsilon = F_2(x, y)$, the frequencies must satisfy,

$$f(\lambda) \equiv \lambda^4 + \left(4\gamma^2 - 2\omega^2\right)\lambda^2 + \omega^4 - \epsilon^2 = 0. \tag{5.23}$$

As this is a quartic polynomial, it admits four solutions for the frequencies, and depending on the value of ϵ there are three possibilities: all real frequencies, all complex frequencies, two real and two complex frequencies. The equilibrium state, or the PT-symmetric phase, corresponds to the case of all real solutions because complex frequencies indicate either decaying amplitudes or exponentially growing ones. As (5.23) is quadratic in λ^2, its solutions are,

$$\lambda^2 = \left(\varkappa - \gamma^2\right) \pm \sqrt{\epsilon^2 - 4\gamma^2\varkappa}. \tag{5.24}$$

This makes apparent the PT-symmetric regime as,

$$\epsilon_1 \equiv 2\gamma\sqrt{\varkappa} \leq \epsilon \leq \varkappa + \gamma^2 \equiv \epsilon_2. \tag{5.25}$$

Paraphrasing the above equation, outside of this range of ϵ the system does not reach an equilibrium state in which energy bounces back-and-forth between the two oscillators and is rather uni-directional. For the case of $\epsilon < \epsilon_1$ the two oscillators are too weakly coupled for the energy to be redirected and likewise for the ultra-strongly coupled regime of $\epsilon > \epsilon_2$. The latter case is less explored in literature due to being less analytically tractable than the other ones as well as a corresponding experimental difficulty to implement it. It is only the regime $\epsilon_1 \leq \epsilon \leq \epsilon_2$ that admits real frequencies with unbroken PT-symmetry, and has dynamics that attain *nirvana*, aka equilibrium in physics. However, an exception to this occurs in the limit $\epsilon \to \infty$ with the Hamiltonian being diagonalized by position basis and an account of this is found in [37].

As in the case of *composite* Bateman oscillator, we can compute the Hamiltonian for the linearly *coupled* Bateman oscillator by appropriate Legendre transformations,

$$\begin{aligned} H_{cB} &= p_x p_y + \gamma(y p_y - p_x x) + \varkappa xy + \frac{\epsilon}{2}\left(x^2 + y^2\right) \\ &= (p_x + \gamma y)(p_y - \gamma x) + (\varkappa + \gamma^2)xy + \frac{\epsilon}{2}(x^2 + y^2), \end{aligned} \tag{5.26}$$

which reduces to the composite Bateman oscillator Hamiltonian (5.5) in the limit $\epsilon \to 0$.

As in the case of composite system, we can diagonalize the linearly coupled system in the Fock basis by shifting to ladder operators,

$$\begin{aligned}\left[\frac{1}{2}\left(a^\dagger a + aa^\dagger\right), a^\dagger\right] &= a^\dagger,\\ \left[\frac{1}{2}\left(b^\dagger b + bb^\dagger\right), b^\dagger\right] &= b^\dagger,\end{aligned} \tag{5.27}$$

where we've chosen the following re-definitions,

$$a = \frac{x + ip_x}{\sqrt{2}}, \quad \text{and} \quad b = \frac{y + ip_y}{\sqrt{2}}. \tag{5.28}$$

An interesting distinction vis-a-vis the commutation relations of (a, b) and $\left(a_x, a_y\right)$ is that the former are only defined for $\varkappa > 0$ while the latter are well-defined in general. This arises due to the fact that the coupled system naturally accommodates complex frequencies and thereby doesn't require $\varkappa > 0$. Furthermore, we note that the algebra associated with the linearly coupled system is a rank-2 (sub-)algebra, of $\mathfrak{so}(5, \mathbb{C})$, with ten generators: twelve possible quadratic combinations of the ladder operators and taking away $[x, p_x]$ as well as $[y, p_y]$ as they are constants. As in the case of Kitaev chain we've identified that the Hamiltonian, H_{cB}, is part of a Lie algebra which lends utility to the spread complexity calculation simplifying and, in certain cases, analytically possible. We'd now like to understand the generalized coherent states associated with this Lie algebra [154] so as to be able to compute the spread complexity. The generalized coherent states can be obtained by the action of the group elements on a fixed state in the relevant Hilbert space and as we observed in the case of Kitaev chain, the lowest-weight state $|0, 0\rangle$ seems to be the most compatible choice of this fixed state with the definition,

$$\frac{1}{2}\left(b^\dagger b + bb^\dagger\right)|0, 0\rangle = \frac{1}{2}\left(a^\dagger a + aa^\dagger\right)|0, 0\rangle = \frac{1}{2}|0, 0\rangle, \tag{5.29}$$

and, by definition, coherent states are the eigenstates of the annihilation operator which can be expressed as,

$$\frac{1}{2}aa|0, 0\rangle = \frac{1}{2}bb|0, 0\rangle = ab|0, 0\rangle = b^\dagger a|0, 0\rangle = a^\dagger b|0, 0\rangle = 0. \tag{5.30}$$

With the above as the lowest-weight coherent state, all other coherent states can be obtained by actions of the group element,

$$\boxed{|z_a, z_b, z_{ab}) = e^{\frac{z_a}{2}a^\dagger a^\dagger} e^{\frac{z_b}{2}b^\dagger b^\dagger} e^{z_{ab}a^\dagger b^\dagger}|0, 0\rangle,} \tag{5.31}$$

with all other group elements having trivial action on $|0, 0\rangle$ and hence absorbed into the Baker-Campbell-Hausdorff application. (C.7) indicates that the complexity is associated with an overlap of coherent states which in this case is,

$$\boxed{(\bar{z}_a, \bar{z}_b, \bar{z}_{ab}|z_a, z_b, z_{ab}) = \left(1 - (|z_a|^2 + |z_b|^2 + 2|z_{ab}|^2) + (z_{ab}^2 - z_a z_b)(\bar{z}_{ab}^2 - \bar{z}_a \bar{z}_b)\right)^{-\frac{1}{2}}.} \tag{5.32}$$

We remark that the lowest-weight state $|0, 0\rangle$ isn't apriori guaranteed to be the vacuum state (even if the occupation numbers are represented as 0) since (a, b) operators don't have to function as ladder operators

for the Bateman Hamiltonian. This can be demonstrated by considering transformations like,

$$e^{-i\frac{\alpha}{2}(xp_x+p_xx)}ae^{i\frac{\alpha}{2}(xp_x+p_xx)} = \sqrt{\frac{e^\alpha}{2}}x + \frac{i}{\sqrt{2e^\alpha}}p_x, \tag{5.33}$$

that can transform the $|0,0\rangle$ lowest-weight state to the vacuum. Let us consider the vacuum state in the under-damped regime for the (A,B) oscillators given as,

$$|0,0\rangle_{A,B} \equiv e^{-i\frac{\log(\hbar\sqrt{\varkappa})}{4}(xp_x+p_xx+yp_y+p_yy)}|0,0\rangle. \tag{5.34}$$

This mandates a corresponding transformation in the Hamiltonian H_{cB}, (5.26),

$$\begin{aligned} &e^{-\frac{i}{4}\alpha(xp_x+p_xx+yp_y+p_yy)}H_{cB}e^{\frac{i}{4}\alpha(xp_x+p_xx+yp_y+p_yy)} \\ &= e^{-\alpha}\left(p_xp_y + e^\alpha\gamma(yp_y - xp_x) + e^{2\alpha}\varkappa xy + e^{2\alpha}\frac{\epsilon}{2}\left(x^2+y^2\right)\right), \end{aligned} \tag{5.35}$$

as $e^{-\alpha}$ is factorized in the above it's possible to absorb it into various re-definitions. Explicitly, the following re-scalings of the timescale and coefficients recover the non-transformed Hamiltonian H_{cB}: $t \to e^{\frac{-\alpha}{2}}t$, $\gamma \to e^{\frac{-\alpha}{2}}\gamma$, $\varkappa \to e^{-\alpha}\varkappa$, and $\epsilon \to e^{-2\alpha}\epsilon$. We must also note the rather contentious case of the existence of a sensible ground state $\lim_{\epsilon\to 0} H_{cB}$ which has been subjected to a heated debate in literature [155–159]. Following [155], we consider a similarity-transformation on the operators A and B,

$$\begin{aligned} e^{-\theta(A^\dagger B^\dagger + AB)}Ae^{\theta(A^\dagger B^\dagger + AB)} &= \cos\theta A + \sin\theta B^\dagger, \\ e^{-\theta(A^\dagger B^\dagger + AB)}Be^{\theta(A^\dagger B^\dagger + AB)} &= \cos\theta B + \sin\theta A^\dagger, \end{aligned} \tag{5.36}$$

and correspondingly the Hamiltonian H_B also transforms,

$$\begin{aligned} e^{-\theta(A^\dagger B^\dagger + AB)}(H_0+H_1)e^{\theta(A^\dagger B^\dagger + AB)} &= \sqrt{\varkappa}(A^\dagger A - B^\dagger B) - i\gamma\sin(2\theta)(A^\dagger A \\ &\quad + B^\dagger B + 1) + i\gamma\cos(2\theta)(AB - A^\dagger B^\dagger). \end{aligned} \tag{5.37}$$

Clearly, this transformation breaks the unitarity of the Hamiltonian H_B and even though it preserves the eigenvalues, the inner products are not preserved. A notable exception is the case $\theta \in \mathbb{C}\backslash\mathbb{R}$ which corresponds to a Bogoliubov transformation and is unitarity-preserving. To summarize the contention we consider the same transformation on the $|0,0\rangle_{AB}$ state,

$$e^{-\theta(A^\dagger B^\dagger + AB)}|0,0\rangle_{AB} = \frac{1}{\cos\theta}e^{-\tan\theta A^\dagger B^\dagger}|0,0\rangle_{AB}, \tag{5.38}$$

which is normalized as (unless $\theta = \frac{\pi}{4}$ in the principal period),

$$|\theta,0,0\rangle_{AB} \equiv \frac{\cos(\theta+\theta^*)}{\cos\theta\cos\theta^*}e^{-\tan\theta A^\dagger B^\dagger}|0,0\rangle_{AB}. \tag{5.39}$$

Refs. [155,156] remark that the spectrum of the similarity-transformed Hamiltonian (5.37) may be computed when $\theta = \frac{\pi}{4}$ - as this choice puts the Hamiltonian in a diagonal form. However, other literature [157–159]

points out that the vacuum at $\theta = \frac{\pi}{4}$ is not a physically sensible one owing to the non-normalizability of the state in (5.39) and even though one may compute the eigenvalues for the diagonal similarity-transformed H_B at $\theta = \frac{\pi}{4}$, those eigenvalues do not correspond to physical observables.

We shall utilize spread complexity to add to this discussion and elucidate certain aspects in the next section but at the moment we point out that, mathematically, in terms of the representation theory of the sub-algebra of $\mathfrak{so}(5,\mathbb{C})$ everything is kosher as the lowest-weight state $|0,0\rangle_{AB}$ is defined without nuances. The Hamiltonian-flow originating from H_{cB} in (5.26) is constrained on the manifold of the corresponding coherent states - hence, for the computation of spread complexity the presence or absence of a sensible vacuum is neither necessary nor relevant result of the lowest-weight state being well defined and the restricted Hamiltonian flow.

5.3 Spread Complexity

The coupled Bateman oscillator problem is sufficiently involved that generic closed-form analytic expressions for spread complexity are not straight-forward to compute. However, as demonstrated in [35,106,160], presence of an underlying algebra (specially, if it is low-dimensional) can simplify the computations considerably and, in particular, analytic expressions for return amplitudes as well as corresponding Krylov (spread) complexities can be obtained in closed-form. This is exactly the machinery employed in Ch.4.3.2 to obtain analytic expressions of the spread complexities for three circuits connecting various states in the Kitaev chain. We make an express note of the possibility of obtaining analytic expressions for return amplitude because in the absence of identification of the underlying algebra or if the algebra is not simple then the utility of return amplitude to compute spread complexity is brought into limelight. Furthermore, if return amplitude cannot be computed analytically in closed-form we can still obtain certain interesting results working at the tree-level or low-order corrections to the amplitude [107,108].

5.3.1 Analytic results

In this section we discuss some analytic closed-form expressions of the return amplitude and spread complexities - obtained in specific limits, owing to the difficulty of obtaining generic closed-form results. Certain limits lend themselves well to analytical methods of solutions and hereby we identify these limits as well as compute relevant spread complexities in these limits as functions of the parameters of the coupled Bateman oscillator.

Limits of $\epsilon \to 0$ and $\gamma \to 0$

We demonstrated in Ch.5.1 that the generators of H_{cB} constitute a $\mathfrak{su}(1,1)$ algebra, and that the full set of generators are spanned through the operators written down in (5.15). As our aim is to compute spread complexity, we choose to work with the coherent states and as seen previously the full over-complete manifold of coherent states are connected through these generators via their applications on the lowest-weight state. As $\epsilon \to 0$, we can work with the definitions in (5.12) and analytic solutions become a possibility when the

following coherent state representation is considered,

$$|z\rangle = (1 - z\bar{z})^{\frac{1}{4}}\, e^{zA^\dagger B^\dagger} |0,0\rangle_{AB}. \tag{5.40}$$

The factor $(1 - z\bar{z})^{\frac{1}{4}}$ can be absorbed into re-definitions and we start with a simpler form of the above representation,

$$|z_{ab}\rangle = e^{z_{ab}A^\dagger B^\dagger} |0,0\rangle_{AB}, \tag{5.41}$$

and again, as $\epsilon \to 0$, we have the usual Bateman oscillator so the Hamiltonian is $H_B = H_0 + H_1$ as given in (5.5), with the analytically computed spread complexity expressed as [160],

$$\boxed{C(|z\rangle, |z_{ab}\rangle; H_B) = \frac{(z - z_{ab})(\bar{z} - \bar{z}_{ab})}{(1 - z_{ab}\bar{z}_{ab})(1 - z\bar{z})}.} \tag{5.42}$$

Interestingly, as a result of the Lie algebra being a rank-1 algebra the complexity comes out independent of the parameters that the Hamiltonian H_B depends upon. Note that this expression is independent of the choice of parameters in the Hamiltonian. By contrast, if we consider states that are time-evolved the Hamiltonian parameters do feature in the spread complexity through the time-evolved state's dependence on the same. As discussed previously, this time evolution corresponds to a flow in the coherent-state manifold and more concretely the time-evolved target state is expressed by [2],

$$|z_{ab}(t)\rangle = Ne^{-itH_B} e^{z_{ab}A^\dagger B^\dagger} |0,0\rangle_{AB} = Ne^{\frac{z_0 \cosh(\gamma t) - \sinh(\gamma t)}{\cosh(\gamma t) - z_0 \sinh(\gamma t)} A^\dagger B^\dagger} |0,0\rangle_{AB}. \tag{5.43}$$

This results in the following complexity for the preparation of the time evolved target state,

$$\boxed{C(|z_{ab}(t)\rangle; |z_{ab}(0)\rangle, H_B) = (1 + \sin^2\phi \sinh^2(2\rho)) \sinh^2(\gamma t),} \tag{5.44}$$

where we've substituted $z_{ab} = e^{i\phi} \tanh\rho$. Note that the rate of exponential growth is determined entirely by the damping constant γ, while the choice of coherent reference state affects only the overall constant. It is remarkable to observe the separation of various parameters in the above equation: the parameters related to the choice of target state ($z_{ab} \equiv z_{ab}(\phi, \rho)$) only appear as an overall factor and do not determine the time evolution of spread complexity which is entirely fixed through the damping parameter, γ - an increase in the damping factor leads to spread complexity increasing quickly signifying faster information transport in the system. There is no choice of (ϕ, ρ) that trivializes the spread complexity and hence we can also state that the states in (5.39) are not the eigenstates of the Hamiltonian - which serves to elucidate the same point made in [157–159]. This leads us to conclude that the ground state, which - by definition - is an eigenstate of the Hamiltonian, cannot lie on the manifold of normalizable coherent states traversed through choices of (ϕ, ρ).

(5.31) contains all the reference (coherent) states that can be chosen to compute spread complexity for the Hamiltonian, H_{cB}, corresponding to the linearly coupled Bateman oscillators. It is apparent, as explained previously, that a similarity transformation of Hamiltonian H_{cB} and the circuit states does not change the spread complexity. Consequently, there are similarity-classes of equivalent reference states that result in the

same spread complexity - we chose to work with a subset of the states which correspond to distinct physics. These states are expressed as,

$$|z_{ab}, \Omega\rangle = N e^{-\frac{\log(\Omega)}{4}(a^\dagger a^\dagger - aa + b^\dagger b^\dagger - bb)} e^{z_{ab} a^\dagger b^\dagger} |0, 0\rangle. \tag{5.45}$$

There is a simple interpretation of the parameters describing the coherent state above: z_{ab} is the parameter that connects the state to the Fock basis and Ω values the oscillation scale as per (5.33). The return amplitude is computed to be,

$$\begin{aligned} R(t) &= \langle \bar{z}_{ab}, \Omega | e^{\bar{z}_{ab} ab} e^{\frac{\log(\Omega)}{4}(a^\dagger a^\dagger - aa + b^\dagger b^\dagger - bb)} e^{-itH_1} |z_{ab}, \Omega\rangle \\ &= \left(\frac{(\Omega^2 - k)^2}{4k\Omega^2} (1 + c^2) \sin^2(\sqrt{k}t) + \left(\cosh(\gamma t) + ic \sinh(\gamma t)\right)^2 \right)^{-\frac{1}{2}}, \end{aligned} \tag{5.46}$$

where,

$$c = -i \frac{z_{ab} - \bar{z}_{ab}}{1 - z_{ab}\bar{z}_{ab}}. \tag{5.47}$$

This can be seen to be equivalent to the spread complexity for the standard Bateman system, expressed through the Hamiltonian H_B, given in (5.42) with a choice of $\Omega^2 = \varkappa$ - and in which case the state of the system is an eigenstate of the free part, H_0, of the standard Bateman system H_B. Additionally, without any damping the system is nothing but a couple of harmonic oscillators, so one expects the system to be periodic and this is precisely what's observed *i.e.* the return amplitude's $\gamma \to 0$ limit has a period of $\sqrt{\varkappa}$ for $\varkappa > 0$ (otherwise the frequencies are complex and system is not conservative). When $\Omega^2 \neq \varkappa$, in addition to H_0 imparting oscillating features to the spread complexity, there is also H_1 which is responsible for the interaction between the two systems and hence imparts growing behavior to the spread complexity as well as in return amplitude. As the state evolves in time, the tension between these two complementary behaviors can be observed - depending on an appropriate choice of parameters and timescale. This is beautifully captured in the Figs.(8) and (10). Furthermore, it turns out that the Krylov basis is infinite-dimensional for the linearly coupled Bateman system - this is owed to the fact that the states we consider never cease growing. This leads to an interesting phenomenon that H_0 attempts to restrict the state of the system to an average position on the Krylov chain (recalling their ordered nature) while H_1 attempts to push the state along the Krylov chain - at an exponential pace.

To see this in more precise terms, we compute the derivative of the return amplitude (which necessarily contains all the information and spread complexity is merely extracting a specific part of that information),

$$R'(t) = R(t)^{-\frac{3}{2}} \left(\frac{(1 + c^2)(k - \Omega^2)^2}{8\sqrt{k}\Omega^2} \sin(2\sqrt{k}t) - \frac{1 - c^2}{2} \gamma \sinh(2\gamma t) - ic\gamma \cosh(2\gamma t) \right). \tag{5.48}$$

As $\gamma \to 0$, we just have two harmonic oscillators oscillating without any damping so we expect the system to be periodic and correspondingly - the derivative above vanishes an infinite number of times in this limit,

indicating the system's oscillatory behavior. For a finite non-vanishing γ the derivative may vanish only a finite number of times - this arises from the recurring overlap of the time-evolved state with the reference state (which has zero complexity!) and hence is a local maxima in the derivative of the return amplitude. As the system evolves so does the target state, and the overlap between the time-evolved state and the reference state grows non-existent leading to the derivative not vanishing. This contrasting behavior, demonstrated neatly in Fig.(8), of trigonometric functions and hyperbolic functions (for appropriate choice of parameters) leads to a slower-than-usual growth rate of complexity at initial times - with the former type of functions responsible for oscillations and the latter ones for exponential growth. We do note that this analysis only applies to the under-damped regime with $\varkappa > 0$ becuase for the over-damped regime $\varkappa < 0$ both H_0 and H_1 lead to hyperbolic functions (as the frequencies are complex) and no similar competition is observed.

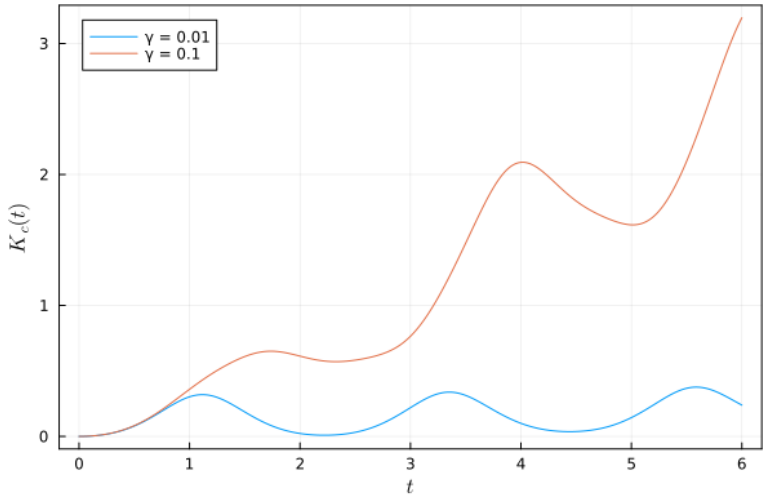

Figure 8: In this figure, we illustrate the time profile of spread complexity of the time-evolved reference state, using parameters $\varkappa = 2.0$, $\epsilon = 0.0$, while varying the value of γ for the weakly-coupled under-damped Bateman oscillator system. The reference state is defined as the coherent state with $\Omega = 1.0$ and $z_{ab} = 0$, chosen consistently throughout this work. The first 50 probability amplitudes are taken to contribute to the spread complexity, accounting for at least 95% of the total probability. This plot highlights the interplay between oscillation vs exponential growth time-scales. Specifically, for $\gamma = 0.01$, the oscillation time-scale is shorter than the growth time-scale, making growth difficult to observe. Conversely, with $\gamma = 0.1$, the growth in complexity is apparent even at initial time-scales.

5.3.2 General Case

In the previous section we considered the behavior of the spread complexity (and return amplitude) to get a physical intuition of the system and to ascertain that the spread complexity is indeed physically relevant. We also remarked that it is not straightforward to obtain a generic closed-form analytic expression for the return amplitude, and consequently the spread complexity. It may not be straightforward, however, it is possible to

compute the return amplitude for an arbitrary coherent-state circuit. An indispensable tool towards this are the Baker-Campbell-Hausdorff formulae - the discussion of which is deferred to App.(D). The computation is, as in the case of Kitaev chain, facilitated by the Hamiltonian constituting a finite-dimensional algebra as charted out in Chs.5.1 and 5.2. The generic coherent states can be uniquely identified by three parameters which are complex and the corresponding return amplitude assumes the form,

$$\boxed{R(t) = \left(1 + c_{++}e^{(\omega_1+\omega_2)t} + c_{+-}e^{(\omega_1-\omega_2)t} + c_{-+}e^{(-\omega_1+\omega_2)t} + c_{--}e^{-(\omega_1+\omega_2)t}\right)^{-1/2},} \tag{5.49}$$

where,

$$i\omega_1 = \sqrt{\varkappa - \gamma^2 - \sqrt{\epsilon^2 - 4\gamma^2\varkappa}}, \quad i\omega_2 = \sqrt{\varkappa - \gamma^2 + \sqrt{\epsilon^2 - 4\gamma^2\varkappa}}. \tag{5.50}$$

The nature of these frequencies (complex, real, or purely imaginary) dictates the physics featuring in the return amplitude. The choice of a specific coherent state only serves to modify the coefficients $c_{\pm\pm}$ and a generic choice of coherent states serves little purpose - so we might as well choose a specific value of these coefficients with no loss of generality,

$$\langle 0,0|e^{\frac{i}{4}\log(\Omega)(xp_x+p_xx+yp_y+p_yy)}e^{-itH}e^{-\frac{i}{4}\log(\Omega)(xp_x+p_xx+yp_y+p_yy)}|0,0\rangle = \left(\frac{\Sigma^2-\Delta^2-\tau^2}{16(\omega_2^2-\omega_1^2)\Omega^2}\right)^{-\frac{1}{2}}, \tag{5.51}$$

where,

$$\begin{aligned}
\Sigma &= -2\Omega(\omega_1^2-\omega_2^2)\left(\cosh(\omega_1 t) + \frac{i\epsilon}{2\Omega\omega_1}\sinh(\omega_1 t) + \cosh(\omega_2 t) + \frac{i\epsilon}{2\Omega\omega_2}\sinh(\omega_2 t)\right) \\
&\quad + 2i\epsilon(\varkappa+\Omega^2)\left(\frac{\sinh(\omega_1 t)}{\omega_1} - \frac{\sinh(\omega_2 t)}{\omega_2}\right), \\
\Delta &= 4\epsilon\Omega\left(\cosh(\omega_2 t) + \frac{i\epsilon}{2\Omega}\frac{\sinh(\omega_2 t)}{\omega_2} - \cosh(\omega_1 t) - \frac{i\epsilon}{2\Omega}\frac{\sinh(\omega_1 t)}{\omega_1}\right) \\
&\quad + i(\varkappa+\Omega^2)\left((4\gamma^2+\omega_1^2-\omega_2^2)\frac{\sinh(\omega_1 t)}{\omega_1} + (-4\gamma^2+\omega_1^2-\omega_2^2)\frac{\sinh(\omega_2 t)}{\omega_2}\right), \text{ and} \\
\tau &= 4\gamma\left((\varkappa-\Omega^2)(\cosh(\omega_2 t)-\cosh(\omega_1 t)) + i\epsilon\Omega\left(\frac{\sinh(\omega_1 t)}{\omega_1} - \frac{\sinh(\omega_2 t)}{\omega_2}\right)\right).
\end{aligned} \tag{5.52}$$

Ω marks the scaling of the Bateman oscillators and does not feature in the trigonometric functions which determine the time dependence of return amplitude (and, in turn, spread complexity) thereby indicating that it only affects the superposition. Here onwards, there are (at least) two prominent ways to compute the spread complexity: firstly, by using the moments method; and secondly, by the typical Lanczos algorithm. We note that, to capture the time-evolved state precisely we must include a sufficient number of probability amplitudes associated with the Krylov basis (complexity wavefunctions). At around $t = 0$ only the first few probability amplitudes are non-vanishing and contribute to the spread complexity - however, as the state evolves exponentially more and more Krylov basis vectors or probability amplitudes become significant. There are three regimes of distinct dynamics depending on the value of $\varkappa$: under-damped, over-damped,

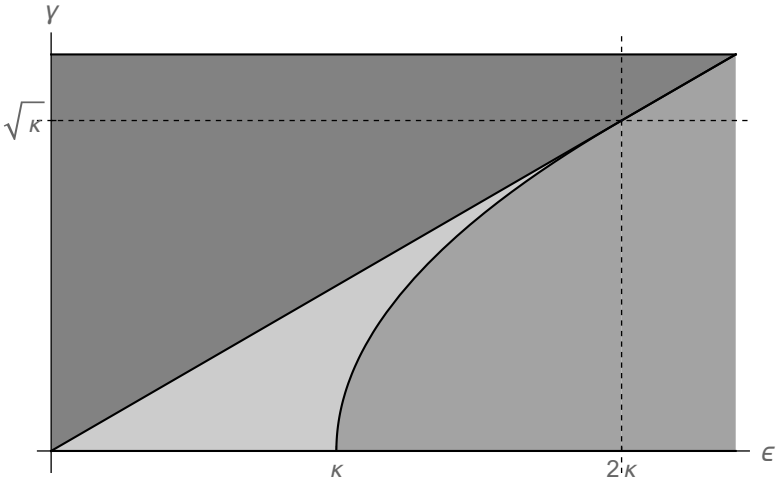

Figure 9: In the under-damped case with $\varkappa > 0$, three distinct regimes can be identified based on the frequencies. When the conditions $\epsilon > 2\sqrt{\varkappa}\gamma$ and $\epsilon < \gamma^2 + \varkappa$ hold, the frequencies are real, as indicated by the lightest shading in the figure. This range diminishes as γ approaches $\sqrt{\varkappa}$, and once γ exceeds $2\sqrt{\varkappa}$, it becomes impossible to obtain two real frequencies.

and critically damped. We shall now focus on each of these regimes and compute spread complexity's behavior to observe if it can distinguish these distinct dynamical regimes. We defer a detailed discussion of the numerical methods utilized to obtain the following results to App.(E).

5.3.3 Under-damped Regime

The first region in the parameter space is the under-damped region which corresponds to the $\varkappa > 0$ in the phase space of parameters. The frequencies in this regime can be put into three categories [37] which are demonstrated in Fig.(9). We observe that the most analytically accessible expressions are obtained when $\Omega = \sqrt{\varkappa}$ and use this value in the following.

Weak Coupling

ϵ represents the coupling strength and as discussed previously there are two critical values of the coupling. If $\epsilon < \epsilon_1$, we say that the system is weakly coupled and the return amplitude is given as,

$$\begin{aligned}\langle 0,0|e^{-itH}|0,0\rangle = \Bigg(&\frac{\Omega^2\gamma^2}{2\Delta^2\Sigma^2} - \frac{(\Omega^2-\Sigma^2)((\Omega^2-\Sigma^2)\Delta^2+\Omega^4)}{2\Sigma^2(\Delta^2+\Sigma^2)\Omega^2}\cos(2\Sigma t)\Bigg)\\ &+\frac{(\Sigma^2-\Omega^2)^{\frac{3}{2}}\sqrt{\Delta^2+\Omega^2}}{\Sigma(\Delta^2+\Sigma^2)\Omega}\sin(2\Sigma t) + \frac{(\Sigma^2-\Omega^2)^{\frac{1}{2}}(\Delta^2+\Omega^2)^{\frac{3}{2}}}{\Delta(\Delta^2+\Sigma^2)\Omega}\sinh(2\Delta t)\\ &+\frac{(\Delta^2+\Omega^2)(\Delta^2\Sigma^2+\Omega^2(\Sigma^2-\Omega^2))}{2\Delta^2(\Delta^2+\Sigma^2)\Omega^2}\cosh(2\Delta t)\Bigg)^{-\frac{1}{2}},\end{aligned} \tag{5.53}$$

with,

$$
\begin{aligned}
2\Sigma &= \sqrt{\Omega^2 - \gamma^2 + i\sqrt{4\gamma^2\Omega^2 - \epsilon^2}} + \sqrt{\Omega^2 - \gamma^2 - i\sqrt{4\gamma^2\Omega^2 - \epsilon^2}}, \\
2\Delta &= i\left(\sqrt{\Omega^2 - \gamma^2 + i\sqrt{4\gamma^2\Omega^2 - \epsilon^2}} - \sqrt{\Omega^2 - \gamma^2 - i\sqrt{4\gamma^2\Omega^2 - \epsilon^2}}\right).
\end{aligned}
\tag{5.54}
$$

It is observed that the return amplitude consists of two types of functions: trigonometric functions and hyperbolic functions. The former has a time-scale of Σ, while the latter has a time-scale of Δ. For small values of Δ the spread complexity is roughly oscillatory as the coefficients multiplying the trigonometric and hyperbolic functions are comparable. This feature is distinguished in the early-time regime but is also present at later times. The presence of hyperbolic functions in return amplitude, as discussed previously, implies that the spread complexity grows without bound and that the probability amplitudes become (highly) delocalized on the Krylov basis, eventually. Hence, the overall behavior of spread complexity is oscillatory on a small time-scale but with growth apparent on more coarse-grained ones. This is demonstrated in Fig.(10). The spread complexity shows exponential growth, such that the time-scale is roughly estimated by the quantity Δ in (5.54). In this $\epsilon < \epsilon_1$ weak coupling regime, the probability amplitudes consist of trigonometric functions, with frequency Σ. For $\Sigma > \Delta$, spread complexity is exponentially growing on longer scales but oscillating on the shorter ones, Fig.(8).

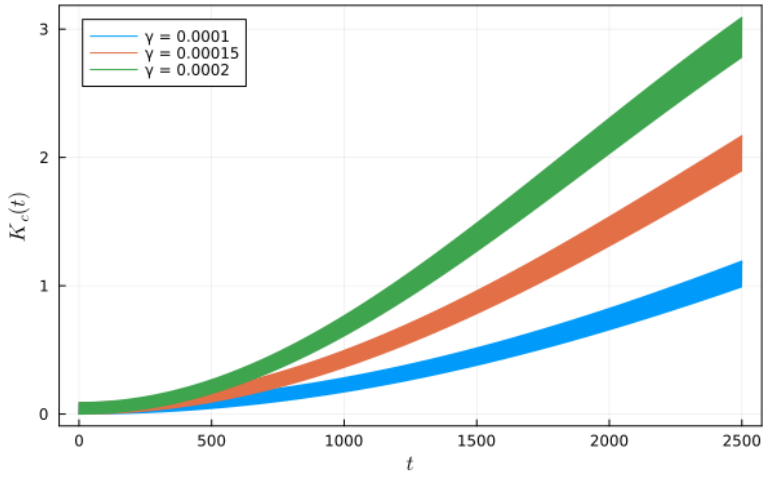

Figure 10: The spread complexity is analyzed for the parameters $\varkappa = 1.5$, $\Omega = 1.0$, $N = 30$, and $\epsilon = 0.5\epsilon_1$ across different values of γ. At least 95% of the total probability is accounted for. Larger values of γ result in more pronounced exponential growth. Because the parameters are sufficiently small, setting $\epsilon = 0$ does not significantly modify the spread complexity owing to the very weakly coupled system. The observed 'band-like' pattern reflects closely spaced oscillations.

Rabi Oscillations

The linearly coupled Bateman oscillator features Rabi oscillations in the PT-symmetric phase which the system exhibits when the coupling between the two oscillators falls within the two critical values of couplings

i.e. when $\epsilon_1 < \epsilon < \epsilon_2$. The corresponding return amplitude is expressed as,

$$\begin{aligned}\langle 0,0|e^{-itH}|0,0\rangle = &\left(-\frac{\Omega^2\gamma^2}{2\Delta^2\Sigma^2} + \frac{(\Omega^2-\Sigma^2)(-(\Omega^2-\Sigma^2)\Delta^2+\Omega^4)}{2\Sigma^2(\Delta^2+\Sigma^2)\Omega^2}\cos(2\Sigma t)\right)\\ &- i\frac{(\Sigma^2-\Omega^2)^{\frac{3}{2}}\sqrt{\Delta^2-\Omega^2}}{\Sigma(\Sigma^2-\Delta^2)\Omega}\sin(2\Sigma t) + i\frac{(\Sigma^2-\Omega^2)^{\frac{1}{2}}(\Delta^2-\Omega^2)^{\frac{3}{2}}}{\Delta(\Delta^2-\Sigma^2)\Omega}\sin(2\Delta t)\\ &\left(+\frac{(\Delta^2-\Omega^2)(\Delta^2\Sigma^2+\Omega^4-\Sigma^2\Omega^2}{2\Delta^2(\Delta^2-\Sigma^2)\Omega^2}\cos(2\Delta t)\right)^{-\frac{1}{2}},\end{aligned} \tag{5.55}$$

for which,

$$\begin{aligned}2\Sigma &= \sqrt{\Omega^2-\gamma^2+\sqrt{\epsilon^2-4\gamma^2\Omega^2}} + \sqrt{\Omega^2-\gamma^2-\sqrt{\epsilon^2-4\gamma^2\Omega^2}}\\ 2\Delta &= \sqrt{\Omega^2-\gamma^2+\sqrt{\epsilon^2-4\gamma^2\Omega^2}} - \sqrt{\Omega^2-\gamma^2-\sqrt{\epsilon^2-4\gamma^2\Omega^2}}.\end{aligned} \tag{5.56}$$

For this regime, the return amplitude - and, consequently, the spread complexity - are composed entirely of periodic functions and have exclusively real frequencies (with a discrete spectrum for the Hamiltonian) since this regime corresponds to the conservative phase space such that the roles of the driven and damped oscillators are periodically interchanged. More precisely, when (ω_1, ω_2) are rational the coupled Bateman oscillator system is periodic, subject to Σt and Δt both being multiples of π. Generically, for arbitrary non-rational practical values of (ω_1, ω_2) the system is only only roughly periodic as real numbers can be approximated via rational ones. More importantly, we note that the spread complexity is periodic and bounded - a property characterizing the Rabi oscillation *i.e.* PT-symmetric phase, as seen in Fig.(11).

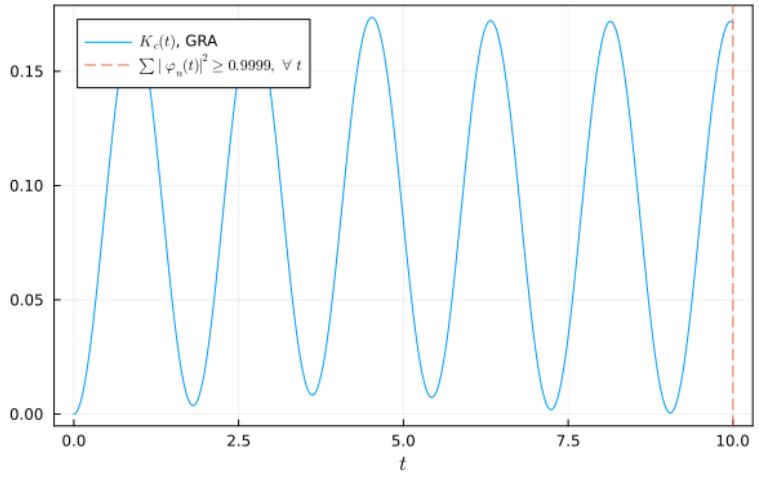

Figure 11: The spread complexity is estimated using the first 40 probability amplitudes for the parameters $\varkappa = 2.0,\ \Omega = 1.0, \gamma = 0.01, \epsilon = 1.014$. This selection captures at least 99.99% of the time-evolved reference state through the first 40 complexity-wavefunctions within the shown time-range.

Ultra-Strong Coupling

The last remaining regime for under-damped system is that of the ultra-strong coupling which corresponds to $\epsilon > \epsilon_2$ in the parameter space. We note the following relation for the return amplitude,

$$\begin{aligned}\langle 0,0|e^{-itH}|0,0\rangle = &\left(-\frac{\Omega^2(\Omega^2+2(\omega_1^2-\omega_2^2))}{2(\omega_1^2+\omega_2^2)^2}+\frac{\Omega^4+2\Omega^2(\omega_1^2-\omega_2^2)+2(\omega_1^2+\omega_2^2)^2}{2(\omega_1^2+\omega-2^2)^2}\cosh(2\omega_1 t)\cos(2\omega_2 t)\right)\\ &+i\frac{\sqrt{\Omega^4+2\Omega^2(\omega_1^2-\omega_2^2)+(\omega_1^2+\omega_2^2)^2}}{2\Omega(\omega_1^2+\omega_2^2)}\times\\ &\times\left(\frac{\Omega^2+\omega_1^2+\omega_2^2}{\omega_2}\cosh(2\omega_1 t)\sin(2\omega_2 t)+\frac{\Omega^2-\omega_1^2-\omega_2^2}{\omega_1}\times\sinh(2\omega_1 t)\cos(2\omega_2 t)\right)\\ &\left[-\frac{\Omega^6(\omega_1^2-\omega_2^2)+2\Omega^4(\omega_1^2-\omega_2^2)^2+2\Omega^2(\omega_1^2-\omega_2^2)(\omega_1^2+\omega_2^2)^2+(\omega_1^2+\omega_2^2)^4}{4\Omega^2\omega_1\omega_2(\omega_1^2+\omega_2^2)^2}\right.\\ &\left.\times\sinh(2\omega_1 t)\sin(2\omega_2 t)\right]^{-\frac{1}{2}},\end{aligned} \tag{5.57}$$

with the following notations for ω_1 and ω_2,

$$\omega_1=\frac{1}{2}\sqrt{\sqrt{\epsilon^2-4\gamma^2\Omega^2}-(\Omega^2-\gamma^2)},\quad \omega_2=\frac{1}{2}\sqrt{\sqrt{\epsilon^2-4\gamma^2\Omega^2}+(\Omega^2-\gamma^2)}. \tag{5.58}$$

Clearly, every term has hyperbolic-function dominant features and hence we do not observe any regimes with periodic behavior. Consequently, the spread complexity grows exponential, as demonstrated in Fig.(12). On a purely computational level, it is interesting to observe that to faithfully encapsulate the time-evolved target state we required more number of probability amplitudes, compared to the weakly-iterating $\epsilon < \epsilon_1$ regime, to be summed for any desired time evolution duration. This correlates with the difficulty of engineering the system in the strongly-coupled $\epsilon > \epsilon_2$ regime.

5.3.4 Overdamped Regime

Having studied the under-damped regime in detail and having observed that the profile of spread complexity accurately captures the underlying dynamics quite precisely, we turn our attention to the less-physically relevant case of over-damped regime which corresponds to the $\varkappa < 0$ parameter space and with the presence of complex frequencies, (5.50). Again, the choice of $\varkappa = -\Omega^2$ leads to a remarkably simple form for the return amplitude,

$$R(t)=\left[\left(\cosh(\omega_1 t)+\frac{i\epsilon}{2\sqrt{-\varkappa}\omega_1}\sinh(\omega_1 t)\right)\left(\cosh(\omega_2 t)+\frac{i\epsilon}{2\sqrt{-\varkappa}\omega_2}\sinh(\omega_2 t)\right)\right]^{-\frac{1}{2}}. \tag{5.59}$$

The frequencies here are,

$$\begin{aligned}\omega_1&=\sqrt{\Omega^2+\gamma^2-\sqrt{\epsilon^2+4\Omega^2\gamma^2}},\\ \omega_2&=\sqrt{\Omega^2+\gamma^2+\sqrt{\epsilon^2+4\Omega^2\gamma^2}},\end{aligned} \tag{5.60}$$

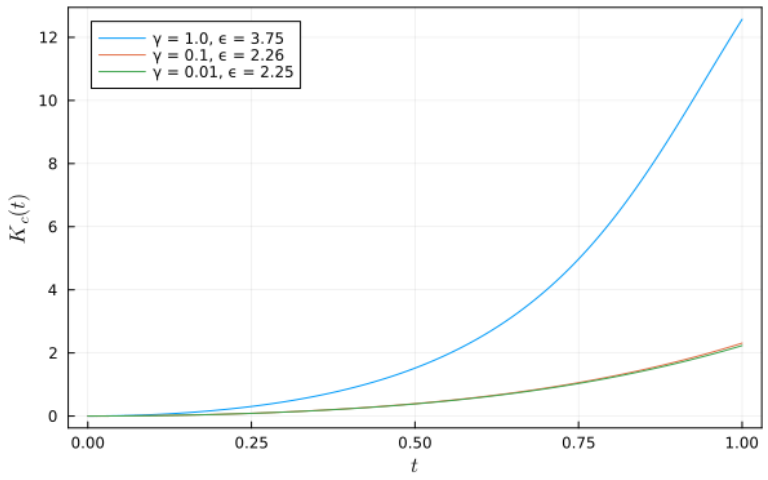

Figure 12: The spread complexity is determined for $\varkappa = 1.5$, $\Omega = 1$, and $N = 80$ across different values of γ. This analysis captures at least 99% of the total probability. The exponential growth becomes increasingly evident with larger values of γ, which is associated with an increase in ϵ, fixed at $1.5\epsilon_2$ for all three scenarios, indicating that the system is strongly coupled.

and $\omega_1 \in \mathbb{C}\backslash\mathbb{R}$ purely imaginary if $\epsilon > |\gamma^2 + \varkappa| = \epsilon_2$. Hence, there appear to be two dynamical patterns for the over-damped system: the first, with exclusively hyperbolic-dominant growth; and the second, with a superposition of both hyperbolic and trigonometric growth. Interestingly, the case with purely hyperbolic function dominant growth is reminiscent of the ultra-strongly coupled under-damped case - with a caveat that, here $\omega_1 < \omega_2$ identically, which leads to a faster growth patterns in the spread complexity as compared to the under-damped case. Consequently, we could not identify the phase space which corresponds to the oscillatory growth becoming apparent at any time-scale for the over-damped system. Hence, spread complexity is devoid of interesting features and simply shows exponential growth as observed in Fig.(13).

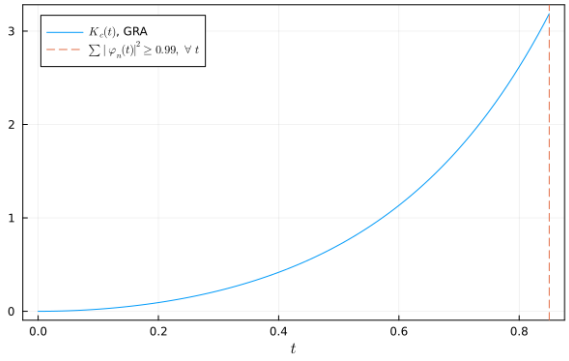

(a) $\epsilon = 0.007\epsilon_2$

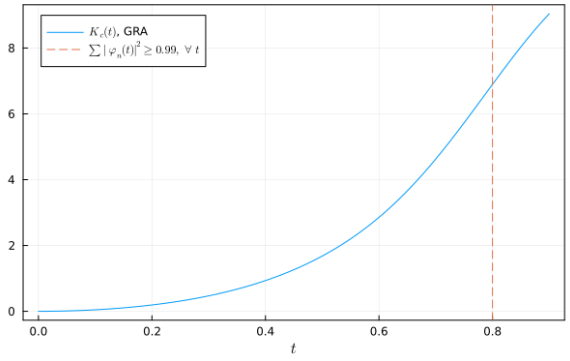

(b) $\epsilon = 1.5\epsilon_2$

Figure 13: The spread complexity for over-damped oscillator system with $\varkappa = -2.0$, $\epsilon_2 = 2.0$, $\gamma = 0.01$, $\Omega = 1.0$, and $N = 50$.

5.3.5 Critically Damped Regime

The final case under consideration is that of the critically-damped regime with $\varkappa = 0$, for which the return amplitude is computed to be,

$$R(t) = \left[\left(\cosh(\sqrt{\gamma^2+\epsilon}t) + i\frac{(\epsilon-\Omega^2)\sinh(\sqrt{\gamma^2+\epsilon}t)}{2\Omega\sqrt{\gamma^2+\epsilon}}\right)\left(\cosh(\sqrt{\gamma^2-\epsilon}t) + i\frac{(\epsilon+\Omega^2)\sinh(\sqrt{\gamma^2-\epsilon}t)}{2\Omega\sqrt{\gamma^2+\epsilon}}\right)\right] + \left[\frac{\gamma^2\Omega^2}{2\epsilon^2}\left(\cosh(\sqrt{\gamma^2-\epsilon}t)\cosh(\sqrt{\gamma^2+\epsilon}t) - \frac{\gamma^2\sinh(\sqrt{\gamma^2-\epsilon}t)\sinh(\sqrt{\gamma^2+\epsilon}t)}{\sqrt{\gamma^4-\epsilon^2}} - 1\right)\right]^{-\frac{1}{2}}. \tag{5.61}$$

As this is the critically-damped case, both critical points merge into a single transition point at $\epsilon = \gamma^2$. We observe precisely the same behavior in spread complexity as for the over-damped case with exactly the same physical motivations and the time-scales at which oscillation-dominant growth become apparent are significantly larger than the ones for exponential-dominant growth, leading to an exponentially growing spread complexity, as shown in Fig.(14).

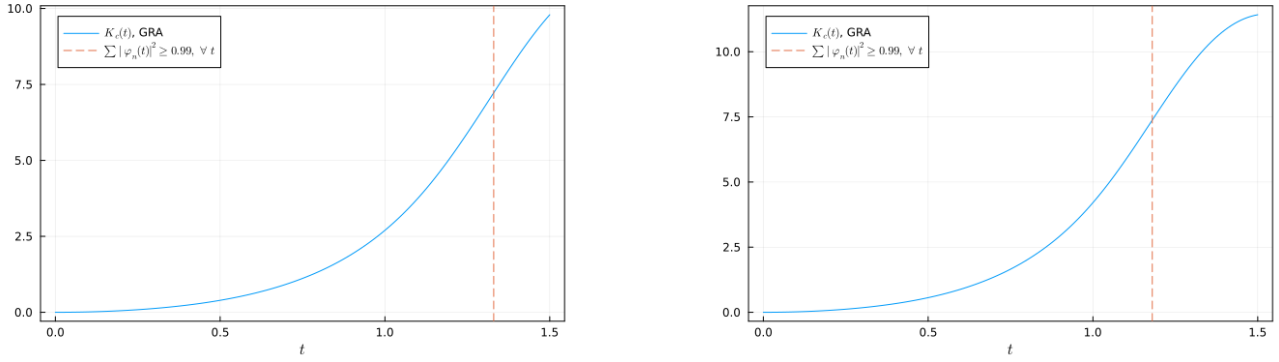

(a) $\epsilon = 0.5 \times \epsilon_2$ (b) $\epsilon = 1.5 \times \epsilon_2$

Figure 14: The spread complexity for critically-damped Bateman oscillator system with $\varkappa = 0.0$, $\epsilon_2 = 1.0$, $\gamma = 1.0$, $\Omega = 1.0$, and $N = 50$.

6 Summary & Outlook

"All truths are easy to understand once they are discovered; the point is to discover them."
- Galileo Galilei

In this thesis, we proposed a modern diagnostic for detecting phase transitions in and out of different phases of quantum matter - the *Krylov complexity*, and more specifically we worked with the Krylov complexity of quantum states, also known as spread complexity (although the same term is technically applicable to K-complexity of operators but canonically its reserved for the K-complexity of states). While Krylov complexity was initially introduced in literature as a diagnostic of quantum chaos, defined through BGS conjecture - we've proposed a repurposing of it as a tool for detecting quantum phase transitions. We've also defended our proposal in two prototypical models: Kitaev chain and linearly-coupled Bateman oscillator, by computing spread complexity of various circuits (reference state to target state) and demonstrating its ability to accurately as well as consistently capture different types of phase transitions.

We began with setting up a premise and background on the field of quantum chaos which primarily deals with understanding transport properties of quantum systems whose classical counterparts demonstrate chaotic characteristics via exponential sensitivity to initial conditions, or RMT-like spectral correlations, or any other probe (like alignment indices). Through important contributions of Dyson and Wigner, among others, RMT-like spectral correlations were discovered in the context of heavy nuclei with high number of degrees of freedom. Further works by BGS and others helped establish a universal link between RMT-like behavior and generic quantum chaotic systems with high degrees of freedom. This link was then extended to an arbitrary number of degrees of freedom by studying quantum systems with low (two) degrees of freedom like Sinai billiards [45] (whose classical version is known to be chaotic) and contrasting the behavior with circular billiards (whose classical version is known to be integrable). Hence, RMT-like or Wigner-Dyson spectral correlations emerged as the *de facto* working definition of quantum chaos by the late 1980s which has persisted to this day; while Poisson-like statistics are widely understood to be a signature of integrable systems. However, the definition of quantum chaos (through the BGS conjecture) as presence of Wigner-Dyson spectral distribution, has not been without some challenges including presence of quantum phenomena like scars and localization. It is interesting to note that classical chaotic systems are non-deterministic while quantum chaotic systems are quite deterministic owing to the linearity of the Schrödinger Equation and in the $\hbar = 0$ classical regime the determinism turns to non-determinism. We then discussed some probes of quantum chaos in literature, including Spectral Form Factor, Out-of-Time-Order Correlators, and Quantum Complexity - which is, in essence, similar to Krylov complexity, the object of interest in this thesis.

We identified the theoretical framework underpinning Krylov complexity as the Krylov subspace and discussed in detail its construction. We observed that, in the Heisenberg representation, operator evolution can be effected through a Liouvillian operator which is just a commutator with the usual Hamiltonian: $\mathscr{L} = [H, \cdot]$. The Liouvillian operator is in-fact a super-operator which means that it acts on the space of

the linear operators which themselves act on the Hilbert space $\mathscr{H}$ *i.e.* $\mathcal{O} : \mathscr{H} \mapsto \mathscr{H}$ and $\mathscr{L} : L(\mathscr{H}) \mapsto L(\mathscr{H})$. This, in turn, means that one can associate a state, $|\mathcal{O})$, with any linear operator $\mathcal{O} \in L(\mathscr{H})$, which acts on $\mathscr{H}$, via the GNS or Choi-Jamiolkowski construction (or any other equivalent construction) and hence, one can treat the Liouvillian as if it were a Hamiltonian - albeit acting on $L(\mathscr{H})$ rather than $\mathscr{H}$. The Hamiltonian dynamical evolution of a generic operator, $\mathcal{O} \in L(\mathscr{H})$, is then represented as, $\mathcal{O}(t) = e^{i\mathscr{L}t}\mathcal{O}(0)$. One can then construct a basis out of the set of various powers of $\mathscr{L}$ acting on $\mathcal{O}$ which can be ortho-normalized to furnish the Krylov basis as well as a set of powerful coefficients called Lanczos coefficients that condense all the dynamical information of the system. The Krylov basis, through construction, is ordered according to the powers of $\mathscr{L}$ or nested commutators. Importantly, it turns out that the Liouvillian operator is tri-diagonal in this basis which leads to a significant reduction in amount of work to compute the time-evolved operator. Krylov complexity is then defined as the average position on the ordered Krylov basis and serves as a probe of quantum chaos, it shows different asymptotic behavior for different dynamical classes of system under time evolution which we summarized in Table 1. We then showed how the operator definition can be easily extended to one for states, wherein complexity is seen as a minima of a specific cost function - reminiscent of Nielsen's circuit complexity, with the additional benefit that one does not need to define an operator to state map. Thereafter, one can unify both the state and operator notions of Krylov complexity in terms of the label operator $l = \sum_{n=0}^{K-1} c_n \, |n\rangle \, \langle n|$, where K is the dimension of the Krylov subspace, by shifting to a doubled Hilbert space in order to effect an operator to state map. This provided some interesting results for the Thermofield Double state, which finds ubiquitous applications in theoretical high-energy physics. A final entry in establishing the framework for Krylov complexity consisted of extending the discrete quantum mechanical definition of Krylov complexity to a field theoretic one, which involves some subtlety in the choice of the inner product, a poor choice of which can lead to false-positives in chaotic signatures, but is otherwise quite straightforward - further supplementing Krylov complexity's utility in applications through various fields in physics. We also briefly touched upon some computational approaches to Krylov complexity that help in simplifying the analytic computation and assist in numerical computations too.

Below, we summarize the key lessons from our investigation of Krylov complexity for the two applications considered in this thesis.

Kitaev Chain

Kitaev chain is a prototypical model in condensed matter physics and is a minimal model hosting topological phases of quantum matter. It is a collection of spin-$\frac{1}{2}$ fermions hopping along a 1-D chain, that are subjected to a chemical potential, and a (p-wave) superconducting interaction. We observed that the Hamiltonian can be decomposed in the Majorana basis and, importantly, it furnishes unpaired Majorana fermions localized at the edges of the chain with zero energy. Tuning the ratio of chemical potential and hopping parameter displays the presence of a topologically trivial and a topologically non-trivial phase characterized through a degeneracy in the ground state. The knowledge that a topological phase exists in the phase diagram of the Kitaev chain serves as a control to test our hypothesis against - the hypothesis, of course, being that the Krylov complexity is able to diagnose the topological phase transition.

We constructed three different circuits for the Kitaev chain, and observed that the Krylov (state) complexity for all three of them demonstrated acute sensitivity towards the transitions in and out of the topologically non-trivial phase. This displays the robustness of Krylov complexity to capture topological phase transitions. However, the imprint of topological phase transitions on Krylov complexity appear to be circuit (state) dependent in our analysis *i.e.* for certain circuits Krylov complexity plateaus in the topological phase while for others it doesn't. We also observed that it is instructive to compute the derivatives of Krylov complexity, since for certain circuits Krylov complexity itself may not clearly indicate the phase transition but the derivatives of Krylov complexity come to the rescue and, in particular, are reminiscent of first and second order classical phase transitions under the Landau paradigm.

Bateman Oscillator

The linearly coupled Bateman oscillator is another ubiquitous model consisting of two damped oscillators which are linearly coupled. It demonstrates three different regimes depending on damping: the under-damped, the critically damped, and the over-damped - which are all self-explanatory as well as discussed in the main text. The regime of most interest to physicists is the under-damped regime as it hosts a rich phase structure. There are three phases depending on the choice of the coupling strength. Describe the phases. and the This model can be used as a building block for system-environment interactions.

We note that in the Kitaev chain study our approach was to directly observe the behavior of Krylov complexity across the phase transition. However, we adapted a slightly different - though equivalent - approach for the study of linearly coupled Bateman oscillator system. We compute the Krylov complexity *inside* each phase *i.e.* we do not explicitly vary Krylov complexity across the phase transition. A reason behind this was that the return amplitude, and consequently Krylov complexity, diverges at both the phase boundaries so it is much simpler to investigate Krylov complexity within each phase in such cases. And again, we observe that Krylov complexity shows distinctive behavior for each of the phase - as it did for Kitaev chain. In the case of linearly coupled Bateman oscillator model we also observed that the Krylov complexity is capable of characterizing the phase. More precisely, we note that the Krylov complexity is extremely sensitive to the minutest interplay of different dynamics and captures them very accurately in the following sense: for under-damped regime with weak coupling, there are two dynamical drivers at play: the linear growth and the oscillatory growth - the former is indicative of the mode which supports uni-directional flow of energy from one oscillator to the other and the latter is indicative of the mode which supports bi-directional flow of energy between the two oscillators. Both these modes have a subtle interplay depending on the precise value of the parameters used, and Krylov complexity beautifully captures this interplay. This is, in hindsight, quite expected because Krylov complexity is but a repackaging of the Lanczos coefficients which themselves encode this interplay - though, visually and mathematically, this encoding is much more apparent in Krylov complexity than the Lanczos coefficients. Additionally, it is difficult to ascribe a physical meaning and build an intuition for the Lanczos coefficients so it is much nicer to work with Krylov complexity.

As concluding remarks to this thesis, we provide an outlook with a few interesting future directions and applications that we're confident our work can be extended towards.

1. The most natural extension of this work is to investigate other exotic phases of quantum matter and

the transitions among them through the lens of Krylov complexity to see how far it can be pushed as a probe of quantum phase transitions, and to demarcate its limitations in detecting the same transitions. These studies may focus on various phases including, but not limited to, quantum spin liquids [161], berry phases [162], fractional quantum states [163], symmetry protected phases [164], and Kondo phase [165][1].

2. Another very promising direction of research is to study if Krylov complexity is merely sensitive to phase transitions or could it be used to classify the quantum phases of matter themselves - this could potentially come in the shape of Table 1 *i.e.* could Krylov complexity show different asymptotic behavior for different phases of matter?

3. Clearly, there is a correlation between critical exponents and Krylov complexity as they both encode information about phase transitions. It would be useful to many different fields in physics to make this correlation more explicit. A useful starting point, is to consider the unification of two notions of Krylov complexity. This unification employs the Choi-Jamiolkowski map, and an operator-state correspondence exists in Conformal Field Theory which is often useful to describe physics near critical points of the phase space. This could be potentially utilized to see if critical exponents can be computed using Krylov complexity.

4. We remarked that a bad choice of inner product for field-theoretic complexity, canonical inner product *vis a vis* microcanonical inner product, can lead to false chaotic signatures in Krylov complexity. However, it has not been investigated if the same ailment affects Krylov complexity's ability to diagnose quantum phase transitions.

5. Studying Krylov complexity in the framework of the KAM theorem [166–168], *e.g.* for kicked rotor model, may assist in understanding the transition from integrable to chaotic dynamics. Furthermore, it may help shed light on the existence of a quantum version of the KAM, and help sharpen the intuition that in the thermodynamic limit even small perturbations are expected to deviate the system away from integrability.

6. Krylov complexity of scar states in otherwise quantum chaotic systems shows non-chaotic signatures. In this sense, it becomes imperative to study if there exist specific states - perhaps, even scar states - that mask the presence of phase transitions to Krylov complexity. We observed in the Kitaev chain study that the Krylov complexity can display very different signatures depending on the states being considered. So it is important to identify states that may make Krylov complexity blind to quantum phase transitions - and it is equally important to identify if there exist specific states that somehow serve to enhance the signatures of quantum phase transitions in Krylov complexity. This may further elaborate why Krylov complexity is able to detect quantum phase transitions - even though the nature of these transitions may be wildly different.

In summary, Krylov complexity has gone through its formative years in the very recent past and has been extensively studied for many systems. While it was initially introduced in literature as a probe of quantum chaos, recent years have seen it being utilized to a number of ends - one among which being a detector of

[1] For a great discussion on these phases see [151].

quantum phase transitions, as this thesis proposes. It is apparent now that the field of quantum/Krylov complexity itself is at a critical point and undergoing a phase transition. It is now well-poised to make groundbreaking contributions in a wide spectrum of applications, and this can already be seen from the vast interest it is garnering across communities. This thesis is but a small step in, what we expect to be, a very fruitful direction.

References

[1] Pawel Caputa, Nitin Gupta, S. Shajidul Haque, Sinong Liu, Jeff Murugan, and Hendrik J. R. Van Zyl. Spread complexity and topological transitions in the Kitaev chain. *JHEP*, 01:120, 8 2023. ^0, ^3, ^23, ^40

[2] Cameron Beetar, Nitin Gupta, S. Shajidul Haque, Jeff Murugan, and Hendrik J. R. Van Zyl. Complexity and operator growth for quantum systems in dynamic equilibrium. *Journal of High Energy Physics*, 2024(8):156, Aug 2024. ^0, ^3, ^58, ^62, ^67

[3] Richard J. Huggett. *Geoecology: An evolutionary approach*. Routledge, 2001. ^2

[4] Francesco Nazzi. The hexagonal shape of the honeycomb cells depends on the construction behavior of bees. *Scientific Reports*, 6(1):28341, Jun 2016. ^2

[5] Anna Grigas. The fibonacci sequence: Its history, significance, and manifestations in nature. 2013. ^2

[6] Ugo Lopez, Jacques Gautrais, Iain D. Couzin, and Guy Theraulaz. From behavioural analyses to models of collective motion in fish schools. *Interface Focus*, 2(6):693–707, Oct 2012. ^2

[7] Susannah Mistr and David Bercovici. A theoretical model of pattern formation in coral reefs. *Ecosystems*, 6(1):0061–0074, Jan 2003. ^2

[8] Eunjin Yang, Jae Hak Son, Sang-im Lee, Piotr G. Jablonski, and Ho-Young Kim. Water striders adjust leg movement speed to optimize takeoff velocity for their morphology. *Nature Communications*, 7(1), Dec 2016. ^2

[9] Peter J. Hore and Henrik Mouritsen. The quantum nature of bird migration. *Scientific American*, 32(15):26, Mar 2023. ^2

[10] Sampriti Mukherjee and Bonnie L. Bassler. Bacterial quorum sensing in complex and dynamically changing environments. *Nature Reviews Microbiology*, 17(6):371–382, Apr 2019. ^2

[11] David A. Relman. "til death do us part": Coming to terms with symbiotic relationships. *Nature Reviews Microbiology*, 6(10):721–724, Oct 2008. ^2

[12] C.H. Papadimitriou. *Computational Complexity*. Theoretical computer science. Addison-Wesley, 1994. ^2

[13] Eric Allender and Catherine McCartin. *Basic complexity*, pages 1–28. De Gruyter, Berlin, New York, 2001. ^2

[14] Spephen Bellantoni and Stephen Cook. A new recursion-theoretic characterization of the polytime functions. *computational complexity*, 2(2):97–110, Jun 1992. ^2

[15] Frank Arute and Kunal *et. al.* Arya. Quantum supremacy using a programmable superconducting processor. *Nature*, 574(7779):505–510, October 2019. ^2

[16] Feng Pan and Pan Zhang. Simulation of quantum circuits using the big-batch tensor network method. *Phys. Rev. Lett.*, 128:030501, Jan 2022. ^2

[17] Jared Duker Lichtman. A proof of the erdős primitive set conjecture. *Forum of Mathematics, Pi*, 11, 2023. ^2

[18] Daniel Harlow and Patrick Hayden. Quantum Computation vs. Firewalls. *JHEP*, 06:085, 2013. ^2

[19] Leonard Susskind. Butterflies on the stretched horizon, Dec 2013. ^2, ^5, ^12

[20] Leonard Susskind. Computational Complexity and Black Hole Horizons. *Fortsch. Phys.*, 64:24–43, 2016. [Addendum: Fortsch.Phys. 64, 44–48 (2016)]. ^2, ^5, ^12

[21] Michael A. Nielsen. A geometric approach to quantum circuit lower bounds, 2005. ^2, ^12, ^38

[22] Michael A. Nielsen, Mark R. Dowling, Mile Gu, and Andrew C. Doherty. Quantum computation as geometry. *Science*, 311(5764):1133–1135, feb 2006. ^2, ^12, ^38

[23] Tibra Ali, Arpan Bhattacharyya, S. Shajidul Haque, Eugene H. Kim, Nathan Moynihan, and Jeff Murugan. Chaos and Complexity in Quantum Mechanics. *Phys. Rev. D*, 101(2):026021, 2020. ^2

[24] Arpan Bhattacharyya, Wissam Chemissany, S. Shajidul Haque, and Bin Yan. Towards the web of quantum chaos diagnostics. *Eur. Phys. J. C*, 82(1):87, 2022. ^2, ^11

[25] Mohsen Alishahiha, Souvik Banerjee, and Mohammad Javad Vasli. Krylov complexity as a probe for chaos, 2024. ^2

[26] Daniel E. Parker, Xiangyu Cao, Alexander Avdoshkin, Thomas Scaffidi, and Ehud Altman. A Universal Operator Growth Hypothesis. *Phys. Rev. X*, 9(4):041017, 2019. ^2, ^3, ^9, ^13, ^22

[27] VS Viswanath and Gerhard Müller. *The recursion method: application to many-body dynamics*, volume 23. Springer Science & Business Media, 2008. ^2, ^9, ^14, ^15

[28] A. Krylov. De la résolution numérique de l'équation servant à déterminer dans des questions de mécanique appliquée les fréquences de petites oscillations des systèmes matériels. *Bull. Acad. Sci. URSS*, 1931(4):491–539, 1931. ^3

[29] Cornelius Lanczos. An iteration method for the solution of the eigenvalue problem of linear differential and integral operators. *J. Res. Natl. Bur. Stand. B*, 45:255–282, 1950. ^3

[30] Eamonn Cahill, Alan Irving, Christopher Johnston, and James Sexton. Numerical stability of lanczos methods. *Nuclear Physics B - Proceedings Supplements*, 83–84:825–827, April 2000. ^3

[31] Horst D. Simon. The lanczos algorithm with partial reorthogonalization. *Mathematics of Computation*, 42(165):115–142, 1984. ^3, ^19

[32] Beresford N. Parlett. *The symmetric eigenvalue problem*. Society for Industrial and Applied Mathematics, 1998. ^3, ^19

[33] W. E. Arnoldi. The principle of minimized iterations in the solution of the matrix eigenvalue problem. *Quarterly of Applied Mathematics*, 9(1):17–29, 1951. ^3, ^19

[34] Youcef Saad and Martin H. Schultz. Gmres: A generalized minimal residual algorithm for solving nonsymmetric linear systems. *SIAM Journal on Scientific and Statistical Computing*, 7(3):856–869, 1986. ^3, ^19

[35] Pawel Caputa, Javier M. Magan, and Dimitrios Patramanis. Geometry of Krylov complexity. *Phys. Rev. Res.*, 4(1):013041, 2022. ^3, ^22, ^37, ^38, ^66, ^97, ^98

[36] A Yu Kitaev. Unpaired majorana fermions in quantum wires. *Physics-Uspekhi*, 44(10S):131–136, oct 2001. ^3, ^40

[37] Carl M. Bender and Mariagiovanna Gianfreda. Twofold Transition in PT-Symmetric Coupled Oscillators. *Phys. Rev. A*, 88(6):062111, Dec 2013. ^3, ^58, ^62, ^63, ^71

[38] Pedro H. S. Bento, Adolfo del Campo, and Lucas C. Céleri. Krylov complexity and dynamical phase transition in the quenched lipkin-meshkov-glick model. *Physical Review B*, 109(22), June 2024. ^3

[39] Takanori Anegawa, Norihiro Iizuka, and Mitsuhiro Nishida. Krylov complexity as an order parameter for deconfinement phase transitions at large n. *Journal of High Energy Physics*, 2024(4), Apr 2024. ^3, ^15, ^27, ^30, ^104

[40] Maitri Ganguli and Aneek Jana. State dependent spread complexity dynamics in many-body localization transition, 2024. ^3

[41] Ahmed Almheiri, Donald Marolf, Joseph Polchinski, and James Sully. Black holes: Complementarity or firewalls? *Journal of High Energy Physics*, 2013(2), Feb 2013. ^5

[42] Henri Poincaré. On the three-body problem and the equations of dynamics. *History of Modern Physical Sciences*, page 368–376, Jul 2003. ^5

[43] R. B. Levien and S. M. Tan. Double pendulum: An experiment in chaos. *American Journal of Physics*, 61(11):1038–1044, 11 1993. ^5

[44] Edward N. Lorenz. Deterministic nonperiodic flow. *Journal of Atmospheric Sciences*, 20(2):130–141, 1963. ^5

[45] Yakov G Sinai. Dynamical systems with elastic reflections. *Russian Mathematical Surveys*, 25(2):137–189, Apr 1970. ^5, ^77

[46] L. A. Bunimovich. On the ergodic properties of nowhere dispersing billiards. *Communications in Mathematical Physics*, 65(3):295–312, Oct 1979. ^5

[47] Michael Berry. Quantum chaology, not quantum chaos. *Physica Scripta*, 40(3):335, sep 1989. ^6

[48] Eugene P. Wigner. Characteristic vectors of bordered matrices with infinite dimensions. *Annals of Mathematics*, 62(3):548–564, 1955. ^6

[49] Eugene P. Wigner. Characteristics vectors of bordered matrices with infinite dimensions ii. *Annals of Mathematics*, 65(2):203–207, 1957. ^6

[50] Eugene P. Wigner. On the distribution of the roots of certain symmetric matrices. *Annals of Mathematics*, 67(2):325–327, 1958. ^6

[51] Freeman J. Dyson. Statistical Theory of the Energy Levels of Complex Systems. I. *Journal of Mathematical Physics*, 3(1):140–156, 01 1962. ^6

[52] Freeman J. Dyson. Statistical Theory of the Energy Levels of Complex Systems. II. *Journal of Mathematical Physics*, 3(1):157–165, 01 1962. ^6

[53] Freeman J. Dyson. Statistical Theory of the Energy Levels of Complex Systems. III. *Journal of Mathematical Physics*, 3(1):166–175, 01 1962. ^6

[54] Freeman J. Dyson. The Threefold Way. Algebraic Structure of Symmetry Groups and Ensembles in Quantum Mechanics. *Journal of Mathematical Physics*, 3(6):1199–1215, 11 1962. ^6

[55] O. Bohigas, M. J. Giannoni, and C. Schmit. Characterization of chaotic quantum spectra and universality of level fluctuation laws. *Phys. Rev. Lett.*, 52:1–4, 1984. ^6

[56] Bohigas, O., Giannoni, M.J., and Schmit, C. Spectral properties of the laplacian and random matrix theories. *J. Physique Lett.*, 45(21):1015–1022, 1984. ^6

[57] Alexander Altland and Martin R. Zirnbauer. Nonstandard symmetry classes in mesoscopic normal-superconducting hybrid structures. *Phys. Rev. B*, 55:1142–1161, Jan 1997. ^6

[58] G. Casati, J. Ford, and Springer-Verlag. *Stochastic Behavior in Classical and Quantum Hamiltonian Systems*. Lecture notes in physics. Springer Berlin / Heidelberg, 1979. ^7

[59] Shmuel Fishman, D. R. Grempel, and R. E. Prange. Chaos, quantum recurrences, and anderson localization. *Phys. Rev. Lett.*, 49:509–512, Aug 1982. ^7

[60] D. R. Grempel, R. E. Prange, and Shmuel Fishman. Quantum dynamics of a nonintegrable system. *Phys. Rev. A*, 29:1639–1647, Apr 1984. ^7

[61] Rahul Nandkishore and David A. Huse. Many-body localization and thermalization in quantum statistical mechanics. *Annual Review of Condensed Matter Physics*, 6(Volume 6, 2015):15–38, 2015. ^7

[62] C. J. Turner, A. A. Michailidis, D. A. Abanin, M. Serbyn, and Z. Papić. Quantum scarred eigenstates in a rydberg atom chain: Entanglement, breakdown of thermalization, and stability to perturbations. *Phys. Rev. B*, 98:155134, Oct 2018. ^7

[63] Črt Lozej, Giulio Casati, and Tomaž Prosen. Quantum chaos in triangular billiards. *Phys. Rev. Res.*, 4:013138, Feb 2022. ^7

[64] Budhaditya Bhattacharjee, Samudra Sur, and Pratik Nandy. Probing quantum scars and weak ergodicity breaking through quantum complexity. *Phys. Rev. B*, 106:205150, Nov 2022. ^7, ^22

[65] D Lippolis. Estimating the spectral density of unstable scars. *Journal of Physics A: Mathematical and Theoretical*, 55(32):324001, jul 2022. ^7

[66] Michael Iversen and Anne E. B. Nielsen. Tower of quantum scars in a partially many-body localized system. *Phys. Rev. B*, 107:205140, May 2023. ^7

[67] Mark Srednicki. Chaos and quantum thermalization. *Phys. Rev. E*, 50:888–901, Aug 1994. ^7

[68] J. v. Neumann. Beweis des ergodensatzes und desh-theorems in der neuen mechanik. *Zeitschrift für Physik*, 57(1):30–70, Jan 1929. ^8

[69] J. von Neumann. Proof of the ergodic theorem and the h-theorem in quantum mechanics. *The European Physical Journal H*, 35(2):201–237, Nov 2010. ^8

[70] James R. Garrison and Tarun Grover. Does a single eigenstate encode the full hamiltonian? *Phys. Rev. X*, 8:021026, Apr 2018. ^8

[71] L.D. Landau and E.M. Lifshitz. *Statistical Physics: Volume 5*. Number v. 5. Elsevier Science, 2013. ^8

[72] Anatoli Polkovnikov Luca D'Alessio, Yariv Kafri and Marcos Rigol. From quantum chaos and eigenstate thermalization to statistical mechanics and thermodynamics. *Advances in Physics*, 65(3):239–362, 2016. ^9

[73] Pratik Nandy, Apollonas S. Matsoukas-Roubeas, Pablo Martínez-Azcona, Anatoly Dymarsky, and Adolfo del Campo. Quantum Dynamics in Krylov Space: Methods and Applications. 5 2024. ^10

[74] Fritz Haake. *Quantum signatures of Chaos*. Springer-Verlag Berlin Heidelberg, 2010. ^10

[75] Luc Leviandier, Maurice Lombardi, Rémi Jost, and Jean Paul Pique. Fourier transform: A tool to measure statistical level properties in very complex spectra. *Phys. Rev. Lett.*, 56:2449–2452, Jun 1986. ^10

[76] Giorgio Cipolloni, László Erdős, and Dominik Schröder. On the spectral form factor for random matrices. *Communications in Mathematical Physics*, 401(2):1665–1700, Jul 2023. ^10, ^11

[77] Arseni Wisniacki. Loschmidt echo. *Scholarpedia*, 7(8):11687, 2012. ^10

[78] Lev Vidmar and Marcos Rigol. Entanglement entropy of eigenstates of quantum chaotic hamiltonians. *Physical Review Letters*, 119(22), November 2017. ^11

[79] Anatoly I. Larkin and Yu. N. Ovchinnikov. Quasiclassical method in the theory of superconductivity. *Journal of Experimental and Theoretical Physics*, 1969. ^11

[80] Stephen H. Shenker and Douglas Stanford. Black holes and the butterfly effect. *Journal of High Energy Physics*, 2014(3):67, Mar 2014. ^11

[81] Stephen H. Shenker and Douglas Stanford. Multiple shocks. *Journal of High Energy Physics*, 2014(12):46, Dec 2014. ^11

[82] Stephen H. Shenker and Douglas Stanford. Stringy effects in scrambling. *Journal of High Energy Physics*, 2015(5):132, May 2015. ^11

[83] Daniel A. Roberts and Douglas Stanford. Diagnosing chaos using four-point functions in two-dimensional conformal field theory. *Phys. Rev. Lett.*, 115:131603, Sep 2015. ^11

[84] Daniel A. Roberts, Douglas Stanford, and Leonard Susskind. Localized shocks. *Journal of High Energy Physics*, 2015(3):51, Mar 2015. ^11

[85] Juan Maldacena, Stephen H. Shenker, and Douglas Stanford. A bound on chaos. *JHEP*, 08:106, 2016. ^11, ^12

[86] Jordan Cotler, Nicholas Hunter-Jones, Junyu Liu, and Beni Yoshida. Chaos, complexity, and random matrices. *Journal of High Energy Physics*, 2017(11), November 2017. ^11

[87] S.V. Syzranov, A.V. Gorshkov, and V.M. Galitski. Interaction-induced transition in the quantum chaotic dynamics of a disordered metal. *Annals of Physics*, 405:1–13, 2019. ^11

[88] Koji Hashimoto, Keiju Murata, and Ryosuke Yoshii. Out-of-time-order correlators in quantum mechanics. *Journal of High Energy Physics*, 2017(10), October 2017. ^11, ^12

[89] S. V. Syzranov, A. V. Gorshkov, and V. Galitski. Out-of-time-order correlators in finite open systems. *Phys. Rev. B*, 97:161114, Apr 2018. ^11

[90] Sagar Vijay and Ashvin Vishwanath. Finite-temperature scrambling of a random hamiltonian. *arXiv: Strongly Correlated Electrons*, 2018. ^11

[91] Josef Rammensee, Juan Diego Urbina, and Klaus Richter. Many-body quantum interference and the saturation of out-of-time-order correlators. *Phys. Rev. Lett.*, 121:124101, Sep 2018. ^11

[92] Alexander Schuckert and Michael Knap. Many-body chaos near a thermal phase transition. *SciPost Phys.*, 7:022, 2019. ^11

[93] B. V. Fine, T. A. Elsayed, C. M. Kropf, and A. S. de Wijn. Absence of exponential sensitivity to small perturbations in nonintegrable systems of spins 1/2. *Phys. Rev. E*, 89:012923, Jan 2014. ^12

[94] Efim B. Rozenbaum, Leonid A. Bunimovich, and Victor Galitski. Early-time exponential instabilities in nonchaotic quantum systems. *Phys. Rev. Lett.*, 125:014101, Jul 2020. ^12

[95] Koji Hashimoto, Kyoung-Bum Huh, Keun-Young Kim, and Ryota Watanabe. Exponential growth of out-of-time-order correlator without chaos: inverted harmonic oscillator. *Journal of High Energy Physics*, 2020(11), November 2020. ^12

[96] Ivan Kukuljan, Sa šo Grozdanov, and Toma ž Prosen. Weak quantum chaos. *Phys. Rev. B*, 96:060301, Aug 2017. ^12

[97] Tianrui Xu, Thomas Scaffidi, and Xiangyu Cao. Does scrambling equal chaos? *Phys. Rev. Lett.*, 124:140602, Apr 2020. ^12

[98] Juan Maldacena and Douglas Stanford. Remarks on the sachdev-ye-kitaev model. *Phys. Rev. D*, 94:106002, Nov 2016. ^12

[99] Leonard Susskind. Three lectures on complexity and black holes, 2018. ^12

[100] Shira Chapman, Jens Eisert, Lucas Hackl, Michal P. Heller, Ro Jefferson, Hugo Marrochio, and Robert C. Myers. Complexity and entanglement for thermofield double states. *SciPost Phys.*, 6:034, 2019. ^13

[101] Adam R. Brown, Daniel A. Roberts, Leonard Susskind, Brian Swingle, and Ying Zhao. Holographic Complexity Equals Bulk Action? *Phys. Rev. Lett.*, 116(19):191301, 2016. ^13

[102] Douglas Stanford and Leonard Susskind. Complexity and Shock Wave Geometries. *Phys. Rev. D*, 90(12):126007, 2014. ^13

[103] Alexandre Belin, Robert C. Myers, Shan-Ming Ruan, Gábor Sárosi, and Antony J. Speranza. Does complexity equal anything? *Physical Review Letters*, 128(8), February 2022. ^13

[104] Alexandre Belin, Robert C. Myers, Shan-Ming Ruan, Gábor Sárosi, and Antony J. Speranza. Complexity equals anything ii. *Journal of High Energy Physics*, 2023(1), January 2023. ^13

[105] E. Rabinovici, A. Sánchez-Garrido, R. Shir, and J. Sonner. Operator complexity: a journey to the edge of Krylov space. *JHEP*, 06:062, 2021. ^15, ^22, ^105

[106] Vijay Balasubramanian, Pawel Caputa, Javier M. Magan, and Qingyue Wu. Quantum chaos and the complexity of spread of states. *Phys. Rev. D*, 106:046007, Aug 2022. ^15, ^21, ^22, ^37, ^47, ^66, ^98, ^104

[107] Mohsen Alishahiha and Souvik Banerjee. A universal approach to Krylov state and operator complexities. *SciPost Phys.*, 15:080, 2023. ^15, ^23, ^25, ^37, ^38, ^66, ^104

[108] Arjun Kar, Lampros Lamprou, Moshe Rozali, and James Sully. Random matrix theory for complexity growth and black hole interiors. *JHEP*, 01:016, 2022. ^15, ^22, ^27, ^30, ^32, ^37, ^66, ^104

[109] Pawel Caputa and Sinong Liu. Quantum complexity and topological phases of matter. *Phys. Rev. B*, 106:195125, Nov 2022. ^15, ^21, ^22, ^51, ^52, ^53, ^92, ^98

[110] Aranya Bhattacharya, Pratik Nandy, Pingal Pratyush Nath, and Himanshu Sahu. Operator growth and Krylov construction in dissipative open quantum systems. *JHEP*, 12:081, 2022. ^16

[111] Chang Liu, Haifeng Tang, and Hui Zhai. Krylov complexity in open quantum systems. *Phys. Rev. Res.*, 5(3):033085, 2023. ^16

[112] Aranya Bhattacharya, Pratik Nandy, Pingal Pratyush Nath, and Himanshu Sahu. On Krylov complexity in open systems: an approach via bi-Lanczos algorithm. *JHEP*, 12:066, 2023. ^16

[113] Cornelius Lanczos. An iteration method for the solution of the eigenvalue problem of linear differential and integral operators. *Journal of research of the National Bureau of Standards*, 45:255–282, 1950. ^18

[114] Zhong-Ying Fan. Universal relation for operator complexity. *Phys. Rev. A*, 105:062210, 2022. ^21, ^22

[115] Markus Heyl. Dynamical quantum phase transitions: a review. *Rept. Prog. Phys.*, 81(5):054001, 2018. ^22

[116] J. L. F. Barbón, E. Rabinovici, R. Shir, and R. Sinha. On The Evolution Of Operator Complexity Beyond Scrambling. *JHEP*, 10:264, 2019. ^22

[117] Javier M. Magán and Joan Simón. On operator growth and emergent Poincaré symmetries. *JHEP*, 05:071, 2020. ^22

[118] Shao-Kai Jian, Brian Swingle, and Zhuo-Yu Xian. Complexity growth of operators in the SYK model and in JT gravity. *JHEP*, 03:014, 2021. ^22

[119] Chao Yin and Andrew Lucas. Quantum operator growth bounds for kicked tops and semiclassical spin chains. *Phys. Rev. A*, 103(4):042414, 2021. ^22

[120] Anatoly Dymarsky and Alexander Gorsky. Quantum chaos as delocalization in Krylov space. *Phys. Rev. B*, 102(8):085137, 2020. ^22

[121] Anatoly Dymarsky and Michael Smolkin. Krylov complexity in conformal field theory. *Phys. Rev. D*, 104(8):L081702, 2021. ^22, ^30, ^39

[122] Pawel Caputa and Shouvik Datta. Operator growth in 2d CFT. *JHEP*, 12:188, 2021. ^22

[123] Matteo Carrega, Joonho Kim, and Dario Rosa. Unveiling Operator Growth Using Spin Correlation Functions. *Entropy*, 23(5):587, 2021. ^22

[124] Joonho Kim, Jeff Murugan, Jan Olle, and Dario Rosa. Operator delocalization in quantum networks. *Phys. Rev. A*, 105(1):L010201, 2022. ^22

[125] E. Rabinovici, A. Sánchez-Garrido, R. Shir, and J. Sonner. Krylov complexity from integrability to chaos. *JHEP*, 07:151, 2022. ^22

[126] Fabian Ballar Trigueros and Cheng-Ju Lin. Krylov complexity of many-body localization: Operator localization in Krylov basis. *SciPost Phys.*, 13(2):037, 2022. ^22

[127] E. Rabinovici, A. Sánchez-Garrido, R. Shir, and J. Sonner. Krylov localization and suppression of complexity. *JHEP*, 03:211, 2022. ^22

[128] Niklas Hörnedal, Nicoletta Carabba, Apollonas S. Matsoukas-Roubeas, and Adolfo del Campo. Ultimate speed limits to the growth of operator complexity. *Communications Physics*, 5(1):207, Aug 2022. ^22

[129] Budhaditya Bhattacharjee, Xiangyu Cao, Pratik Nandy, and Tanay Pathak. Krylov complexity in saddle-dominated scrambling. *JHEP*, 05:174, 2022. ^22

[130] Kiran Adhikari, Sayantan Choudhury, and Abhishek Roy. Krylov complexity in quantum field theory. *Nuclear Physics B*, 993:116263, 2023. ^22

[131] Wolfgang Mück and Yi Yang. Krylov complexity and orthogonal polynomials. *Nucl. Phys. B*, 984:115948, 5 2022. ^22, ^33

[132] Dimitrios Patramanis. Probing the entanglement of operator growth. *PTEP*, 2022(6):063A01, 2022. ^22

[133] R.S. Doran and A.M. Society. *C*-algebras: 1943-1993 : a Fifty Year Celebration : AMS Special Session Commemorating the First Fifty Years of C*-algebra Theory, January 13-14, 1993, San Antonio, Texas*. Contemporary mathematics. American Mathematical Society, 1994. ^22

[134] Michael A. Nielsen and Isaac L. Chuang. *Quantum Computation and Quantum Information*. Cambridge University Press, 2000. ^24

[135] Min Jiang, Shunlong Luo, and Shuangshuang Fu. Channel-state duality. *Phys. Rev. A*, 87:022310, Feb 2013. ^24

[136] Juan Maldacena. The large-n limit of superconformal field theories and supergravity. *International Journal of Theoretical Physics*, 38(4):1113–1133, Apr 1999. ^27

[137] Anatoly Dymarsky and Alexander Gorsky. Quantum chaos as delocalization in krylov space. *Phys. Rev. B*, 102:085137, Aug 2020. ^38

[138] Arnab Kundu, Vinay Malvimat, and Ritam Sinha. State dependence of Krylov complexity in 2d CFTs. *JHEP*, 09:011, 2023. ^38

[139] Zijian Xiong, Dao-Xin Yao, and Zhongbo Yan. Nonanalyticity of circuit complexity across topological phase transitions. *Phys. Rev. B*, 101(17):174305, 2020. ^38

[140] Hao-Hua Sun, Kai-Wen Zhang, Lun-Hui Hu, Chuang Li, Guan-Yong Wang, Hai-Yang Ma, Zhu-An Xu, Chun-Lei Gao, Dan-Dan Guan, Yao-Yi Li, Canhua Liu, Dong Qian, Yi Zhou, Liang Fu, Shao-Chun Li, Fu-Chun Zhang, and Jin-Feng Jia. Majorana zero mode detected with spin selective andreev reflection in the vortex of a topological superconductor. *Phys. Rev. Lett.*, 116:257003, Jun 2016. ^40

[141] Hao-Hua Sun and Jin-Feng Jia. Detection of majorana zero mode in the vortex. *npj Quantum Materials*, 2(1), Jul 2017. ^40

[142] Anindya Das, Yuval Ronen, Yonatan Most, Yuval Oreg, Moty Heiblum, and Hadas Shtrikman. Zero-bias peaks and splitting in an al–inas nanowire topological superconductor as a signature of majorana fermions. *Nature Physics*, 8(12):887–895, Nov 2012. ^40

[143] Graham Kells, Dganit Meidan, and PW Brouwer. Near-zero-energy end states in topologically trivial spin-orbit coupled superconducting nanowires with a smooth confinement. *Physical Review B—Condensed Matter and Materials Physics*, 86(10):100503, 2012. ^40

[144] Vincent Mourik, Kun Zuo, Sergey M Frolov, SR Plissard, Erik PAM Bakkers, and Leo P Kouwenhoven. Signatures of majorana fermions in hybrid superconductor-semiconductor nanowire devices. *Science*, 336(6084):1003–1007, 2012. ^40

[145] Berthold Jäck, Yonglong Xie, and Ali Yazdani. Detecting and distinguishing majorana zero modes with the scanning tunnelling microscope. *Nature Reviews Physics*, 3(8):541–554, Jun 2021. ^40

[146] Martin Greiter, Vera Schnells, and Ronny Thomale. The 1d ising model and the topological phase of the kitaev chain. *Annals of Physics*, 351:1026–1033, 2014. ^41

[147] Kartik Chhajed. From ising model to kitaev chain. *Resonance*, 26(11):1539–1558, Nov 2021. ^41

[148] Haining Pan and Sankar Das Sarma. Majorana nanowires, kitaev chains, and spin models. *Physical Review B*, 107(3), January 2023. ^41, ^42, ^43

[149] Mehran Kardar. *Statistical Physics of Fields*. Cambridge University Press, 2007. ^43

[150] Subir Sachdev. *Quantum Phase Transitions*. Cambridge University Press, 4 2011. ^43

[151] S. Sachdev. *Quantum Phases of Matter*. Cambridge University Press, 2023. ^43, ^80

[152] Aranya Bhattacharya, Rathindra Nath Das, Bidyut Dey, and Johanna Erdmenger. Spread complexity and localization in $\mathcal{PT}$-symmetric systems. *Phys. Rev. B*, 110:064320, Aug 2024. ^58

[153] H. Bateman. On dissipative systems and related variational principles. *Phys. Rev.*, 38:815–819, Aug 1931. ^59

[154] A. M. Perelomov. Coherent states for arbitrary Lie group. *Communications in Mathematical Physics*, 26(3):222 – 236, 1972. ^64, ^102

[155] Shinichi Deguchi, Yuki Fujiwara, and Kunihiko Nakano. Two quantization approaches to the Bateman oscillator model. *Annals Phys.*, 403:34–46, 2019. ^65

[156] Shinichi Deguchi and Yuki Fujiwara. Square-integrable eigenfunctions in quantizing the Bateman oscillator model. 10 2019. ^65

[157] Fabio Bagarello, Francesco Gargano, and Federico Roccati. A no-go result for the quantum damped harmonic oscillator. *Phys. Lett. A*, 383:2836–2838, 2019. ^65, ^67

[158] Fabio Bagarello, Francesco Gargano, and F. Roccati. Some remarks on few recent results on the damped quantum harmonic oscillator. *Annals of Physics*, 414:168091, 02 2020. ^65, ^67

[159] Francisco M. Fern'andez. Algebraic treatment of the bateman hamiltonian. *Canadian Journal of Physics*, 2020. ^65, ^67

[160] Arghya Chattopadhyay, Arpita Mitra, and Hendrik J. R. van Zyl. Spread complexity as classical dilaton solutions. *Phys. Rev. D*, 108(2):025013, 2023. ^66, ^67

[161] C. Broholm, R. J. Cava, S. A. Kivelson, D. G. Nocera, M. R. Norman, and T. Senthil. Quantum spin liquids. *Science*, 367(6475):eaay0668, 2020. ^80

[162] Eliahu *et. al.* Cohen. Geometric phase from aharonov–bohm to pancharatnam–berry and beyond. *Nature Reviews Physics*, 1(7):437–449, Jul 2019. ^80

[163] Horst L. Stormer. Nobel lecture: The fractional quantum hall effect. *Rev. Mod. Phys.*, 71:875–889, Jul 1999. ^80

[164] T. Senthil. Symmetry-protected topological phases of quantum matter. *Annual Review of Condensed Matter Physics*, 6(1):299–324, March 2015. ^80

[165] Sara M. Cronenwett, Tjerk H. Oosterkamp, and Leo P. Kouwenhoven. A tunable kondo effect in quantum dots. *Science*, 281(5376):540–544, 1998. ^80

[166] A N Kolmogorov. On conservation of conditionally periodic motions for a small change in Hamilton's function. *Dokl. Akad. Nauk SSSR*, 98:527–530, 1954. ^80

[167] J Möser. On invariant curves of area-preserving mappings of an annulus. *Nachr. Akad. Wiss. Göttingen, II*, pages 1–20, 1962. ^80

[168] V. I. Arnol'd. Proof of a Theorem of A. N. KOLMOGOROV on the Invariance of Quasi-Periodic Motions Under Small Perturbations of the Hamiltonian. *Russian Mathematical Surveys*, 18(5):9–36, October 1963. ^80

[169] J M Radcliffe. Some properties of coherent spin states. *Journal of Physics A: General Physics*, 4(3):313, may 1971. ^93

[170] Kohei Kawabata, Ryohei Kobayashi, Ning Wu, and Hosho Katsura. Exact zero modes in twisted Kitaev chains. *Phys. Rev. B*, 95(19):195140, 2017. ^97

[171] Luis Benet and David P. Sanders. Taylorseries.jl: Taylor expansions in one and several variables in julia. *Journal of Open Source Software*, 4(36):1043, 2019. ^107

[172] Christopher Rackauckas and Qing Nie. DifferentialEquations.jl–a performant and feature-rich ecosystem for solving differential equations in Julia. *Journal of Open Research Software*, 5(1), 2017. ^108

A Ground State Calculation

The discussion in this appendix follows [109] and is included here for completion. Suppose that we have a generic Hamiltonian of the form,

$$\boxed{H = 2R_3 J_0 + iR_1 \left(J_+ - J_-\right),} \tag{A.1}$$

where $J_{0,\pm}$ are the generators of an $\mathfrak{su}(2)$ algebra. Since, this is a quadratic Hamiltonian we can write down spin coherent states for it. We already have the generators for an $\mathfrak{su}(2)$ algebra so let's build $SU(2)$ spin coherent states out of them. There are two advantages of using generalized coherent states (GCS) to diagonalize a Hamiltonian which is an element of some Lie Algebra :

- construction of GCS from Lie Groups has been studied and various results are available in literature for use;
- the time evolution operator, $e^{\frac{itH}{\hbar}}$, will be an element of the corresponding Lie Group and hence the time evolution of the target state is just a particular parametertization of the GCS - any Lie Group element acting on the target state can be expressed as some parameterization of the GCS.

A generic coherent state can be built like : $e^{aJ_+ + bJ_- + cJ_3} \left|0\right\rangle$ with $\left|0\right\rangle$ being the vacuum state which is destroyed by application of J_-. Now, it's clear that the action of J_0 is trivial on $\left|0\right\rangle$ and J_- destroys it. So, the most

generic unnormalized spin coherent state built from these generators would be,

$$|\Omega\rangle = e^{zJ_+} |0\rangle . \tag{A.2}$$

One can note that since $J_{0,\pm}$ are the generators of an **$\mathfrak{su}(2)$** algebra : $|0\rangle \to |j,-j\rangle$. Also, one can easily normalize this state (see (3.5) of [169] and get the following normalized generic $SU(2)$ coherent state,

$$|\Omega\rangle = \left(1+|z|^2\right)^{-\frac{1}{2}} e^{zJ_+} |j,-j\rangle . \tag{A.3}$$

We can fix the value of z by requiring that the above state be an energy eigenstate, which readily furnishes the energy spectrum,

$$H|\Omega\rangle = \left[2R_3J_0 + iR_1\left(J_+ - J_-\right)\right]\left(1+|z|^2\right)^{-\frac{1}{2}} e^{zJ_+} |j,-j\rangle . \tag{A.4}$$

We will need the equation describing the action of $J_{0,\pm}$ on $|j,-j\rangle$. The action of **$\mathfrak{su}(2)$** generators on Fock basis is given by,

$$\begin{aligned} J_0|J,m\rangle &= (-J+m)|J,m\rangle , \\ J_+|J,m\rangle &= \sqrt{(m+1)(2J-m)}\,|J,m+1\rangle , \\ J_-|J,m\rangle &= \sqrt{m(2J-m+1)}\,|J,m-1\rangle , \end{aligned} \tag{A.5}$$

where $m = 0,1,\cdots,2j$. The above relations can be modified as,

$$\begin{aligned} J_0|J,m\rangle &= \frac{1}{2}(J-m)(J+m+1)|J,m\rangle , \\ J_+|J,m\rangle &= \sqrt{(J-m)(J+m+1)}\,|J,m+1\rangle , \\ J_-|J,m\rangle &= \sqrt{(J+m)(J-m+1)}\,|J,m-1\rangle , \end{aligned} \tag{A.6}$$

where $m = -j,-j+1,\cdots,j$. We have $J=j, m=-j$ for the $SU(2)$ coherent ground state. So,

$$\begin{aligned} J_0|j,-j\rangle &= -j|j,-j\rangle , \\ J_+|j,-j\rangle &= \sqrt{2j}\,|j,-j+1\rangle , \\ J_-|j,-j\rangle &= 0. \end{aligned} \tag{A.7}$$

Evaluating the above term by term,

$$J_0 e^{zJ_+}|j,-j\rangle = J_0\sum_{n=0}^{\infty}\frac{z^n}{n!}J_+^n|j,-j\rangle . \tag{A.8}$$

If we can take J_0 to the RHS of J_+^n then it's action on $|j,-j\rangle$ will be trivially easy to write down,

$$J_0 e^{zJ_+}|j,-j\rangle = \sum_{n=0}^{\infty}\frac{z^n}{n!}J_0J_+^n|j,-j\rangle . \tag{A.9}$$

Let's evaluate how J_0 moves across a factor proportional to J_+^n,

$$\begin{aligned} J_0 J_+^n &= (J_0 J_+) J_+^{n-1} \\ &= (J_+ + J_+ J_0) J_+^{n-1} \\ &= J_+^n + J_+ (J_0 J_+) J_+^{n-2} \\ &= J_+^n + J_+ (J_+ + J_+ J_0) J_+^{n-2} \\ &= 2J_+^n + J_+^2 J_0 J_+^{n-2} \\ &\vdots \\ &= kJ_+^n + J_+^k J_0 J_+^{n-k} \quad : k^{\text{th}} \text{ term} \quad ; \quad k \leq n \\ &\vdots \\ &= nJ_+^n + J_+^n J_0 \quad : k = n. \end{aligned} \tag{A.10}$$

So,

$$\begin{aligned} J_0 e^{zJ_+} |j,-j\rangle &= \sum_{n=0}^{\infty} \frac{z^n}{n!} \left(nJ_+^n + J_+^n J_0\right) |j,-j\rangle \\ &= \sum_{n=0}^{\infty} \left[\left(\frac{z^{n-1}}{(n-1)!} J_+^{n-1} \right) zJ_+ + \left(\frac{z^n}{n!} J_+^n \right) J_0 \right] |j,-j\rangle \\ &= \left(e^{zJ_+}\right) zJ_+ |j,-j\rangle + e^{zJ_+} J_0 |j,-j\rangle \\ &= \left(e^{zJ_+}\right) z\sqrt{2j} |j,-j+1\rangle + e^{zJ_+} (-j) |j,-j\rangle , \end{aligned} \tag{A.11}$$

$\Longrightarrow$

$$\left[2R_3 \left(1 + |z|^2\right)^{-\frac{1}{2}}\right] J_0 e^{zJ_+} |j,-j\rangle = 2R_3 \left(1 + |z|^2\right)^{-\frac{1}{2}} \left[z\sqrt{2j} e^{zJ_+} |j,-j+1\rangle - j e^{zJ_+} |j,-j\rangle\right]. \tag{A.12}$$

The second term will be, $iR_1 \left(1 + |z|^2\right)^{-\frac{1}{2}} \underbrace{J_+ e^{zJ_+}}_{\substack{\text{swap with} \\ \text{impunity}}} |j,-j\rangle$,

$$iR_1 \left(1 + |z|^2\right)^{-\frac{1}{2}} J_+ e^{zJ_+} |j,-j\rangle = iR_1 \left(1 + |z|^2\right)^{-\frac{1}{2}} e^{zJ_+} \sqrt{2j} |j,-j+1\rangle . \tag{A.13}$$

The third term will be,

$$J_- e^{zJ_+} |j,-j\rangle = \sum_{n=0}^{\infty} \frac{z^n}{n!} J_- J_+^n |j,-j\rangle . \tag{A.14}$$

The easier way to get J_- to the RHS of J_+^n would be to consider their commutator. One can show that the commutator will be,

$$\begin{aligned} \left[J_-, J_+^n\right] &= 2nJ_+^{n-1} J_0 + n(n-1) J_+^{n-1}, \\ \Longrightarrow J_- J_+^n &= J_+^n J_- - 2nJ_+^{n-1} J_0 - n(n-1) J_+^{n-1}, \end{aligned} \tag{A.15}$$

So,

$$\begin{aligned} J_- e^{zJ_+} |j,-j\rangle &= \sum_{n=0}^{\infty} \frac{z^n}{n!} J_- J_+^n |j,-j\rangle \\ &= \sum_{n=0}^{\infty} \frac{z^n}{n!} \left[J_+^n \cancelto{0}{J_-} - 2nJ_+^{n-1} J_0 - n(n-1) J_+^{n-1} \right] |j,-j\rangle \\ &= \sum_{n=0}^{\infty} \frac{z^n}{n!} 2njJ_+^{n-1} |j,-j\rangle - \sum_{n=0}^{\infty} \frac{z^n}{n!} n(n-1) J_+^{n-1} |j,-j\rangle \\ &= (2jz) \sum_{n-1=0}^{\infty} \frac{z^{n-1}}{(n-1)!} J_+^{n-1} |j,-j\rangle - z^2 \sum_{n-2=0}^{\infty} \frac{z^{n-2}}{(n-2)!} J_+^{n-2} J_+ |j,-j\rangle \\ &= \left(2jz\right) e^{zJ_+} |j,-j\rangle - z^2 \sqrt{2j} e^{zJ_+} |j,-j+1\rangle , \end{aligned} \tag{A.16}$$

and we get,

$$iR_1 \left(1+|z|^2\right)^{-\frac{1}{2}} J_- e^{zJ_+} |j,-j\rangle = iR_1 \left(1+|z|^2\right)^{-\frac{1}{2}} \left[\left(2jz\right) e^{zJ_+} |j,-j\rangle - z^2 \sqrt{2j} e^{zJ_+} |j,-j+1\rangle \right]. \tag{A.17}$$

Putting the above results together,

$$\begin{aligned} H|\Omega\rangle &= \left(1+|z|^2\right)^{-\frac{1}{2}} \left[2R_3 J_0 + iR_1 \left(J_+ - J_-\right) \right] e^{zJ_+} |j,-j\rangle \\ &= \left(1+|z|^2\right)^{-\frac{1}{2}} \Big[\left\{ \left(-2R_3 j\right) e^{zJ_+} |j,-j\rangle \right\} + \left\{ \left(2R_3 z\sqrt{2j}\right) e^{zJ_+} |j,-j+1\rangle \right\} \\ &+ \left\{ iR_1 \sqrt{2j}\, e^{zJ_+} |j,-j+1\rangle \right\} + \left\{ \left(-2iR_1 zj\right) e^{zJ_+} |j,-j\rangle \right\} + \left\{ \left(iR_1 z^2 \sqrt{2j}\right) e^{zJ_+} |j,-j+1\rangle \right\} \Big] \\ &= \left(1+|z|^2\right)^{-\frac{1}{2}} \left[\left\{ -2j \left(izR_1 + R_3\right) e^{zJ_+} |j,-j\rangle \right\} + \left\{ \sqrt{2j} \left(2zR_3 + iR_1 + iz^2 R_1\right) e^{zJ_+} |j,-j+1\rangle \right\} \right] \\ &= \left[-2j \left(izR_1 + R_3\right) |\Omega\rangle + \boldsymbol{\left(2zR_3 + iR_1 + iz^2 R_1\right)} J_+ |\Omega\rangle \right]. \end{aligned} \tag{A.18}$$

If we require that the bold terms in the above equate to 0 then $|\Omega\rangle$ will be an eigenstate of H. This gives,

$$\boxed{H|\Omega\rangle = \pm 2j \left(\sqrt{R_3^2 + R_1^2}\right) |\Omega\rangle ,} \tag{A.19}$$

$$\boxed{z = i \left(\frac{R_3 \pm \sqrt{R_3^2 + R_1^2}}{R_1} \right).} \tag{A.20}$$

So, we know the ground state of H,

$$\boxed{|\Omega_g\rangle = \sqrt{1 + \frac{\left(R_3 - \sqrt{R_3^2 + R_1^2}\right)^2}{R_1^2}}\, e^{i \frac{R_3 - \sqrt{R_3^2+R_1^2}}{R_1} J_+} |j,-j\rangle ,} \tag{A.21}$$

with eigenvalue $-2j\left(\sqrt{R_3^2+R_1^2}\right)$, and can be easily seen to be equivalent to (4.28) upto some normalization factor and taking into account decomposition of the Hamiltonian over momenta modes. We may also ask that the terms in red be proportional to $\left[-2j\left(izR_1+R_3\right)\right]$ for $|\Omega\rangle$ to be an eigenstate of H but it doesn't lead to any additional insight of significance to this discussion so we shall skip discussing that choice in the favor of *Occam's razor* .

B Odd L and Periodic Boundary Condition for Kitaev chain

The discussion in Ch.4.3.3 makes assumptions of considering only even L and anti-periodic boundary conditions. A natural question to consider is whether the results, *i.e.* spread complexity and/or its derivative being sensitive to the topological phase boundaries, are affected by a different choice e.g. odd L and periodic boundary conditions. In this appendix we argue that relaxing the assumptions of Ch.4.3.3 on the parity of chain length and the boundary condition of the chain do not alter the essence of the results obtained in the referred chapter, in the continuum limit of $L \gg 1$.

We note that the momenta, (4.36) can include $k = 0$ and/or $k = \pi$ when L is chosen to be odd and/or a choice of periodic boundary condition is imposed on the Kitaev chain - and for these values of k it is clear that, $a_k = a_{-k}$. This feature requires more consideration than a cursory mention. As noted in App.(A) of [170], having this symmetry introduces one of the following two terms in the Kitaev chain Hamiltonian in (4.27),

$$\begin{aligned} H_0 &= -(\mu + J)(a_0^\dagger a_0 - a_0 a_0^\dagger), \\ H_\pi &= -(\mu - J)(a_\pi^\dagger a_\pi - a_\pi a_\pi^\dagger). \end{aligned} \tag{B.1}$$

The eigenstates of $H_{0/\pi}$ constitute the number operator basis *i.e.* occupancy of one or none. The ground states for $H_{0/\pi}$ are respectively expressed as,

$$\begin{aligned} |\Omega\rangle_0 &= |0\rangle_0 + \Theta(\mu + J)\left(a_0^\dagger|0\rangle_0 - |0\rangle_0\right), \\ |\Omega\rangle_\pi &= |0\rangle_\pi + \Theta(\mu - J)\left(a_\pi^\dagger|0\rangle_\pi - |0\rangle_\pi\right). \end{aligned} \tag{B.2}$$

Ref. [35] indicates that the spread complexity is obtained via the Heisenberg algebra formulae and this adds a factor of 1 to the total continuum complexity for finite L if $H_{0/\pi}$ is accounted as the boundary condition contribution at $\mu = \pm J$, respectively, and in this case the ground state is distinguished from the reference state by a lone fermion. At these points in the parameter space, the spread complexity assumes a discontinuous profile while in the continuum case its a well behaved continuous function. Fortunately for us, in the continuum limit of $L \gg 1$ these new contributions to complexity are sub-leading and the results of main text do not perturb from the desired behavior.

C Spread Complexity for a Coherent State Circuit

Following [35] we discuss the computation of spread complexity for generalized coherent states. Since the Kitaev chain Hamiltonian is part of an **$\mathfrak{su}(2)$** algebra this discussion is structured around the computation of spread complexity for $SU(2)$ coherent states - this can be easily adapted to other generalized coherent states.

A circuit Hamiltonian here refers to any Hamiltonian that generates a unitary flow on the operator space via a circuit parameter s, which may be thought of as the circuit-time. A generic $SU(2)$ circuit Hamiltonian assumes the following form,

$$L = \alpha J_+ + \alpha^* J_- + \gamma J_0. \tag{C.1}$$

As in the main text, we consider the $SU(2)$ lowest-weight state as the reference state with various available choices for the target state to which the Hamiltonian generates a unitary flow via circuit parameter t. The circuit-parameter evolved reference state can be expressed as,

$$e^{iLs}|j,-j\rangle = \mathcal{N} e^{z(\alpha,\alpha^*,\gamma;s)J_+}|j,-j\rangle \equiv \frac{1}{\sqrt{(\bar{z}|z)}}|z), \tag{C.2}$$

where $\mathcal{N}$ represents the normalization, s the circuit parameter, and z the coherent-state parameter with different choices of $z \equiv z(\alpha,\alpha^*,\gamma;s)$ connecting the reference state $\left|j,-j\right\rangle$ to various target states upon a unitary evolution through e^{iLs}. This can be seen through a simple application of Baker-Campbell-Hausdorff formulae. Throughout this work, we have chosen the target state as the state obtained through the evolution of circuit-parameter from $s = 0 \mapsto 1$ - so effectively, determining $z(\alpha,\alpha^*,\gamma;s=1)$ fixes the target state, or rather, since we choose particular target states in the main text we need to figure out the corresponding $z(\alpha,\alpha^*,\gamma;s=1)$.

The very action of choosing coherent basis to represent the circuit implies the identification of coherent state basis as the Krylov basis [106, 109],

$$|K_n\rangle = \frac{1}{\sqrt{\langle j,-j|J_-^n J_+^n|j,-j\rangle}} J_+^n|j,-j\rangle, \tag{C.3}$$

and as such the Krylov complexity operator is obtained as,

$$\widehat{K} = \sum_{n=0} n \frac{J_+^n|j,-j\rangle\langle j,-j|J_-^n}{\langle j,-j|J_-^n J_+^n|j,-j\rangle}. \tag{C.4}$$

In the notation of Krylov-complexity operator, $\widehat{K}$, the Lanczos coefficients in the $SU(2)$ coherent-state basis

are expressed as,

$$\begin{aligned} b_n &= \alpha \frac{\langle j,-j|J_-^{n-1}J_+^{|j,-j\rangle}}{\sqrt{\langle j,-j|J_-^{n-1}J_+^{n-1}|j,-j\rangle\langle j,-j|J_-^{n}J_+^{n}|j,-j\rangle}} = \alpha\sqrt{n(2j-n+1)}, \\ a_n &= \gamma \frac{\langle j,-j|J_-^{n}J_0J_+^{n}|j,-j\rangle}{\sqrt{\langle j,-j|J_-^{n}J_+^{n}|j,-j\rangle\langle j,-j|J_-^{n}J_+^{n}|j,-j\rangle}} = \gamma(n-j). \end{aligned} \tag{C.5}$$

There are, at least, a couple of equivalent approaches to computing the spread complexity of the desired target state $|\psi_t\rangle$ going forward, keeping in mind that we've fixed the reference state. One of them, and probably the most utilized one in literature, is to use these Lanczos coefficients to obtain the complexity wavefunctions, by solving (3.19), and then the sum of the number-weighted average of the probabilities associated with these complexity wavefunctions would be the spread complexity, by definition, (3.20). Utilizing coherent-state basis furnishes a simpler way to obtain spread complexity as the expectation value of the Krylov-complexity operator,

$$C = \langle\psi_t|\widehat{K}|\psi_t\rangle. \tag{C.6}$$

As such, the Krylov complexity for a circuit connecting reference and target states expressed in terms of a $SU(2)$ coherent basis is computed as,

$$\begin{aligned} C &= \frac{1}{(\bar{z}|z)}(\bar{z}|\widehat{K}|z), \\ &= \sum_{n,m,m'} \frac{n}{(m!)(m'!)} \frac{\langle\psi_0|\bar{z}^m L_-^m L_+^n|\psi_0\rangle\langle\psi_0|L_-^n z^{m'} L_+^{m'}|\psi_0\rangle}{(\bar{z}|z)\langle\psi_0|L_-^n L_+^n|\psi_0\rangle}, \\ &= \sum_n \frac{n}{(n!)^2}\bar{z}^n z^n \frac{\langle\psi_0|L_-^n L_+^n|\psi_0\rangle}{(\bar{z}|z)}, \\ &= z\partial_z \log(\bar{z}|z). \end{aligned} \tag{C.7}$$

This form of spread complexity is manifestly symmetric under the exchange of target and reference states - which makes sense for unitarity preserving flows in the operator space. Interestingly, this is also equivalent to the (normalized) expectation value of the operator $J_0 + j$,

$$\boxed{C = \langle\bar{z}|J_0 + j|z\rangle \equiv z\partial_z \log(\bar{z}|z).} \tag{C.8}$$

Specifically, the overlap of reference and target $SU(2)$ coherent states is expressed as,

$$\begin{aligned} (\bar{z}|z) &= (1+z\bar{z})^{2j}, \\ \implies C &= \frac{2jz\bar{z}}{1+z\bar{z}}, \end{aligned} \tag{C.9}$$

which, for $z \equiv \pm i\tan\phi$ upon choosing $\left(\frac{R_3 \pm \sqrt{R_3^2+R_1^2}}{R_1}\right) = \pm\tan\left(\phi\right)$ in (A.20), yields,

$$C = 2j\sin^2\phi. \tag{C.10}$$

We recall from Ch.3 that the Krylov basis, for spread complexity, is uniquely fixed by the choice of the Hamiltonian as well as the reference state. Consequently, the expression (C.8) is solely applicable to coherent-state circuits connecting the lowest-weight $SU(2)$ reference state to target states.

Even though we state that the above analysis is strictly applicable to the circuits with lowest-weight $SU(2)$ reference states it is easy to see that the analysis is naturally generalized to references states that are obtained by arbitrary $SU(2)$ unitaries acting on the $SU(2)$ lowest-weight coherent state. The states considered in the main text belong to this category and hence one finds this analysis applicable to them with the following minor modifications. For a reference state, $|\phi_0\rangle$ evolved through the lowest-weight $SU(2)$ reference state by an arbitrary $SU(2)$ unitary U,

$$|\phi_0\rangle = U|j,-j\rangle, \tag{C.11}$$

the Krylov basis is given by,

$$\boxed{|K_n\rangle = \frac{1}{\langle j,-j|J_-^n J_+^n|j,-j\rangle} U J_+^n |j,-j\rangle,} \tag{C.12}$$

There are a couple of straightforward ways to see this:

1. the Krylov basis in (C.3) is independent of the parameters α, α^*, and γ with the only effect of a $SU(2)$ unitary acting on the lowest-weight $SU(2)$ coherent state is to change these parameters, as remarked earlier, leading to the Krylov basis just picking up a factor of U through its dependence on the reference state; and,
2. in the same vein as above, a $SU(2)$ unitary transformation of circuit Hamiltonian, expressed as,

$$U^\dagger L U = \alpha' J_+ + (\alpha')^* J_- + \gamma' J_0, \tag{C.13}$$

simply represents a transformation of the coefficients α, α^*, and γ - leading to a Hamiltonian which only differs in the parameters from the non-transformed one and results in the same structure of the Krylov basis.

The spread complexity of a generic $SU(2)$ coherent state set as the target state is quickly evaluated as,

$$C = \langle \bar{z}|U^\dagger J_0 U + j|z\rangle. \tag{C.14}$$

One may simply absorb the arbitrary $SU(2)$ unitary U into the coherent state label, z.

So we've established that the above result (C.14) is applicable to any generic circuit connecting lowest-weight state or $SU(2)$-evolved lowest-weight states to other $SU(2)$ coherent target states. This is sufficiently general to capture all the three circuits considered in the Ch.4.

D BCH Formulae

The aim of this appendix is to describe the ubiquitous utility of Baker-Campbell-Hausdorff (BCH) formulae to facilitate the computation of spread complexity when the corresponding Hamiltonian constitutes some symmetry algebra - specially if it is a low-dimensional algebra. These formulae also lend themselves well to facilitating computation of return amplitudes or two-point functions as well.

In this appendix, we work in reference to the linearly coupled Bateman oscillator problem. However, this machinery is readily generalized to other systems - albeit ones with relevance to some underlying algebra in the context of spread complexity. We begin by considering the following faithful matrix representation of the operators that are exactly quadratic (term by term) in the ladder operators. To this end, note the following finite dimensional faithful 4×4 matrix representation of the operators quadratic in creation and annihilation operators,

$$\begin{aligned}
\frac{\alpha}{2}a^\dagger a^\dagger + \frac{\alpha^*}{2}aa + \frac{\gamma}{4}\left(a^\dagger a + aa^\dagger\right) &= \begin{pmatrix} \frac{\gamma}{2} & i\alpha & 0 & 0 \\ i\alpha^* & -\frac{\gamma}{2} & 0 & 0 \\ 0 & 0 & 0 & 0 \\ 0 & 0 & 0 & 0 \end{pmatrix}, \\
\frac{\alpha}{2}b^\dagger b^\dagger + \frac{\alpha^*}{2}bb + \frac{\gamma}{4}\left(b^\dagger b + bb^\dagger\right) &= \begin{pmatrix} 0 & 0 & 0 & 0 \\ 0 & 0 & 0 & 0 \\ 0 & 0 & \frac{\gamma}{2} & i\alpha \\ 0 & 0 & i\alpha^* & -\frac{\gamma}{2} \end{pmatrix}, \\
\rho a^\dagger b^\dagger + \rho^* ab &= \begin{pmatrix} 0 & 0 & 0 & i\rho \\ 0 & 0 & i\rho^* & 0 \\ 0 & i\rho & 0 & 0 \\ i\rho^* & 0 & 0 & 0 \end{pmatrix}, \\
\rho a^\dagger b + \rho^* ab^\dagger &= \begin{pmatrix} 0 & 0 & \rho & 0 \\ 0 & 0 & 0 & -\rho^* \\ \rho^* & 0 & 0 & 0 \\ 0 & -\rho & 0 & 0 \end{pmatrix}.
\end{aligned} \tag{D.1}$$

This representation is a 4×4 finite dimensional matrix representation of the algebra. Using this representation one can readily compute BCH formulae that are useful for evaluating the return amplitude, and by extension the spread complexity. As an illustrative example, we take the following rather simple (but sufficient to demonstrate the utility of BCH formulae) reference state,

$$|\phi_r\rangle = |0,0\rangle. \tag{D.2}$$

The BCH formulae are an instruction on the process to decompose an exponential of non-commuting elements *i.e.* it define as map: $e^{A+B} \mapsto f(e^A, e^B)$, for non-commuting A and B - which in the context of spread

complexity take the form of the generators of the algebra which the Hamiltonian constitutes. For the generators in (D.1) the following decomposition serves our purposes,

$$U = e^{\frac{z_{aa}}{2}a^\dagger a^\dagger} e^{\frac{z_{bb}}{2}b^\dagger b^\dagger} e^{\frac{z_{ab}}{2}a^\dagger b^\dagger} e^{\zeta b^\dagger a} e^{\Delta_a(a^\dagger a + aa^\dagger)} e^{\Delta_b(a^\dagger a + aa^\dagger)} e^{\zeta' a^\dagger b} e^{\frac{z'_{ab}}{2}ab} e^{\frac{z'_{bb}}{2}bb} e^{\frac{z'_{aa}}{2}aa}. \tag{D.3}$$

The parameters z_{aa}, z_{bb}, etc. are complex however, they are not independent. The faithful representation of the group suggests that there are 10 real parameters characterizing the group while the right-hand side of (D.3) clearly has 20 real parameters (10 complex parameters, each having 2 real parameters). The unitarity of the group element U, $U^\dagger U = \mathbb{I}$ determines half of these parameters. Now, the action of the decomposed group element on the reference state is given as,

$$\begin{aligned} U|\phi_r\rangle &= e^{\Delta_a+\Delta_b} e^{\frac{z_{aa}}{2}A^\dagger A^\dagger} e^{\frac{z_{bb}}{2}B^\dagger B^\dagger} e^{z_{ab}A^\dagger B^\dagger} |0,0\rangle \\ &= \mathcal{N} e^{\frac{z_{aa}}{2}A^\dagger A^\dagger} e^{\frac{z_{bb}}{2}B^\dagger B^\dagger} e^{z_{ab}A^\dagger B^\dagger} |0,0\rangle, \end{aligned} \tag{D.4}$$

where $\mathcal{N}$ is some normalization factor. These constitute the generalized coherent states [154] for the group associated with the algebra that the Hamiltonian is an element of and each coherent state corresponds uniquely with the elements of the factor group G/H with H being the stationary subgroup linked with our chosen reference state. More precisely, these group elements are given as,

$$e^{ic_a(a^\dagger a + aa^\dagger) + ic_b(b^\dagger b + bb^\dagger) + \zeta ab^\dagger - \bar{\zeta} ba^\dagger} \in H, \tag{D.5}$$

whose action on the reference state $|\phi_r\rangle = |0,0\rangle$ is trivial.

While the above analysis is valid for any element of the group, we are concerned with evaluating the return amplitude (to eventually compute spread complexity) and hence we'd like to utilize the BCH formulae to decompose the time-evolution generating group element in this way. This amounts to computing the following return amplitude,

$$\langle\phi_r|e^{-itH}|\phi_r\rangle = e^{\Delta_a(t)+\Delta_b(t)}. \tag{D.6}$$

As a result, to obtain the return amplitude we merely need to figure out the parameters Δ_a and Δ_b - which can be done using BCH-decomposing the time-evolution group element. This is not a straightforward (or even, possible) in the infinite-dimensional representation of the group elements. However, as we've identified a finite dimensional faithful representation in (D.1) this is a quick computation and in particular, it suffices to evaluate the group multiplication identities like (D.3). Expressing (D.3) in terms of the finite-dimensional matrix representation,

$$\begin{aligned} U = &\begin{pmatrix} 1 & iz_{aa} & 0 & i(z_{ab} - z_{aa}\zeta) \\ 0 & 1 & 0 & -\zeta \\ \zeta & iz_{ab} & 1 & i(z_{bb} - z_{ab}\zeta) \\ 0 & 0 & 0 & 1 \end{pmatrix} \begin{pmatrix} e^{2\Delta_a} & 0 & 0 & 0 \\ 0 & e^{-2\Delta_a} & 0 & 0 \\ 0 & 0 & e^{2\Delta_b} & 0 \\ 0 & 0 & 0 & e^{-2\Delta_b} \end{pmatrix} \\ &\times \begin{pmatrix} 1 & 0 & \zeta' & 0 \\ iz'_{aa} & 1 & iz'_{ab} & 0 \\ 0 & 0 & 1 & 0 \\ i(z'_{ab} - z_{aa}\zeta') & -\zeta' & i(z'_{bb} - z'_{ab}\zeta') & 1. \end{pmatrix}. \end{aligned} \tag{D.7}$$

Hence, it is quite straightforward from here onwards to compute the return amplitude (or other 2-point functions) by evaluating the coefficients on the right-hand-side of the above expression of U, and, thereby, the spread complexity by performing matrix exponentiations. We may choose any desired Hamiltonian or generator from the algebra as well as any coherent reference state - the two aspects which uniquely determine the spread complexity. Consequently, this method proves quite powerful in evaluating closed-form analytic solutions of the spread complexity (and, return amplitude) for an arbitrary circuit (expressed in the corresponding coherent basis) of an arbitrary Hamiltonian - provided that the Hamiltonian participates in an group algebraic structure.

E Numerical Analysis for Spread Complexity

Spread complexity is an incredibly useful tool to detect phase transitions, conservatively, in quantum-mechanical setups - as we've seen in the main text. The analytic closed-form computations of it, however, remain challenging and we often need to resort to numerical approaches to extract the desired dynamical information from the system. This appendix is dedicated to charting out some of the numerical methods and techniques used to obtain spread complexity. In particular, we discuss the numerical analysis in the context of the linearly coupled Bateman oscillator system, and elaborate the complexities - pun intended - in computing the Lanczos coefficients and Krylov (spread) complexity. We discuss these numerical techniques in sufficient generality that they are readily adapted to other discrete quantum-mechanical systems. For continuum quantum-mechanical setups, one needs to frame the theory appropriately as discussed in [39, 107, 108] and develop relevant numerical tools, which are beyond the scope of this thesis. In our implementation, the analytic parts of the results were obtained in `Mathematica` while `Julia` was chosen for the numerical results for its well-professed computational power.

As discussed in Ch.3, Krylov Complexity is the weighted sum of the complexity wavefunction probabilities - computed on the ordered Krylov basis with the weight being the same as the order/position of the complexity wavefunction on the Krylov chain. These complexity wavefunctions are determined through two distinct sets of Lanczos coefficients, $\{a_n\}$ and $\{b_n\}$, with $n \in [0, D]$, where D is the dimension of the Krylov subspace associated to the operator or state whose evolution is under consideration. The Krylov basis vectors are computed using a version of Gram-Schmidt orthogonalization procedure that is appropriate for the Hamiltonian under study; or one may find that the Hamiltonian constitutes some symmetry algebra and it has been shown [106] that the generalized coherent states correspond to the Krylov basis. What, then, about the computation of Lanczos coefficients - which contain all the dynamical information of the system? We saw in Ch.3 that using the standard Krylov subspace method already generates both the sets of coefficients. However, there's an alternate way to obtain them which eschews the determination of the Krylov basis entirely: through the *moments method* which employs moments of the return amplitude to generate the Lanczos coefficients. We briefly recount it for completeness and discuss the relevant numerical analysis for the linearly coupled Bateman oscillator system.

E.1 Lanczos coefficient computation via return amplitude

For a return amplitude, $G(t)$, the n^{th} moment is expressed as,

$$m_n = \frac{1}{G(0)} \left(-i \frac{d}{dt}\right)^n G(t)\Big|_{t=0} . \tag{E.1}$$

One can then define a "moment matrix" $M_{ij} = m_{i+j}$ and a Hankel transform on it generates the $\{b_n\}$ coefficients,

$$b_1^{2n} b_2^{2(n-1)} \dots b_n^2 = \det(M_{ij})\Big|_{0\le i,j\le n} . \tag{E.2}$$

The essence of the above Hankel transformed result is that the coefficients $\{b_n\}$ can be computed by selecting incrementally larger values of n. Starting with $n = 1$, we find $b_1^2 = \det(M_{ij})\big|_{0\leq i,j\leq 1}$, which can be substituted into the $n = 2$ relation $b_1^4 \cdot b_2^2 = \det(M_{ij})\big|_{0\leq i,j\leq 2}$ to evaluate b_2, and so on.

The advantage of the moments method is that it provides an efficient approach for analytically calculating the Lanczos coefficients and is relatively easy, as well as computationally resource efficient (specially compared to the usual Krylov subspace methods) to implement numerically. However, it can encounter numerical instabilities, necessitating careful attention to the precision used. `Julia` is particularly well-suited for this task. A significant portion of the computational time, for the numerical implementation, is devoted to calculating the determinant of the moment matrix for each n; therefore it is advisable to pre-process the moments matrix. e.g. lower/upper decomposition, before computing its determinant. One may also note that there is a simple relation between the determinants for successive n, as observed through (E.2), which may serve to reduce the computational time even further. With increasing n, the size of the moment matrix grows, and hence computation of determinants takes longer - which dictates the maximum number of coefficients that can be obtained within a reasonable time frame. For instance, our code takes approximately 5 minutes to compute the first 200 coefficients in `Julia` using the moments method.

Generically we observe that, the GRA method (see App.(E.2)) outperforms the SOE method when fewer coefficients are needed. Conversely, when a larger number of coefficients is required, numerical instabilities in the moments method can accumulate quickly, rendering it unreliable even with very high numerical precision. This can be illustrated by considering (E.1). The moments method requires computing the n^{th} order derivative of the return amplitude, which scales as $n!$, to obtain the n^{th} coefficient. For instance, to compute b_{100} and a_{100}, for example, one would need to compute the 100^{th} derivative which is of the order of $100! \sim 10^{157}$. Then, the moments method further entails taking determinants of the moment matrices for each n, with very large entries, and a ratio of these determinants - necessitating a careful consideration on the usage of numerical precision. This positions the numerical implementation of the moments method at a disadvantage compared to the more standard Krylov subspace methods. Despite this limitation, we found it feasible to efficiently obtain up to 200 coefficients using the moments method and high-precision computations, although this s contingent on the complexity, pun intended, of the return amplitude's form. Pragmatically, the most crucial aspect of these computations is the duration for which the complexity can be accurately approximated with a specific choice of the artificial cut-off, N, on the Krylov subspace - which is often infinite dimensional for interesting models.

The significance of computing Lanczos coefficients lies in the fact that they encapsulate all the dynamical information about the system [105] - the spread complexity is just one (of many) ways to re-package that information in a form that corresponds to observables with a clear physical interpretation. Consequently, there may be valid concerns that the moments method might not yield enough coefficients to accurately explore the time regimes of interest and adequately capture the underlying physics. Nonetheless, our numerical analysis indicates that, at least for this specific class of problems, appropriately selecting the system parameters can make even $N = 30$ sufficient to capture the expected physics—allowing for some degree of tolerance—as confirmed by our analytical computations in various analytically tractable limiting cases (see

Fig.(10). Figs.(15), and (16) illustrate a comparison of the complexity upon increasing N.

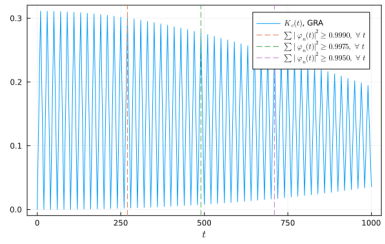

(a) $N = 10$

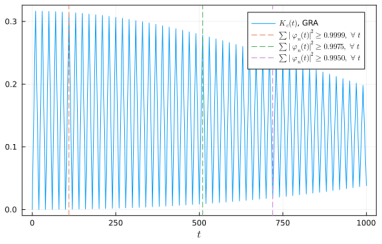

(b) $N = 30$

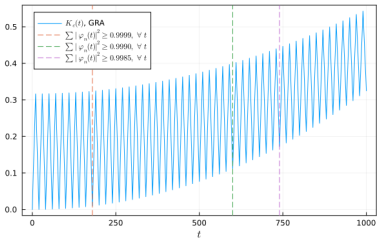

(c) $N = 50$

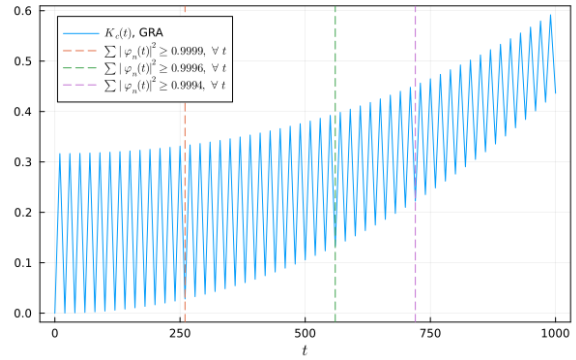

(d) $N = 80$

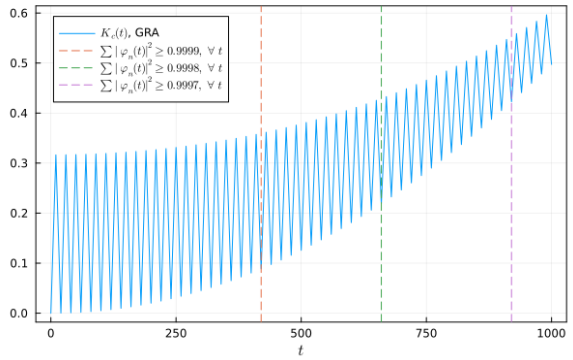

(e) $N = 120$

Figure 15: We compare the complexity as the artificial Krylov space cut-off N is tuned, keeping the parameters fixed at: $\varkappa = 2.0$, $\epsilon = 0.0001414 < \epsilon_1$, $\gamma = 0.0001$, $\Omega = 1.0$ *i.e.* the system is under-damped and weakly coupled. Parameter choice is optimized to contrast the contrast the oscillatory and linear growths. We observe that for low N, it is possible to be blind to important features even if the total probability captured is, $\geq 99.75\%$ - hence, it's advisable to have a sufficiently large N along with capturing most of the probability amplitudes. We found it sufficient to capture essential physics with $N = 50$ (for the results in this appendix), and this ballpark figure is robust at late times too. Furthermore, $N = 50$ is sufficiently low that that the Generated from Return Amplitude (GRA) method out-performs System of Equations (SOE) method significantly; see Ch.E.2. An increase in N assists in exploring progressively smaller time differences & later time physics more accurately (*i.e.*, with a lower tolerance for fault or a higher percentage of total probability captured).

As previously mentioned, the moments method involves computing high-order derivatives of the return amplitude. To enhance the efficiency of this process, we found that performing a power series expansion of the return amplitude is more effective to obtain these derivatives compared to using a generic derivative function. The latter often limits one to only the first few derivatives when dealing with a sufficiently complex return amplitude, as is the case here. While this approach is beneficial in finite-dimensional systems, it proves indispensable when the Krylov subspaces are infinite-dimensional, where numerical implementation necessitates the introduction of a cut-off in the Krylov space dimension. For our implementation, we uti-

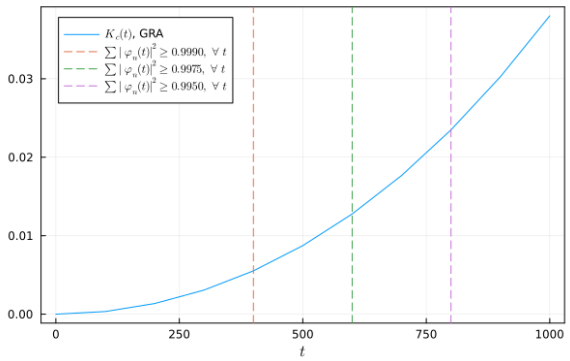

(a) $N = 30$

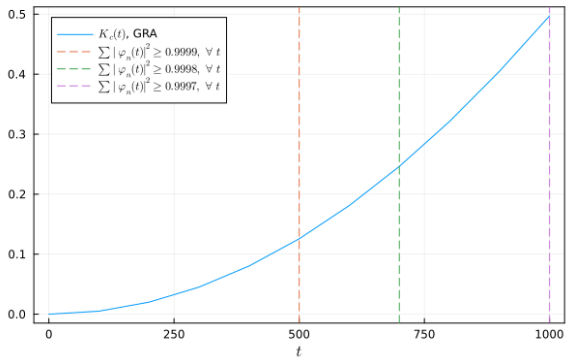

(b) $N = 120$

Figure 16: This figure highlights the need for choosing an appropriate time interval to probe. With same parameters as Fig.(15), the oscillatory behavior is absent in this figure even with $N = 120$ since the time interval of the probe is $\Delta t = 50.0$ compared to $\Delta t = 1.0$ for Fig.(15) (as well as, all other plots in this appendix). Upon increasing N, the ratio $\frac{\Delta t}{t_{\text{max.}}}$ can be reduced, where $t_{\text{max.}}$ is the total time up to which the system is evolved, to get more accurate complexity *i.e.* an increase in N, expectedly, leads to better results by allowing for probing the system for smaller time intervals and allowing for longer time evolution of the system.

lized `TaylorSeries.jl` [171].

Finally, it is crucial to manage precision when applying the moments method, given the technique's inherent numerical instability. In finite-dimensional spaces, this instability can lead to the non-truncation of the Krylov space as successive coefficients are calculated through ratios. If precision is lost, a coefficient expected to be zero may instead yield a very small value, which can cause the subsequent coefficient to become excessively large (as the coefficients are computed via successive ratios in the moments method); similar issues arise in infinite-dimensional Krylov spaces. Nevertheless, these loss-of-precision errors are generally straightforward to handle.

E.2 Computing the complexity wavefunctions

After computing the Lanczos coefficients, as described in the previous section, there are - at least - two simple methods that furnish the complexity wavefunctions - the probabilities of which determine the spread complexity.

- System of Equations (SOE) : this is the standard method and it involves looking for simultaneous solutions of the following systems of equations,

$$\begin{pmatrix} \dot{\phi}_0(t) \\ \dot{\phi}_1(t) \\ \vdots \\ \dot{\phi}_n(t) \end{pmatrix} = -i \begin{pmatrix} a_0 & b_1 & 0 & 0 & \cdots & 0 \\ b_1 & a_1 & b_2 & 0 & \cdots & 0 \\ 0 & b_2 & a_2 & b_3 & \cdots & 0 \\ \vdots & \vdots & \vdots & & \ddots & \\ 0 & 0 & 0 & & \cdots & a_n \end{pmatrix} \times \begin{pmatrix} \phi_0(t) \\ \phi_1(t) \\ \vdots \\ \phi_n(t) \end{pmatrix}, \tag{E.3}$$

with the boundary conditions : $\phi_0(0) = 1$ and $\phi_n(0) = 0 \; \forall \; n > 0$ - which encode that at initial time, $t = 0$, all the support is on the first complexity wavefunction (and hence, the first Krylov basis vector) while the rest are zero. As the target state evolves, increasingly more complexity wavefunctions contribute to the spread complexity - and the manner of their contribution determines the chaotic/integrable dynamics of the system under consideration. Note that, the system is limited to a finite-dimensional approximation of the full system due to the introduction of artificial cut-off N. All N complexity wavefunctions are determined for all times after solving equation (E.3). However, it is clear that because of the cut-off, the solutions will not accurately reflect the true complexity wavefunctions (and hence, the spread complexity) beyond a certain time - which depends on the cut-off as well as the parameters of the system.

- Generated from Return Amplitude (GRA) : The complexity wavefunctions can also be derived from the return amplitude, where the first wavefunction is simply the return amplitude, $G(t) = \phi_0(t)$. The subsequent wavefunctions are generated successively, not by a simultaneous solution of (E.3), but by using the boundary conditions, $\phi_0(0) = 1$ and $\phi_n(0) = 0 \; \forall \; n > 0$. The tridiagonal structure of (E.3) permits efficiency improvements, making this method preferable to SOE when the dimension (or the cut-off) of the Krylov space is sufficiently small. The cut-off implies that we will only be able to generate the first N wavefunctions. While higher-valued wavefunctions still exist within this framework, we choose not to compute them (due to the rather strict limitation of having merely finite computational power); unlike in SOE, we do not restrict ourselves to a finite-dimensional approximation of the system. In SOE, selecting a finite cut-off leads to the assumption that $\phi_{n>N}(t) = 0 \; \forall \; t$ —a statement that holds strictly only at $t = 0$ and may be approximately true for longer times, but not universally so. In contrast, GRA does not impose such an assumption. Thus, as time evolves, one might expect that a portion of the total probability will not be captured, as it is lost to the wavefunctions $\phi_n(t)$ with $n > N$ which have been assumed to vanish identically.

The GRA method presents two key benefits compared to the SOE method: (*i*) it operates several orders of magnitude faster, and (*ii*) the probability sum of the complexity wavefunctions, given by, $\sum_{n=0}^{N} \left|\phi_n(t)\right|^2$, quantifies the total probability captured by the cut-off at N. In contrast, the corresponding probability sum for the SOE method reflects the accuracy of the differential equation solver with respect to this cut-off. Consequently, while assessing the error in the SOE results is challenging, the GRA method provides an immediate estimate through this probability sum. Initially, for early times, the GRA probability sum is expected to equal to 1.0 even with small N. However, as time progresses, this value is likely to decrease due to the presence of non-zero contributions from $\phi_{N+1}(t > t_0) \neq 0$, for some t_0. The SOE method, however, operates under the assumption that, due to a fixed cut-off at N, all $\phi_{M>N}$ vanish identically. Thus, the GRA method effectively accounts for missing probabilities, a feature the SOE method lacks. The error computed in the GRA framework can, therefore, serve as a qualitative indicator of the error in the SOE results.For our SOE computations, we utilized the `DifferentialEquations.jl` [172] package. The outcomes from both methods align up to a certain time, which varies based on the parameters used in the return amplitude calculations, as shown in Fig.(17). A general simultaneous differential equation solver must recognize the system's characteristics to perform well with the SOE method and must also adaptively select appropriate parameter intervals during integration, which significantly adds to the computational time. In contrast, the

GRA method's efficiency remains unaffected by the equations' structural complexities.

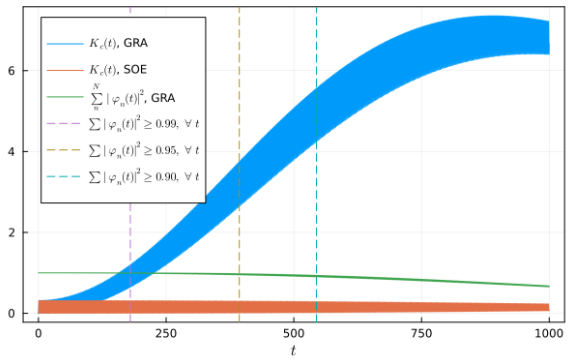

(a) $\gamma = 0.001,\ \epsilon = 0.001414 < \epsilon_1$

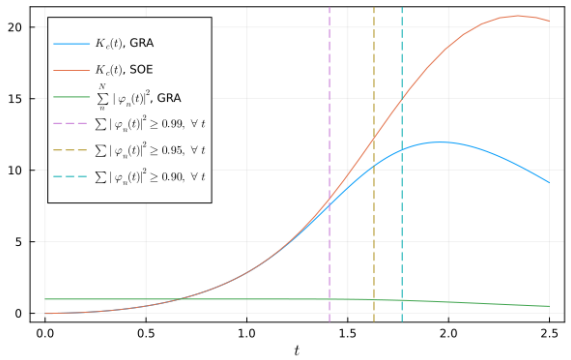

(b) $\gamma = 1.0,\ \epsilon = 1.414 < \epsilon_1,\ \Delta t = 0.01$

Figure 17: We compare the two methods of computing Krylov complexity, the GRA method and the SOE method. We fix the parameters as, $\varkappa = 2.0,\ \Omega = 1.0,\ N = 50$ such that the system is in the under-damped weakly coupled phase. The two methods concur for early times as observed in (a) and (b) subplots, but afterwards the SOE method is unreliable. The time up to which SOE method can be trusted clearly depends on the choice of parameters and (b) illustrates that there is a portion of parameter space for which SOE and GRA both fail to capture the physics around the same time. Nonetheless, GRA method is generically the better choice to compute Krylov complexity.

Finally, for the under-damped weakly coupled system, our analytical analysis predicts that the spread complexity should oscillate superposed with a linearly growing envelope. This expectation is validated by the numerical analysis presented in Fig. (10). Upon further examination, the numerical results reveal an intriguing phenomenon. In Fig.(18), we see a brief time interval around $t = 17.0$ where the linear growth in complexity predominates over the oscillations. Additionally, for various parameter choices, we notice a periodic transition between regimes dominated by oscillations and those characterized by linear growth. This behavior corresponds with changes in the associated Lanczos coefficients, as illustrated in Fig.(20), which is expected since these coefficients encapsulate all the dynamical information of the system. Fig.(19) compares spread complexity across different values of N. The linear-growth-dominant regime in complexity is absent when N is selected such that the relevant regime is not represented in the Lanczos coefficients, particularly the b_n values, as shown in Fig.(20). We hypothesize that the lack of linear-growth dominance is not merely a consequence of using a small N but rather an intrinsic characteristic of the system itself, as opposed to a numerical artifact. This behavior appears to be particularly specific to the case of under-damped weakly coupled oscillators, suggesting that it would be worthwhile to investigate this phenomenon in other similar systems.

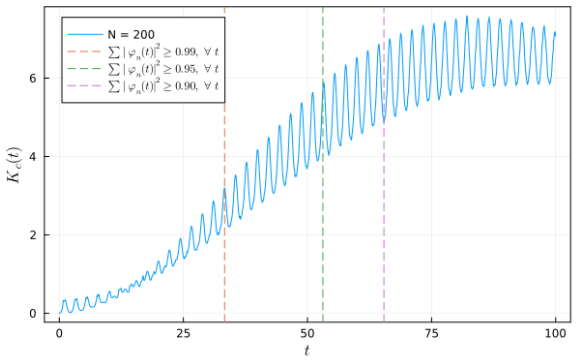

(a) $\varkappa = 2.0,\ \epsilon = 0.01414,\ \gamma = 0.01,\ \Omega = 1.0,$ $N = 200.$

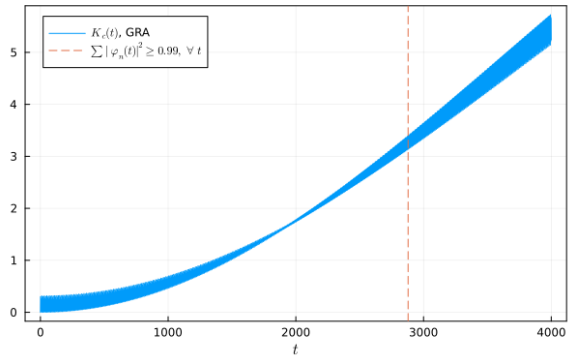

(b) $\varkappa = 2.0,\ \epsilon = 0.0001414,\ \gamma = 10^{-4},\ \Omega = 1.0,$ $N = 120.$

Figure 18: The Krylov (spread) complexity exhibiting features of two characteristic growth behaviors: linear-growth mode; and oscillation mod. There is a clear interplay between the two modes and, in particular, we observe that the linear-growth mode becomes the sole driver of dynamics around $t = 2000$ due to suppression of the oscillation-growth mode, as seen in Fig.(18b). This highlights the robustness of Krylov (spread) complexity to capture the minutest details of a system's dynamics.

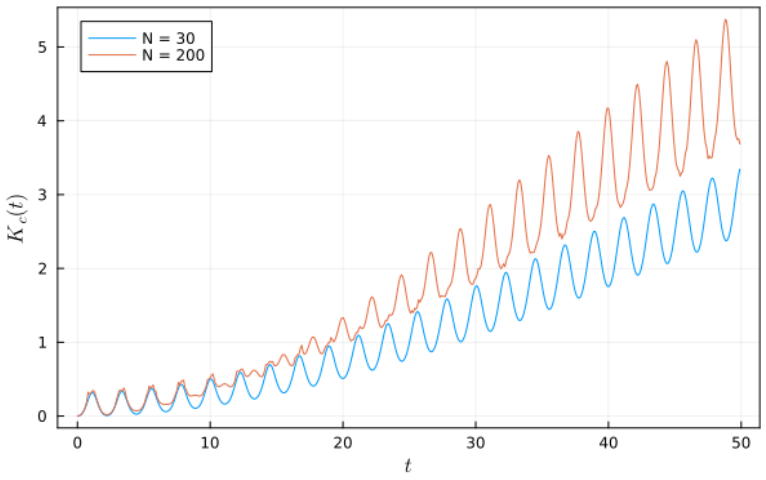

Figure 19: We demonstrate the Krylov (spread) complexity for two values of N, keeping other parameters fixed at: $\varkappa = 2.0,\ \epsilon = 0.01414,\ \gamma = 0.01$, and $\Omega = 1.0$. We note the presence of two growth modes, exactly as in Fig.(18a). The suppression of the oscillation growth mode in not apparent with $N = 30$, while it is so for $N = 200$. This originates from the behavior of Lanczos coefficients, which are mostly oscillation mode dominant for $N \leq 50$, and hence fail to capture the suppression of the oscillation mode (since that is all Krylov complexity "sees"), as noted in Fig.(20). This plot serves to highlight the fact that subtler effects need more data (*i.e.* larger N) to be reflected in Krylov complexity.

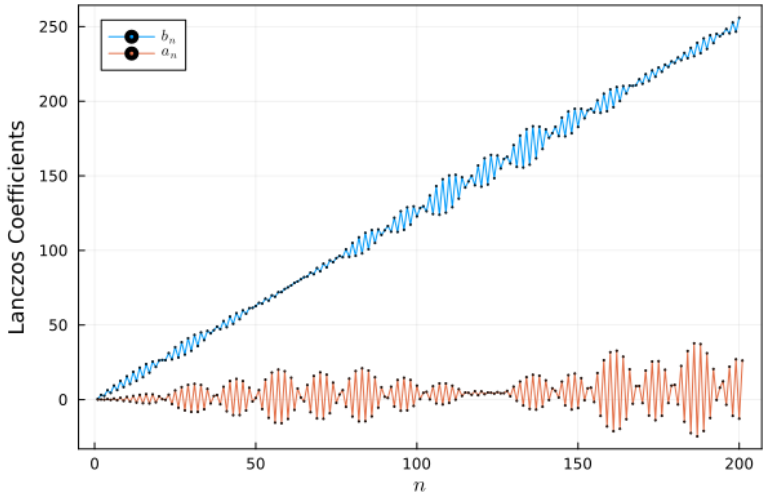

Figure 20: For a parameter choice of: $\varkappa = 2.0$, $\epsilon = 0.01414$, $\gamma = 0.01$, and $\Omega = 1.0$, this plot demonstrates the behavior of first $N = 200$ Lanczos coefficients. As in Figs.(18a) and (19), we observe the two growth modes: the oscillation mode and the linear mode. As remarked, for $N \leq 50$ the Lanczos coefficients are mostly populated by the oscillation mode and the linear mode is absent - which gets reflected in the Krylov (spread) complexity.